9-29-2016 12:00 AM

Geochemical and Petrographic Study of Melt Veins at the West Clearwater Lake Impact Structure, Canada

Rebecca Wilks
The University of Western Ontario

Graduate Program in Geology
A thesis submitted in partial fulfillment of the requirements for the degree in Master of Science

Abstract

The formation of central uplifts in complex impact craters is poorly understood. It is generally accepted that a weakening mechanism is a necessary precursor to accommodate such a large movement of rock. It has been hypothesized that impact-generated melt may have a significant role in weakening the rock of a crater floor to allow for uplift, but it is uncertain if this melt rock is a product of *in situ* melting or injected melt. In this study, melt veins within surface and drill core samples of target rocks from the West Clearwater Impact Structure were analysed using optical microscopy,electron microprobe analysis, and bulk chemistry analysis to determine their formation process. Mixing model results suggest that melt vein structures within the very centre of the crater, collected from the surface and at depth exhibit *in situ* melting; whereas veins around the periphery of the central uplift are formed by the injection of impact melt.

Keywords

West Clearwater Lake Impact Structure; impact cratering; impact melt; melt veins; pseudotachylite.

Acknowledgments

I would like to thank my supervisor Gordon Osinski for the wonderful opportunity to study at Western University and be a part of the Centre for Planetary Science and Exploration and also for the once in a lifetime experience of conducting fieldwork at the West Clearwater Lake Impact Structure.

Thanks also to my undergraduate supervisor Bill Buhay at the University of Winnipeg for introducing me to scientific research and giving me a love for fieldwork. I must also thank Ed Cloutis of the University of Winnipeg for the introduction to planetary science.

Thank you to my family and friends back in Winnipeg Manitoba for being so supportive of my move out east to pursue a masters degree. This unending support made it easy for me to commit to my studies.

I must thank the tight-knit group of friends I was lucky enough to make during my time in London Ontario;Patrick, Mary, Zach, Ian, Danny, Diego, and Taylor. These have been two phenomenal years and a lot of that is owed to you guys.

Table of Contents

List of Figures

List of Appendices

Chapter 1

1 Introduction

Impact cratering is one of the most common geological processes evident throughout the Solar System and can be studied in order to understand the geological history of Earth and other planetary bodies. The process of impact cratering is not fully understood, in particular, how the uplift of underlying rocks occurs in the centre of complex impact structures. This work involves studying the occurrence of melt veins collected from within an impact structure in order to better understand the central uplift formation processes. This study was conducted at the West Clearwater Lake Impact Structure in Northern Quebec, Canada. This structure has a series of central islands, which are interpreted to be the remnants of a central uplift structure and impact melt sheet. The central islands of the structure expose outcrops of impact melt rock, impact breccia and the fractured basement.

It is generally accepted that some weakening mechanism is a necessary precursor for central uplift formation. It has been hypothesized that "melt" may play a major role in the weakening of the rocks which make up the crater floor, allowing for the central uplift process to occur (Spray and Thompson, 1995; Lana et al., 2003; Senft and Stewart, 2009). Melt is thought to lubricate faults which in turn can make blocks of rock more susceptible to displacement, but whether this "melt" is a product of the initial shock (i.e., whole rock impact melt) or due to friction during crater collapse (i.e., pseudotachylite) is currently debated. Here we study these instances of melt observed as vein structures within basement host rock collected from the central islands and drill core at the West Clearwater Lake Impact Structure using petrography and geochemistry in order to determine the process(es) by which they formed.

1.1 Impact Cratering Process

Impact craters are the result of a hypervelocity impact where a projectile of at least 25–50 m in diameter collides with the surface of a planetary body. These impactors travel through the atmosphere with little resistance allowing collisions to occur at cosmic

velocities resulting in high-pressure shock waves that resonate throughout the target. The process that follows collision can be divided into three stages; 1) contact and compression, 2) excavation and 3) modification (Gault et al., 1968) (Figure 1.1).

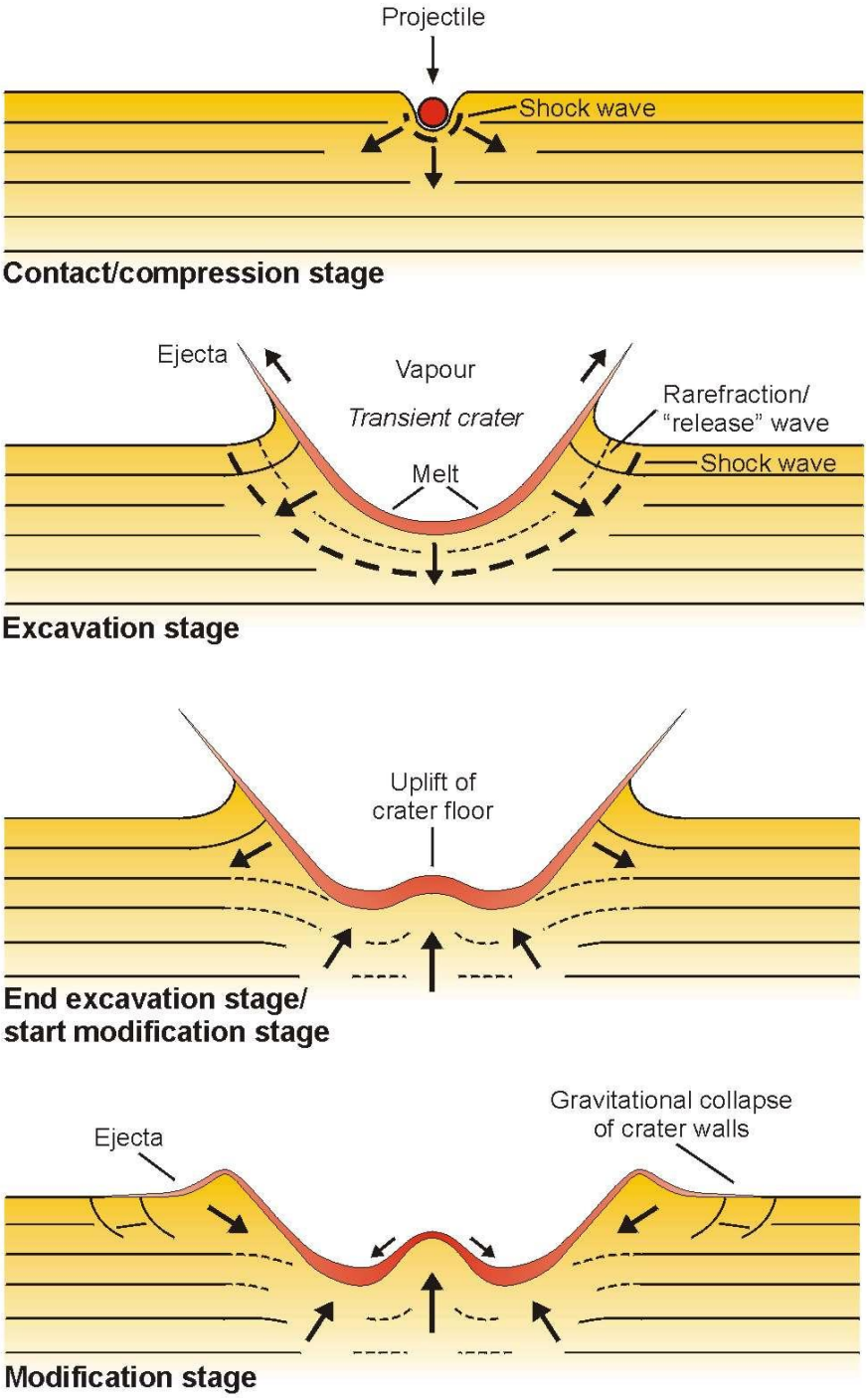

Figure 1.1: Impact cratering stages as illustrated by Osinski (2004).

The contact and compression stage begins when the impactor strikes the surface. On Earth this occurs at a minimum impact velocity of 11.2 km/s, which is the Earth's escape velocity (Melosh, 1989). The force of the collision transports and ejects target material away from the impact area while also compressing these materials; during this time the target's resistance rapidly decelerates the projectile (Melosh, 1989). The resulting pressures at the point of contact reach up to hundreds of GPa creating shock waves between the compressed and uncompressed materials (Melosh, 1989). The shock waves then propagate into both the target material and projectile, these shock pressures far exceed the yield strength of both materials and as a result during the unloading of these pressures the projectile undergoes complete melting and/or vaporization (Melosh, 1989; Osinski and Pierazzo, 2012). Most of the projectile's kinetic energy is transferred to the target materials which undergo compression, acceleration, and heating to a degree where melting and vaporization occurs (Melosh, 1989). The end of the contact and compression stage is considered to be when the projectile has been completely unloaded (Melosh, 1989).

The excavation stage immediately follows contact and compression and its principal result is the expansion of the crater cavity. This expansion is caused by the expanding shock wave and is not the result of the projectile impacting the surface as it has been completely melted and/or vaporized at this point in the process. The generally hemispherical shock wave propagates into the target material weakening as it engulfs more material (Melosh, 1989). During this time, downward directed rarefaction waves are created by initial contact waves reaching the ground surface and rebounding back into the target, this combination with the outward directed shock waves mobilizes target material and results in a subsonic excavation flow of material, opening the crater (Melosh, 1989; Osinski and Pierazzo, 2012). The resultant crater is termed a transient cavity, which can be divided, into two zones; an upper excavated zone and a lower displaced zone. The material from the upper zone has been excavated out of the crater ballistically, causing an ejecta blanket to form and overlay the adjacent terrain (Melosh, 1989; Osinski and Pierazzo, 2012). Materials in the lower displaced zone line the bottom of the transient cavity and are composed of melt and shocked materials. A point is

reached where no more displacement of target rock and melt occurs, however, the end of the excavation is less definitive than the end of contact and compression; as some computer simulations have modelled the cavity reaching a maximum depth and the floor beginning to rise prior to completion of cavity widening (Melosh, 1989; Melosh and Ivanov, 1999).

The final stage of crater formation, modification, is governed by transient cavity size, as smaller craters undergo different modification processes than larger transient cavities. Simple craters (generally less than 4 km across on Earth) undergo moderate modification; this includes slumping of the crater walls as loose materials slides down the steep sides and pool on the crater floor resulting in a bowl shaped depression (Osinski and Pierazzo, 2012). Larger transient cavities undergo modification from gravitational forces to form complex craters; these are defined by their central uplift formation, which occurs when the transient crater floor is uplifted (Osinski and Pierazzo, 2012). Complex craters also experience collapse of the crater walls due to gravitational forces which results in listric fault bounded blocks producing slumped terraces. The modification stage does not have a definite end as the modification processes grade into the normal processes of geological mass movement such as erosion, sedimentation, and isostatic uplift (French, 1998).

1.1.1 Central Uplift Formation

The processes that allow for the formation of central uplifts in impact craters are not fully understood. There is a widely accepted concept that a weakening mechanism is a necessary prerequisite for crater collapse to occur; however, there is considerable debate about the specifics.

The process of acoustic fluidization was first suggested by Melosh (1979) as a means to explain seismic faulting, crater slumping and long runout landslides. The basic concept is that if subjected to strong vibrations rock debris can flow like a fluid even in the absence of air or water as the vibration is transmitted from rock to rock contact as a sound wave. The pressure in a sound wave alternates between more than ambient in compression parts of the wave and less than ambient in rarefactions, due to this difference sliding and failures in the rock debris can occur sporadically throughout the wave where strong

rarefactions cancel out most of the overburden pressure (Melosh, 1989). This random difference in pressure allows for failures to occur throughout the debris mass at a steady rate, resulting in a creeping movement of the rock debris, which produces a finite strain rate (Melosh, 1989). This debris creeps according to rheologic law like that which governs the movement of glacial ice or flow of hot crystalline rock; the strain rate becomes proportional to the applied stress as the acoustic field approaches infinity, the rheology of the acoustically fluidized material then approximates a Newtonian fluid.

This sufficiently strong acoustic wave in rock debris that temporarily relieves the static overburden pressure in certain regions of the rock allows for movement in the unloaded areas (Melosh, 1979). The on going occurrence of these waves can result in the entirety of the rock mass undergoing abundant flow. During the cratering process the initial acoustic energy needed to fluidize the rock is provided by the shock wave and rarefaction, which follow the impact (Melosh, 1979). The dominant wavelength in the acoustic field is roughly the diameter of the impactor (Melosh, 1989). Once the fluidized debris begins to flow this movement can also contribute acoustic energy to the ongoing process; this can result in acoustic fluidization becoming a self supporting process as these acoustic waves add to the general field and promote more sliding (Melosh, 1979). When the acoustic energy is largest flow will occur at low differential stresses and this may result in the materials within the crater acting as a liquid – sloshing back and forth – producing central peaks or peak rings (Melosh, 1989). Materials not within this limited region surrounding the crater do not experience this flow and instead remain effectively rigid throughout this time, allowing for the material acting as a liquid to remain within a hemispherical bowl (Melosh, 1989). The acoustic energy will dissipate once crater collapse is complete and the debris will regain its normal strength properties (Melosh, 1989).

Crater slumping modifies a bowl shaped crater and produces terraced walls; however, these features require very low angles of internal friction (a measure of the ability of a rock unit to withstand shear stress) to form (McKinnon, 1978). Acoustic fluidization can help to explain how these low angles of internal friction are met as these vibrations can temporarily lessen the normal stress of a fault allowing for slipping to occur at lower

shear stresses; if the crater is big enough for differential stresses to be sufficiently large the continued debris flow can produce acoustic energy which would make up for losses from elastic vibrations (Melosh, 1979, 1996). In terms of central uplift formation it is hypothesized that acoustic fluidization aids in the production of a hydrodynamic flow phenomenon similar to that of a water droplet producing a central jet when impacting a body of water.

The block model developed by Melosh and Ivanov (1999) is a variation of Melosh's (1979) original acoustic fluidization model. This model acknowledges that rock medium does not deform as a plastic metal-like continuum but as a system of discrete blocks (Ivanov and Kostuchenko, 1997). The block model applies a variation of the acoustic fluidization equation to a simpler model of a single block sliding along a surface. This modified model of block oscillations is commonly implemented in crater collapse models and can be used to formulate a rheological law for sub crater flow.

Thin veinlets of melt observed in the drill core retrieved from the West Clearwater Lake Impact Structure have been characterized as pseudotachylite by Dence (1965). Pseudotachylite is a dense fault rock that is produced in compression and shear conditions associated with intense and extensive fault movements (Reimold, 1995). It is commonly detected in the crater floor and central uplifts of impact structures, such as those seen at Manicougan (Dressler, 1970), Vredefort (Dietz, 1961), Sudbury (Dietz, 1964) and Ries (Dressler and Graup, 1969). There is some dispute over whether pseudotachylites are formed from frictional melting or by shock wave induced brecciation, which is then followed by thermal metamorphism and melting (Reimold, 1995). The classification of pseudotachylites has been reviewed in depth by Reimold (1995) who discusses how the various interpretations of pseudotachylite differ amongst those in the geologic community. The influence that pseudotachylites may have on central uplift formation has not been studied in depth. The possibility of this connection is worth noting due to the high frequency of pseudotachylite at crater central uplifts, and the potential for pseudotachylite to either promote or act as a weakening mechanism.

The idea of melt and pseudotachylites playing a major role in central uplift formation was examined by Spray and Thompson (1995). Here they define "pseudotachylite rich zones" as areas of large displacement, where there is crushing and heating between basement blocks with frictional melting as well as pseudotachylite injection. They go on to state how the combination of these features can act as a means to accommodate impact induced displacement, or central uplift formation (Spray and Thompson, 1995). Lana et al. (2003) discussed the Vredefort dome central uplift structure and hypothesized that pseudotachylitic breccia vein fractures accommodated the movement of megablocks, due to shear and rotation along these fractures. Melts were also mobilized along the fracture network during the compression and modification stages of the impact event (Lana et al., 2003). Both of these processes are thought to have contributed to the collapse of the crater walls and subsequent central uplift formation, although the role of pseudotachylite is thought to be restricted to transient wall slumping and not associated with the formation of collapse related super faults (Lana et al., 2003). Senft and Stewart (2009) examine dynamic fault weakening as a means to explain crater collapse and subsequent central uplift. Dynamic fault weakening occurs when transiently weakened material in fault zones reduced the bulk strength of the collapsing rock. It is hypothesized that this weakening may be caused by frictional melting (Senft and Stewart, 2009). As these hypotheses suggest, it is likely that melt has some role in contributing to central uplift emplacement.

To summarize, there are two common formation processes for melt veins in impact structures; transport and injection of shock induced melt and *in situ* frictional melting. Shock induced melting occurs during decompression from high shock pressures; whereas frictional melting occurs during crater collapse and uplift formation when rapid slip displacement along faults allow for fragmentation and comminution of the rock (Osinski and Pierzzo, 2012). The latter process results in pseudotachylite. In order to differentiate pseudotachylite from injected impact melt breccia an analysis of the chemical composition of the vein must be performed (Reimold, 1995). If formed *in situ* (pseudotachylite), the composition should be similar to that of the host rock, whereas if the composition is chemically different from the environment it is emplaced, it must be

considered injected impact melt presumably derived from the melt sheet that lines the crater cavity at the end of the excavation stage of crater formation (Reimold, 1995).

There are added complications as recent work by Riller et al. (2010) argues against pseudotachylite being solely generated *in situ* as a product of wall rock melting, and instead states that some allochthonous component must be required. The study's main argument is that the current assumption of fragmentation and melting occurring during a single process in pseudotachylite formation is incorrect. Instead these authors argue that these processes are separated by time and space. Their study focused on Vredefort and Sudbury as examples where the pseudotachylite structures are fragment and melt filled fractures, rather than *in-situ* melt. They used structural and geochemical evidence to support their conclusion that pseudotachylitic melt at Sudbury and Vredefort is partially composed of material from the impact melt sheet, stating that large volumes of the impact melt sheet would have been emplaced into tensional fracture zones.

1.2 The West Clearwater Lake Impact Structure

The West Clearwater Lake Impact Structure is located in northern Quebec, centred at 56°08′N 74°18′W, approximately 110 km east of Hudson Bay. Until recently, the West Clearwater Lake Impact Structure was interpreted to have formed during a binary impact event approximately 290 ± 26 Ma resulting in the formation of Lac à l'Eau Claire (Clearwater Lake) which are two circular lobes separated by a string of small islands and differentiated as West Clearwater and East Clearwater (Figure 1.2). In a recent publication by Schmeider et al. (2015), $^{40}Ar/^{39}Ar$ dating of melt rocks was performed on samples from both the west and east impact structures and a difference in age of approximately 180 Ma was determined. Schmeider et al. (2015) dated the West Clearwater Lake Impact Structure to 286 ± 2.2 Ma and the East Clearwater Lake Impact Structure to a much older Middle Ordovician age of 460–470 Ma.

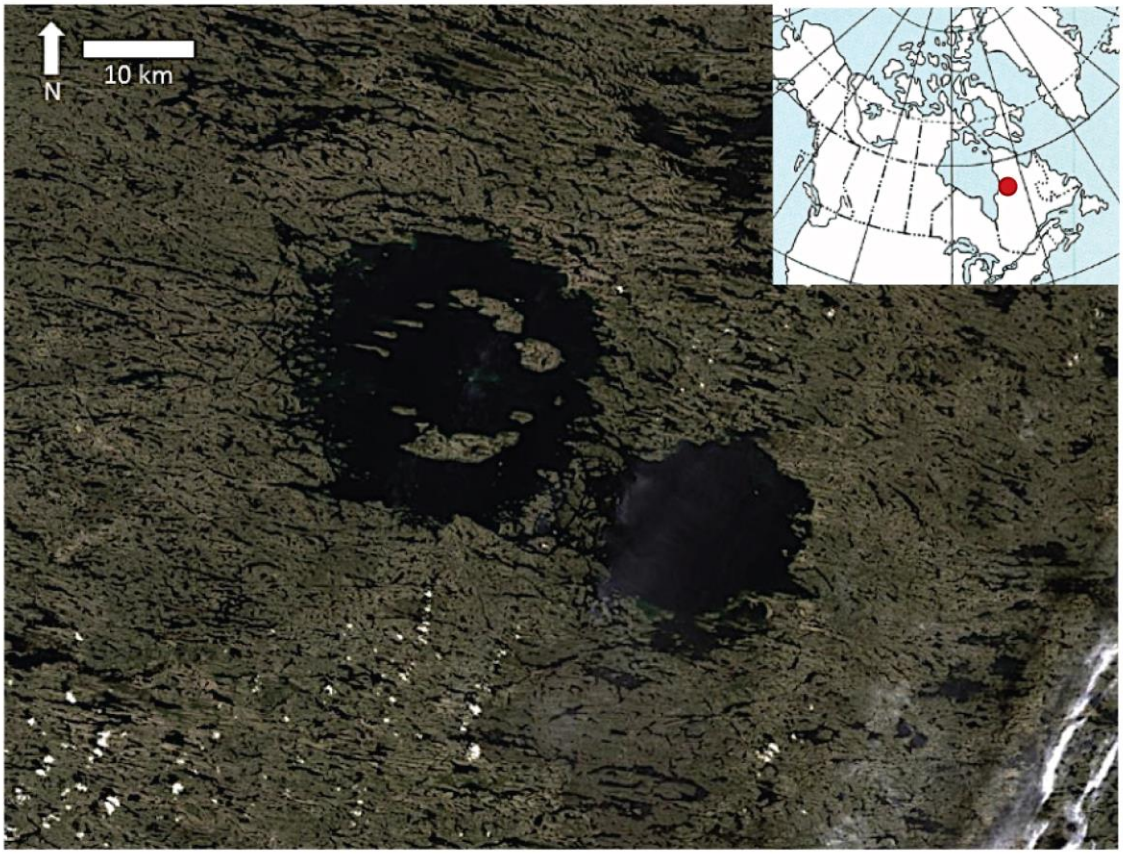

Figure 1.2: Satellite image of Clearwater Lakes, red dot in inset map denotes the location of the impact structures within Canada

The first report of Clearwater Lakes was by George Atkinson II, a Hudson Bay Company employee who came across the lakes while doing reconnaissance in 1818. In 1920 another Hudson Bay Company employee, James Clouston, also doing reconnaissance surveyed the lakes as well; both men noted how clear the body of water was, and Clouston observed the strange shape of the lakes which appeared like two circles joined (Bostock, 1969). The unique shape of the lakes could not go unnoticed while examining aerial photography of the region, which is what lead Beals et al. (1956) to include Clearwater Lake in a survey of potential Canadian impact structures in the Canadian Shield.The West Clearwater Lake Impact Structure is the larger of the two impacts with a diameter of 32km compared to the smaller East Clearwater Lake Impact Structure, which has a 24km diameter (Grieve 2006). The western lake measures 25 km in diameter with a poorly defined rim interpreted to be approximately 5–10 km from the shoreline and rising

to a maximum height of ~425 m. A ~16 km diameter ring of islands within West Clearwater Lake rise to a maximum height of 340 m and centred in this ring are smaller islands less than 100 m across. These central islands are the surface expressions of a central topographical uplift which measures ~5 x 8 km (Hische, 1995). There is an annular trough with maximum depths exceeding 100 m evident between the shoreline and ring of islands and a less defined trough of ~50 m between the ring of islands and the central islands (Grieve, 2006). The West Clearwater Lake Impact Structure has undergone a high degree of erosion, primarily due to glaciation. This heavy erosion makes it impossible to know whether the remnant central islands are linked to the original morphology of the impact, making them what is left of an initial topographically high ring formation, or are simply an artefact of erosional processes (Grieve, 2006).

The West Clearwater Lake Impact Structure was visited by S.H. Kranck of the Geological Survey of Canada in 1963 where he observed red breccia and what he described as red and grey massive dacite. He later published this work (Kranck and Sinclair, 1963) and concluded that the West Clearwater Lake Impact Structure was volcanic in origin. The most extensive study of the West Clearwater Lake Impact Structure by a volcanic origin advocate and the first detailed report of the structure was by Bostock (1969). His work included geologic mapping, petrographic observations as well as major element analysis of both country rock and melt rock. Bostock (1969) concluded that the West Clearwater Lake Impact Structure complex was a result of doming and collapse above a magma chamber.

Throughout the winters of 1962–1963 and 1963–1964 a drilling expedition was conducted by the Dominion Observatory; 2 drill holes were bored in East Clearwaterand 5 were collected from West Clearwater, this was also accompanied by a gravity survey. During the drilling program, observations were made of shatter cones and shock induced mineral phases, as well as thin veinlets of melt, all of which supported the theory of a meteoritic impact origin (Dence, 1964; Dence et al., 1965). The impact origin hypothesis was further supported by the observation of impact induced metamorphic features (McIntyre, 1968; Bunch, 1968; Robertson et al., 1968). Additional backing for an impact

origin was given by Grieve (1978) who was able to accurately model the composition of the West Clearwater Lake Impact Structure impact melt sheet using a mixture of the West Clearwater Lake Impact Structure country rock lithologies. Impact melt rock samples from both the East and West craters were analysed for siderophile trace elements in an attempt to quantify a meteoritic component to the structures (Palme et al., 1978). Results of these studies showed siderophile trace elements present at the East Clearwater Lake impact structure but not detectable at the West Clearwater Lake Impact Structure; the East Clearwater Lake impact structure was estimated to have approximately 7% CI-chondrite component (Grieve, 1978; Palme et al., 1978; Palme et al., 1979; Grieve et al., 1980).

The first attempt at dating the Clearwater Lakes impacts was by Wanless et al. (1964) who used whole rock K-Ar dating methods on the clast poor impact melt rocks to determine an age of 285 ±30 Ma for the West Clearwater Lake Impact Structure and 300± 30 Ma for the East Clearwater Lake impact structure. Later work using the Rb-Sr dating method determined an East Clearwater Lake Impact Structure age of 287 ± 26 (Reimold et al., 1981). However, as mentioned above, there has been a recent argument against the binary impact hypothesis with $^{40}Ar/^{39}Ar$ dating determining the notably different ages of 286 ± 2.2 Ma and 460-470 Ma for the West Clearwater Lake Impact Structure and the East Clearwater Lake Impact Structure impacts respectively (Schmeider et al., 2015).

C. H. Phinney and W. C. Simonds conducted the most detailed geologic investigation of West Clearwater Lake Impact Structure in the summer of 1977 that resulted in two separate publications. Simonds et al. (1978) describes the field and the structural relations; whereas Phinney et al. (1978) covers a detailed petrographic and chemical study of the impact and target lithologies. More recent study of the Clearwater Lakes have focused on the meteoritic body which produced the East Clearwater Lake impact structure. McDonald (2002) re-evaluated platinum group element data retrieved from East Clearwater impact melt to determine that the East Clearwater Lake Impact Structure impactor was more likely composed of ordinary chondritic material rather than

carbonaceous chondritic material. Similarly, Koeberl et al. (2007) found ordinary chondritic material to be the most likely projectile composition based on the chromium isotope signature of the East Clearwater Lake Impact Structure impact melt. A pair of theses from Daniel F. Rosa of McGill University are the latest works on the West Clearwater Lake Impact Structure. Rosa's Masters thesis studied the contact metamorphism of limestone blocks within the West Clearwater Lake Impact Structure (Rosa, 2005); whereas his Ph.D. was a detailed study of the impact melt sheet (Rosa, 2011). Unfortunately, only his Masters work has been published (Rosa and Martin, 2010).

1.2.1 Geology of The West Clearwater Lake Impact Structure

1.2.1.1 Country Rock Lithologies

The impact that formed the West Clearwater Lake Impact Structure, was into plutonic rocks of the Superior craton, specifically, the Bienville sub province, which is distinguished by abundant plutonic rocks, including tonalitic gneiss with mafic enclaves as well as massive felsic plutons (Card and Ciesielski, 1986). The main orthogneissic constituent, "the Bienvilleorthogneiss", contains amphibolite, ultramafic, and metasedimentary inclusions, this orthogniess varies northeastwardly from tonalite to granulite moving from James Bay to Clearwater Lakes (Ciesielski 1991). The country rocks of the West Clearwater Lake Impact Structure were described by Bostock (1969) as being mainly massive to slightly foliated granodiorite, quartz monzonite, minor granite and amphibolite with minor mafic intrusions. Metamorphism to amphibolite-granulite facies is evident for some of the country rock (Grieve, 2006). These country rocks have also been characterized into felsic rocks of the Desbergeres Suite, intermediate rock of the Loups Marins complex and mafic rock of the Qullnaaraluk Suite by Simard et al. (2004). The Desbergeres Suite is made up of biotite and hornblende bearing granites and granodiorites, they are predominately located to the east and southeast of the Clearwater Lakes. The Loup Marins complex is a group of intrusive and metamorphic clinopyroxene and orthopyroxene bearing rocks, which Simard et al. (2004) placed the intermediate rocks of West Clearwater Lake Impact Structure in; these lithologies are seen to intrude the Desbergeres Suite. The Qullnaaraluk Suite is composed of metamorphosed mafic to

ultramafic intrusions into the Desbergeres Suite. The Archean basement rock is intruded by younger diabase dikes of Proterozoic age (Bostock, 1969). There is no genetic connection between the diabase dikes and the impact melt sheet (Simonds et al., 1978); however, evidence of the fragmental breccia cross cutting the diabase dikes has been observed (Bostock, 1969) making the diabase dykes older than the impact. A middle-upper Ordovician limestone unit occurs as blocks in the melt but does not have any depositional contact with the Archean country rock; it is hypothesized to have been only a fraction of the depth penetrated during the impact (Simonds et al., 1978).

1.2.1.2 Impact Related Lithologies

Overlying the fractured basement are three Pennsylvanian aged impact related lithologies: (1) fragmental breccia, (2) clast-rich impact melt rock, and (3) clast-poor impact melt rock. These three units vary in thickness throughout the structure but always occur in this same sequence. Simonds et al. (1978) and Phinney et al. (1978) proposed that these three units are composed of various ratios of the same two components, one being super heated melt, and the other cooler-less shocked debris.

A fragmental breccia unit overlies the fractured basement; this unit can be equated to Bostock's (1969) friable volcanic breccia unit and varies in thickness from a few metres to a maximum of 20 m, which is evident on one of the tadpole islands (Phinney et al. 1978). The fragmental breccia is a friable rock with 50% of its fragments coarser than 1 mm and clasts ranging from <1 cm to > 10 m (Simonds et al., 1978). Flow foliation textures are evident in the breccia around the larger clasts, the distribution of clasts is highly irregular making the unit appear to have two distinct regions, sometimes more clast rich, other times predominantly melt rich (Simonds et al., 1978). Overlying this fragmental breccia is a unit of clast rich impact melt rock. This melt rock ranges in colour from red to purple and has a coherent structure and abundance of columnar cooling joints (Simonds et al., 1978). This unit is less clast rich than the fragmental breccia unit with only 25% of fragments coarser than 1 mm. The clast rich melt has a relatively constant thickness of 15 m and a sharp contact with the underlying fragmental breccia (Simonds et al., 1978; Phinney et al., 1978). There is a decreasing trend in clast content as you move up through the unit, with only 1% of debris in the 1 cm to 1 m range once 15 m above the

base. This is much lower than at the base where 10% of clast content falls within the 1cm to 1 m range (Simonds et al., 1978). The clast-rich impact melt is overlain by a purple to grey clast-poor melt unit, which is coarser and has poorer jointing. Grain size increases from the base of this unit as clast content decreases, there is also little oxidation occurring further from the base as the highest rocks appear blue-grey in colour (Simonds et al., 1978). A portion of this unit has been removed due to erosion but the preserved thickness is 85 m (Simonds et al., 1978). The clast poor unit also hosts large Ordovician limestone blocks, which have undergone some contact metamorphism.

The 2014 expedition to the West Clearwater Lake Impact Structure was conducted in part with NASA's FINESSE (Field Investigations to Enable Solar System Science and Exploration) team, which is a program that conducts field-based research with the goal of gathering unique knowledge applicable to further human and robotic exploration of our solar system. Since the conclusion of this expedition work has been presented on the re-examination of the West Clearwater Lake Impact Structure, specifically a slightly different classification of the impactites and an examination of hydrothermal mineralization. Kerrigan and Osinski (2015) identify various forms of impact generated hydrothermal alteration within the West Clearwater Lake Impact Structure, including sulphur alteration, quartz veins and vugs, as well as highly vesicular zones of alteration, this work will include further study of fluid inclusions in order to understand the origin and generation of the hydrothermal system at the West Clearwater Lake Impact Structure. Osinski et al. (2015) re-classified the impactites into more discrete groups than previously classified by Bostock (1969) and later by Phinney et al., (1978) and Simonds et al., (1978). The fragmental breccia is divided into two categories; monomict lithic breccia, which is the lower strata and in contact with a fractured basement, and impact melt-bearing lithic breccia overlying the monomict variety. Next the clast-rich and clast-poor melt has been reclassified into three varieties from lowest to highest: clast-rich fine-grained impact melt rock, clast-poor fine-grained impact melt rock and clast-poor medium-grained impact melt rock.

1.3 Thesis Objectives

The goal of this study is to determine the origin processes of the melt veins at the West Clearwater Lake Impact Structure and what influence they may have on central uplift formation. In order to determine whether the melt is formed *in situ* or if it is injected into fractures, an analysis of the geochemistry of the melt veins, the target rocks and the impact melt rocks was necessary. The bulk chemistry of the samples was determined using Fusion X-ray Fluorescence (XRF) and Lithium Borate Fusion Inductively Coupled Plasma Mass Spectroscopy (ICP-MS). A petrographic examination of melt vein and host rock textures and compositions from both surface and drill core samples was also conducted in order to determine if there is any evidence to support either *in situ* or injected melt. The relative contributions of host rock and impact melt to the vein was determined using a mixing model in which multiple potential end members may be inputted into the model in an attempt to recreate the chemical compositions of the vein. The hypothesis is that *in situ* melt will have a similar chemical composition to the host rock; whereas injected melt will differ in chemistry when compared to the host rock and should approximate the coherent impact melt sheet at the West Clearwater Lake Impact Structure.

1.4 References

Beals C. S., Ferguson G. M., and Landau A. 1956. A search for analogies between lunar and terrestrial topography and photographs of the Canadian Shield. Journal of the Royal Astronomical Society of Canada 50:203-211.

Bostock H. H. 1969. The Clearwater Complex, New Quebec. Geological Survey of Canada 178:63p.

Bunch T. E. 1968. Some characteristics of selected minerals from craters. In Shock metamorphism of natural materials, edited by French B.M. and Short N.M. Baltimore: Mono Book Corp. pp. 413-432.

Card K. D. and Ciesielski A. 1986. Subdivision of the Superior Province of the Canadian Shield. Geoscience Canada 13:5-13.

Ciesielski A. 1991. Geology of the East Superior Province, James Bay and the Bienville Subprovinces, Quebec. Geological Survey of Canada. Open File 2398. Natural Resources Canada.

Dence M. R. 1964. A comparative structural and petrographic study of probable Canadian meteorite craters. Meteoritics 2:249-269.

Dence M. R. 1965. The extraterrestrial origin of Canadian craters. Annals New York Academy of Science 123:941-969.

Dietz R. S. 1961. Vredefort Ring structure: Meteorite impact scar? The Journal of Geology 69:499-516.

Dietz R. S. 1964. Sudbury Structure as an astrobleme. The Journal of Geology 72:412-434.

Dressler B. and Graup G. 1969. Pseudotachylite aus dem Nördlinger Ries. Geologica Bavarica 60:170-171.

Dressler B. O. 1970. Die Beanspruchung der prakambrischen Gesteine in der Kryptoexplosionsstruktur von Manicouagan in der Provinz Quebec, Canada. Ph. D. dissertation,University of Munich, Germany.

French B. M., 1998. Traces of catastrophe: A handbook of shock-metamorphic effects in terrestrial meteorite impact structures. LPI Contribution No. 954. Lunar and Planetary Institute, Houston, TX. 120 p.

Gault D. E., Quaide W.L., and Oberbeck V.R. 1968. Impact cratering mechanics and structures. In Shock metamorphism of natural materials, edited by French B.M. and Short N.M. Baltimore: Mono Book Corp. pp. 87-99.

Grieve R. A. F. 1978. Meteoritic component and impact melt composition at the Lac à l'Eau Claire, Quebec.Geochimica et Cosmochimica Acta 42:429-431.

Grieve R. A. F., Palme H., and Plant A.G. 1980. Siderophile-rich particles in the melt rocks at E. Clearwater Impact Structure, Quebec: Their characteristics and relationships to the impacting body. Contributions to Mineralogy and Petrolology 75:187-198.

Grieve R. A. F. 2006. Impact Structures in Canada.GEOtext 5, Geological Association of Canada: 210 p.

Hische R. 1995. Geologie des Clearwater Impakstruktur / Quebec. Ph. D. thesis, WestfälichenWilhemsUniversität, Münster, Germany.

Ivanov B. A. and Kostuchenko V. N. 1997. Block oscillation model for impact crater collapse (abstract #1655) 28th Lunar and Planetary Science Conference.

Melosh H. J. and Ivanov B. A. 1999. Impact crater collapse. Annual Review of Earth and Planetary Sciences 27:385-415.

Kerrigan M. C., and Osinski G. R. 2015. Overview of impact-generated hydrothermal activity at the West Clearwater Lake Impact Structure, Canada (abstract #1508) 46th Lunar and Planetary Science Conference.

Koeberl C., Shukolyukov A., and Lugmair G. W. 2007. Chromium isotopic studies of terrestrial impact craters: Identification of meteoritic components at Bosumtwi, Clearwater East, Lappajärvi, and Rochechouart. Earth and Planetary Science Letters 256(3):534-546.

Krank S. H. and Sinclair G. W.1963. Clearwater Lake, New Quebec. Geological Survey of Canada 100:25p.

Lana C., Gibson R. L., and Reimold W. U. 2003. Impact tectonics in the core of the Vredefort dome, South Africa: Implications for central uplift formation in very large impact structures. Meteoritics & Planetary Science38:1093-1107.

McDonald I. 2002. Clearwater East impact structure: a re-interpretation of the projectile type using new platinum-group element data from meteorites. Meteoritics & Planetary Science 37:459-464.

McIntyre D.B. 1968. Impact metamorphism at Clearwater Lake, Quebec. In Shock metamorphism of natural materials, edited by French B.M. and Short N.M. Baltimore: Mono Book Corp. pp. 363-366.

Melosh H. J. 1989. Impact Cratering: A Geologic Process. Oxford University Press, 245 p.

Melosh H. J., and Ivanov B. A. 1999. Impact crater collapse. Annual Review of Earth and Planetary Science 27:385-415.

Osinski G. R. 2004. Hypervelocity impact into sedimentary targets: Processes and products. PhD thesis, University of New Brunswick, Canada.

Osinski G. R. and Pierazzo E. 2012. Impact cratering: Processes and products. John Wiley & Sons, 330 p.

Osinski G. R., Brunner A., Collins G., Cohen B. A., Coulter A., Elphic R., Grieve R. A. F., Heldmann J. L., Hodges K., Horne A., Kerrigan M., Lim D. S. S., Misener R., Morgan J. V., Rae A. S. P., Saint-Jacques D., Skok J. R., Squyres S., Tornabene L. L., Wilks R., and Young, K. 2015. Revisiting the West Clearwater Lake Impact Structure, Canada (abstract #1621) 46th Lunar and Planetary Science Conference.

Palme H., Janssen M. J., Takahashi H., Anders E. and Hertogen J. 1978. Meteoritic

material at five large impact craters. Geochimicaet Cosmochimica Acta 42:313-323.

Palme H., Göbel E., and Grieve R. A. F. 1979. The distribution of volatile and siderophile elements in the impact melt of East Clearwater (Quebec). Proc. 10th Lunar and Planetary Science Conference: pp. 2465-2492.

Phinney W. C., Simonds C. H., Cochran A., and McGee P. 1978. West Clearwater, Quebec, Impact Structure, part II: Petrology Proc. 9th Lunar and Planetary Science Conference: pp. 2659-2693.

Reimold W. U., Grieve R. A. F., and Palme H. 1981. Rb-Sr dating of the impact melt from East Clearwater, Quebec. Contributions to Mineralology and Petrology (76):73-76.

Reimold W. U. 1995. Pseudotachylite in impact structures—generation by friction melting and shock brecciation?: A review and discussion. Earth-Science Reviews 39(3):247-265.

Riller U., Lieger D., Gibson R. L., Grieve R. A., and Stöffler D. 2010. Origin of large-volume pseudotachylite in terrestrial impact structures. Geology38(7):619-622.

Robertson P. B., Dence M. R. and Vos M. A. 1968. Deformation in rock-forming minerals from Canadian craters. In Shock metamorphism of natural materials, edited by French B.M. and Short N.M. Baltimore: Mono Book Corp: pp. 433-452.

Rosa D. F. 2005. Marble enclaves in the melt sheet at the West Clearwater Lake Impact Crater, Northern Quebec. M.Sc. thesis, McGill University, Montreal, Quebec, Canada.

Rosa D. F., and Martin R. F. 2010. A spurrite-, merwinite-and srebrodolskite-bearing assemblage, West Clearwater Lake impact crater, northern Quebec. The Canadian Mineralogist 48(6):1519-1532.

Rosa D. F. 2011. The sheet of impact melt at the West Clearwater Lake, Northern Quebec. Ph.D. thesis, McGill University, Montreal, Quebec, Canada.

Schmieder M., Schwarz W. H., Trieloff M., Tohver E., Buchner E., Hopp J., and Osinski G. R. 2015. New 40 Ar/39 Ar dating of the Clearwater Lake impact structures (Québec, Canada)–Not the binary asteroid impact it seems?. Geochimicaet Cosmochimica Acta 148:304-324.

Senft L. E., and Stewart S. T. 2009. Dynamic fault weakening and the formation of large impact craters. Earth and Planetary Science Letters 287:471-482.

Simard M., Parent M., Thériault R., David J., Lacoste J., and Sharma K. 2004. Géologie de la région du lac à l'Eau Claire (34B et 34C).Ministère des RessourcesNaturelles du Québec, RG 2003-8: 46 p.

Simonds C. H., Phinney W. C., McGee P. and Cochran A. 1978. West Clearwater, Quebec, Impact Structure, part I: Field geology, structure and bulk chemistry. Proc. 9th Lunar and Planetary Science Conference: 2633-2658.

Spray J. G., and Thompson L. M. 1995.Friction melt distribution in a multi-ring impact basin. Nature 373:130-132.

Wanless R. K., Stevens R. D., Lachance G. R. and Rimsaite J. Y. H. 1964. Age determinations and geologic studies (part 1). Isotopic ages, report 5. Geological Survey of Canada Paper 64:17.

Chapter 2

2 Geochemical and Petrographic Study of Melt Veins at the West Clearwater Lake Impact Structure, Canada

2.1 Introduction

It is well known that as impact craters increase in size, their morphology changes. On Earth, craters with diameters of <2−4 km undergo moderate modification, which results in simple craters that have a bowl shaped crater morphology (Melosh, 1989). Above this threshold diameter, crater morphology changes due to gravitational forces during the modification stage, producing so-called complex craters (Dence, 1965). Complex craters differ from simple craters in that they form central peaks due to the uplifting of the crater floor and as diameter increases peak rings form (Melosh, 1989). On Earth, morphology can be difficult to discern due to erosion, therefore, the term central uplift is preferred, as it is typically unknown whether the central region was in fact a peak (Grieve, 2004). The process of central uplift formation in complex craters is poorly understood. It is generally accepted that a weakening mechanism must act as a necessary precursor to uplift but what this mechanism may be is still undetermined (Melosh, 1989). Impact-generated melt has been hypothesized to have a role in this process (Senft and Stewart, 2009); melt can potentially accommodate impact-induced displacement and central uplift formation via cataclasis, frictional melting and subsequent melt injection (e.g., Spray and Thompson, 1995). During the compression and modification stages of crater formation impact melt can be mobilized along fracture networks (Lana et al. 2003). The melt responsible for this mobilization may be formed *in situ* – where it is referred to as pseudotachylite – or it may be formed elsewhere, transported and injected into pre existing fractures. There are, however, competing theories as to how pseudotachylite in impact craters form. The different classifications and origins of pseudotachylite were reviewed by Reimold (1995). The two main models discussed were that pseudotachylite is either formed through frictional melting or via shock induced brecciation and further thermal metamorphism. There is also a recent hypothesis proposed by Riller et al. (2010) that argues against pseudotachylite being formed *in situ.* Instead, this model proposes that a significant

component of pseudotachylite is allochthonous material from a crater's impact melt sheet that has been injected into fractures. In order to differentiate between pseudotachylite and injected melt the chemical composition of the melt must be examined. If the melt is formed *in situ* then a similar chemical composition to that of the host rock can be expected; whereas injected melt would have a different chemical composition than that of the host rock, specifically, a similar composition to that of the impact melt sheet. In this study we examine melt veins within basement host rock of the West Clearwater Lake Impact Structure using petrography and geochemistry in order to determine their formation process and their potential role in central uplift formation.

2.1.1 Geological Setting and Previous Work

The West Clearwater Lake Impact Structure is located in Northern Quebec ~110 km east of Hudson Bay. It was formed 286 ± 2.2 Ma (Schmeider et al., 2015) when a hypervelocity impact occurred into the Archean plutonic rocks of the Superior Province. It was originally believed to be part of a binary impact event, as the East Clearwater Lake Impact Structure lies directly adjacent to it, however the East Clearwater Lake Impact Structure has recently been dated to 460–470 Ma (Schmeider et al., 2015). The West Clearwater Lake Impact Structure is approximately 32 km in diameter and has a central lake measuring 25 km in diameter (Grieve 2006). Since the ~425 m high topographic rim is poorly defined and can occur anywhere from 5 to 10 km from the shoreline of the lake (Grieve 2006) the actual diameter of the structure may be significantly larger. Within the lake are multiple islands in a ring-like distribution and there are also a group of small islands located in the very centre of the lake (Figure 2.1). These central islands are exposures of basement materials from an uplifted region in the centre of the lake measuring 5 x 8 km (Hische, 1995). There are two defined troughs within the lake, one between the shoreline and the island rings, with depths exceeding 100 m, and a second between the island rings and central islands with a maximum depth of 50 m (Grieve, 2006).

The West Clearwater Lake Impact Structure was first studied by Kranck and Sinclair (1963) of the Geological Survey of Canada, whose main observations of red breccia and greydacite, lead them to conclude a volcanic origin for the structure. Bostock (1969) was

the first to study the structure in depth and came to the same volcanic origin conclusion. This research included geologic mapping, petrographic observations and bulk chemical analysis. The first evidence in support of an impact origin was observed during a drilling expedition in the winter of 1963, these observations included shock induced mineral phases, shatter cones and thin veinlets of melt (Dence, 1964; Dence, 1965). An impact related origin hypothesis was later supported by further evidence of impact induced shock metamorphism (McIntyre, 1968; Bunch, 1968; Robertson et al., 1968). The most detailed investigation of the West Clearwater Lake Impact Structure was conducted by W. C. Phinney and C. H. Simonds who carried out a study of the field geology and structural relations (Simonds et al., 1978) as well as a petrographic and chemical examination of the impact and target lithologies (Phinney et al., 1978).

The target rocks of the West Clearwater Lake Impact Structure consist mainly of granodiorite, quartz monzonite, granite and amphibolite (Bostock, 1969). These Archean rocks are intruded by diabase dykes of Protoerzoic age (Bostock, 1969). Imbedded within the impact melt are limestone outcrops of Ordovician age, which are hypothesized to have only been 130 m in thickness at the time of impact (Hishe, 1995).

A variety of allochthonous impactites overlay the fractured basement rocks, with a fragmental breccia occurring at the base (Phinney et al. 1978). This breccia is a friable rock with flow foliations evident within the breccia especially around larger clasts (Simonds et al., 1978).The unit has an irregular distribution of clasts, making some areas more melt rich (Simonds et al., 1978) and varies in thickness from only a couple metres to a maximum thickness of 20 m (Phinney et al. 1978). The unit was classified differently by Osinski et al. (2015) and divided into two separate units: a monomict lithic breccia and a melt-bearing polymict lithic breccia. Overlying these breccias is a clast-rich impact melt which has a much more coherent structure than the breccia and a lower clast content (Simonds et al., 1978). The clast rich melt varies in colour from red to purple and has an average thickness of 15 m; this unit contacts the underlying fragmental breccia sharply (Simonds et al., 1978; Phinney et al., 1978). Finally a clast poor impact melt rock caps the islands. This unit is purple to grey in colour and is coarser than the clast poor melt.

Clast content decreases away from the base of the clast poor unit as grain size increases (Simonds et al., 1978).

Thin veinlets of melt have been observed in the basement lithologies of the drill core and characterized as pseudotachylite (Dence, 1965). Simonds et al., (1978) also makes mention of these small melt dykes in the basement, stating that they are either pseudotachylite formed *in situ* or formed by injected melt.

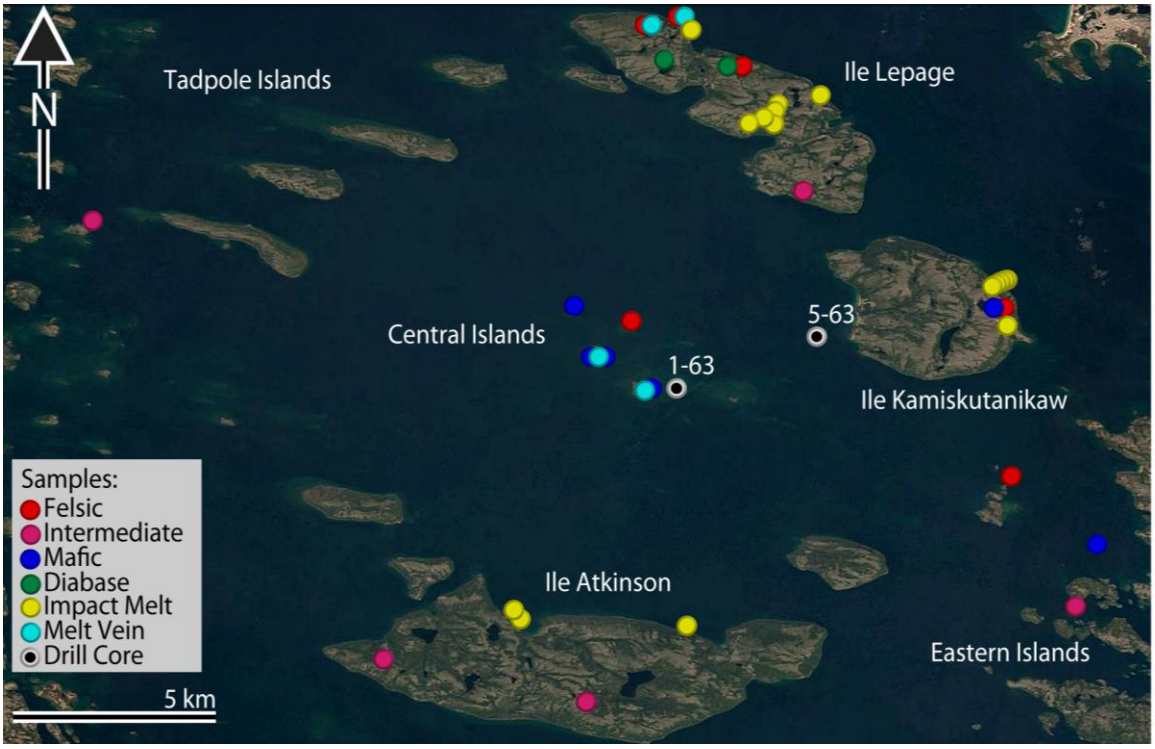

Figure 2.1: Map of the West Clearwater Lake Impact Structure showing sample locations.

2.2 Methods

Fieldwork was conducted over the span of four weeks in August and September of 2014 as part of a Canadian-US-UK expedition with approximately 300 samples being collected from the interior ring of islands, the edge of the mainland, and the eastern islands that divide the West Clearwater Lake Impact Structure and the East Clearwater Lake Impact Structure. Drill core samples were also obtained from the 1963 drilling program conducted by The Dominion Observatory and supervised by M.R. Dence. The drill core

has a diameter of 3.2 cm and begins at various depths below lake level, with a total of 5 cores being sampled throughout the lake (1-63, 3-63, 4-63, 4a-63 and 5-63). The core was logged and sampled at the Geological Survey of Canada in Ottawa, Ontario. A suite of 21 samples from this total were selected from drill cores 1-63 and 5-63 and were cut and sampled for bulk chemistry analysis. Petrographic analysis was conducted at the University of Western Ontario using a Nikon Eclipse LV100 POL microscopes and NIS-Element photographic software package. Mineral analysis was done by wavelength dispersive spectroscopy using a JEOL JXA-8530F field-emission electron microprobe housed at the Earth and Planetary Materials Analysis Laboratory (EPMA) at the University of Western Ontario. This instrument was also used to look at micro textures, acquire element maps and backscattered electron images. Bulk chemical data were obtained from the Biotron Laboratory atthe University of Western Ontarioand from ALS Laboratories. Major and trace element concentrations were measured using Fusion X-ray Fluorescence (XRF) and Lithium Borate Fusion Inductively Coupled Plasma Mass Spectroscopy (ICP-MS).

In this study we used a mixing model developed by Weirich et al. (2016) and used successfully by O'Callaghan et al., (2016) to model breccia at the Sudbury Impact Structure. The model uses IDL software to replicate the geochemical signature of the melt veins using up to four end members. The impact melt average is always included as an end member and the remainder of end members are selected from country rock lithologies. By using four end members we are able to model more complex localities with many potential contributing lithologies as is the case with the West Clearwater Lake Impact Structure. A total of 53 samples were analysed for bulk chemistry, the host rock and melt rock were separated using a rock saw and rotary tool and were then powdered.This resulted in 17 samples for mixing model analysis in addition to the remaining samples which were used to acquire averages for the end member lithologies.

The model evaluates the contributions from up to four end members and performs a principle component decomposition of the geochemical data. The model places threeconstraints on the data; firstly, the sum of all contributions from the end members

must equal 100% (Eq. 1) where $X_i$are the per cent contributions from each end member. Secondly, the modelled melt vein must have the same SiO_2 content as the measured melt vein (Eq. 2) where X_{SiO_2} are the per cent contributions of silica from each end member and they must equal the silica content of the measured vein (M_{SiO_2}).

$$A_i + B_i + C_i + D_i = 1(100\%) \text{ (Eq.1)}$$

$$A_{SiO_2} + B_{SiO_2} + C_{SiO_2} + D_{SiO_2} = M_{SiO_2} \text{ (Eq. 2)}$$

Although the model is capable of modelling up to 63 discrete elements the user is able to select elements of interest. The elements of interest must satisfy a similar criteria to Eq.2, where each end member's contribution of that element of interest must sum to equal the value of that element in the measured vein sample (Eq. 3). The equation 3 values are controlled by the values in equation 2 (equation 2 is the independent variable).Since a chi-squared value is produced for each element or oxide inputted to the model, this allows for discrimination between elements which may be contributing high chi-squared values and therefore distorting the results, in this case those elements would be avoided in the user's selection of elements of interest. The total number of elements of interest must also be selected with caution as too many can make the model inflexible as it must try to satisfy all element contributions, however too few elements can lead to a very flexible model which results in too many degrees of freedom and affects the validity of the results.

$$A_{EOI} + B_{EOI} + C_{EOI} + D_{EOI} = M_{EOI} \text{ (Eq. 3)}$$

Once these constraints are satisfied the mixing model then determines what combination of the oxides and elements produces the lowest chi squared value, which is a measure of difference between the modelled vein and the measured vein (Eq. 4) where $O_i$is the measured vein or observed value and E_i is the modelled vein or expected value for each of the inputted oxides and elements. The higher the chi-squared value the greater the variation is between the modelled and measured results.

$$X^2 = \sum \frac{(O_i - E_i)^2}{E_i} \text{ (Eq. 4)}$$

The output also provides a p-value for each modelled combination to assess the probability that the chi-squared value is low by chance. The p-value acts as a function of the chi-squared values and can vary between 0 and 1. The p-value is used in determining whether or not your hypothesis is correct (in this case whether or not the chi-squared value is significant or if it is low by chance). A pre determined threshold value of 0.05 or 5% was used; meaning p-values between ≥ 0.05 and < 1.0 are considered acceptable. The lower the p-value the less likely the modelled results are accurately explaining the measured values, in contrast, an especially high p-value, such as 1.0 likely means there are too many end members and therefore too much variability in the modelled values. Too high or too low a p-value can also be due to a missing component (missing end member lithology or alteration), which would restrict the model. One shortcoming of the model is that it is not weighted and, therefore, it cannot be used to discriminate between specific elements and their relative proportions from each end member.

A total of 7 vein samples were modelled successfully, 4 of which were surface samples and 3 were retrieved from the drill core. To discriminate between *in situ* melting and injected melt, the end members were chosen based on proximity to the melt vein sampled and how realistic they were to be included in the melt vein composition. In order to have a direct comparison of injected (melt average) and *in situ* (host rock) melting this resulted in all samples having the impact melt average and their associated host rock included in the mixing model. The other one to two end members would vary based on the lithology of outcrops located near to the sample sites.

2.3 Results

2.3.1 Target Rocks

In order to ascertain the origin of the melt veins, knowledge of the geochemistry of the target rocks is critical. The target rocks used in this study were sampled from both the surface and the drill core. Surface samples were almost always heavily fractured and altered in comparison to the drill core samples. The target rock lithologies were divided

into three broad categories; mafic (gabbro, diabase, amphibolite, tonalite), felsic (granites, quartz monzonite), and intermediate (granodiorite, diorite, monzonite) rocks.

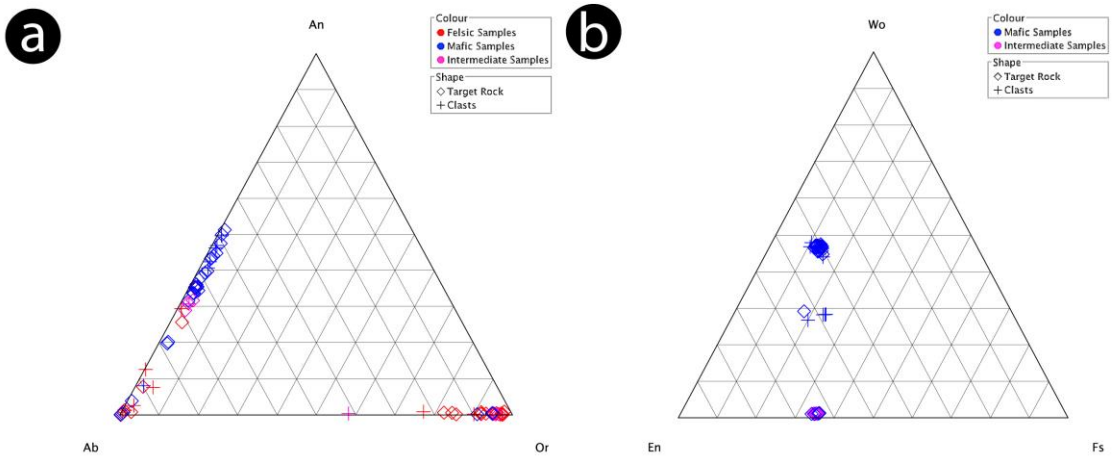

Figure 2.2: Ternary diagrams showing mineral compositions of target rocks and clasts from within melt veins analysed. a) Feldspar ternary diagram of mineral compositions from felsic (red), intermediate (pink) and mafic (blue) target rocks. b) Pyroxene ternary diagram of mineral compositions from intermediate (pink) and mafic (blue) target rocks.

2.3.1.1 Mafic Rocks

Of the mafic target rock samples used in this study, 10 were from the drill core and 8 were hand samples. The mafic hand samples were mainly collected from the central and eastern islands, with only 1 sampled from Ile Kamisutinikaw, and 2 diabase samples from Ile Lepage (Figure 2.1). The drill core samples are from cores 1-63 and 5-63; samples from core 1-63 are amphibolite; however, the 4 samples from core 5-63 have less amphibole and contain quartz. They were, therefore, classified as tonalite in the core logs. These tonalite samples have been grouped with mafic samples for the purposes of this study due to their very low silica content (49–52%).

The most common minerals within the mafic samples are plagioclase with either clinopyroxene or amphibole as the second most abundant mineral (Figure 2.3a and Figure 2.3b). The samples are generally fine to medium grained; however, some core samples display larger grain sizes of plagioclase of up to 1.5 cm. Overall, grain sizes are typically similar throughout the mafic sample suite and they exhibit a granoblastic texture. Common accessory minerals within the mafic target rocks include biotite, pyrite and iron oxides. Biotite is usually in tabular form ranging from 0.01−1mm in size. Some alteration to chlorite is observed in biotite and this usually occurs on the perimeter but at times can occur within the centre of the grain along irregular pathways (Figure 2.4a). Calcite is present as a secondary alteration phase. This obvious infilling of lenticular pores by calcite allows for clear evidence of kink banding in at least one sample (Figure 2.4b). Occasional epidote alteration is also observed, but only in the core samples. Chloritization of minerals is abundant in some drill core samples, often displaying a flow like texture.

In mafic samples plagioclase grains vary from 0.2–2.5 mm with the most common grain size being ~1 mm. Most plagioclase grains display undulatory extinction; polysynthetic twinning is rarely seen and is often poorly developed, especially in the more heavily altered samples. The grains take on a brown appearance in the more altered samples as well. Maskelynite is present in at least one of the shocked samples from the central islands (MK-041) and one drill core sample (1-502.2). This maskelynite in drill core 1-502.2 (Figure 2.3b) becomes completely isotropic in cross polarized light.The composition of the plagioclase feldspar is $An_{0-51}Ab_{48-99}Or_{0-3,}$ predominantly centred on an andesine−labradorite composition, with only 4 feldspars falling within an oligoclase−albite composition (Figure 2.2a). Alkali feldspars were rare in the mafic samples with only 2 detected in sample 1-720.9; they were almost purely orthoclase and ranged from $An_{0.2-0.5}Ab_{5-9}Or_{90-94}$ (Figure 2.2a).

Pyroxene has a similar size range as plagioclase from 0.3–3 mm and often occurs irregularly and congregated together, rather than dispersed throughout the thin section.

Pyroxenes in the mafic surface samples often display irregular growth lamellae in XPL but this was not observed in the drill core samples. Clinopyroxenes were the most common pyroxene observed. The average pyroxene composition is $Wo_{39}En_{45}Fs_{16}$ ranging from $Wo_{1\text{-}48}En_{40\text{-}65}Fs_{12\text{-}36,}$ and is predominately augite and diopside, with minimal clinoenstatite (Figure 2.2b).

As stated earlier amphibole is not present in all mafic samples but where present it usually occurs as medium to large grains ranging from 0.5–3 mm in size. It is predominantly hornblende but kaersutite has also been observed.

2.3.1.2 Felsic Rocks

A total of 13 felsic rocks were investigated; 7 were retrieved from the drill core and 6 from the surface. Of the surface samples 3 were collected from Ile Lepage, 1 from Ile Kamisutinikaw, 1 from the central islands, and 1 from the east islands (Figure 2.1). These surface samples are predominately granites, with one classified as a quartz monzonite. The felsic samples from core 1-63 and 5-63 are coarse-grained gneiss and have undergone varying degrees of shock metamorphism. The main minerals in these pink-grey felsic rocks are alkali feldspar, plagioclase and quartz, with accessory minerals including iron oxide, biotite and apatite (Figure 2.3c and Figure 2.3d); epidote alteration was also observed in the core samples. Plagioclase, alkali feldspar and quartz are all relatively equigranular ranging from 0.2 mm to as large as 1 cm in some pegmatite drill core samples, but on average these minerals are ~1 mm in size.

Plagioclase grains display undulatory extinction and polysynthetic twinning is absent or poorly developed. Plagioclase exhibits an axiolitic texture pattern in at least one sample where long parallel poorly defined grains radiate outwards and have very wavy extinctions. Plagioclase feldspars within the granite samples range in compositions from $An_{0\text{-}35}Ab_{63\text{-}99}Or_{0\text{-}3,}$ with most falling within an albite classification and a few within andesine (Figure 2.2a). The alkali feldspars are equally common in the felsic samples and have a composition which fall close to pure orthoclase, averaging at $An_{0.4}Ab_{7}Or_{93,}$ with some samples having as high as Or_{97} values (Figure 2.2a).

Myrmekite texture is abundant in the granite samples. This appears as either quartz intergrowths in plagioclase feldspar or more commonly antiperthite alkali feldspar in plagioclase feldspar (Figure 2.3d). The texture is composed of vermicular inclusions (of quartz or alkali feldspar). In rare instances the feldspars are reversed and there are plagioclase intergrowths within alkali-feldspar instead. Granophyric intergrowths are also common, where quartz grows within alkali feldspar rather than the plagioclase feldspar.

2.3.1.3 Intermediate Rocks

A total of 6 intermediate surface samples were included in the study; 2 were retrieved from Ile Lepage, 2 from Ile Atkinson and 1 from the eastern islands (Figure 2.1). A drill core sample of coarse-grained gneiss has been included in this description of intermediate rocks due its high content of pyroxene and amphibole. Following bulk chemistry analysis it was determined to be closer to diorite than granite in composition. For the most part the intermediate rocks are quite similar to the felsic samples, as some felsic samples had very low quartz compositions. The intermediate samples have similar plagioclase feldspar characteristics (undulatory extinction, lack of twinning, myrmekite texture) but significantly less alkali feldspar and quartz. One surface sample, RW-011, displays abundant planar deformation features (PDFs) in quartz (Figure 2.4d). The main division between the felsic and intermediate is an almost complete absence of coarse-grained quartz and higher frequency of minerals such as pyroxene, biotite, apatite and amphibole; however, plagioclase remains the most common mineral (Figure 2.3e and Figure 2.3f). Another big difference is the range of grain sizes from <0.1 mm to 2 mm, compared to the felsic and mafic samples, which are fairly equigranular. Plagioclase feldspars in intermediate samples do not vary much in composition and average $An_{31}Ab_{67}Or_{2}$ (Figure 2.2a). Alkali feldspars are much smaller in grain size than when observed in the felsic samples and are almost pure orthoclase with an average composition of $An_{0.3}Ab_{4}Or_{95}$ (Figure 2.2a).

The pyroxenes are clinoenstatite in composition with an average composition of $Wo_1En_{64}Fs_{34}$ and do not vary much (Figure 2.2b). Pyroxenes appear as 0.1–0.2mm grains often proximal to amphibole along with biotite and iron oxides.

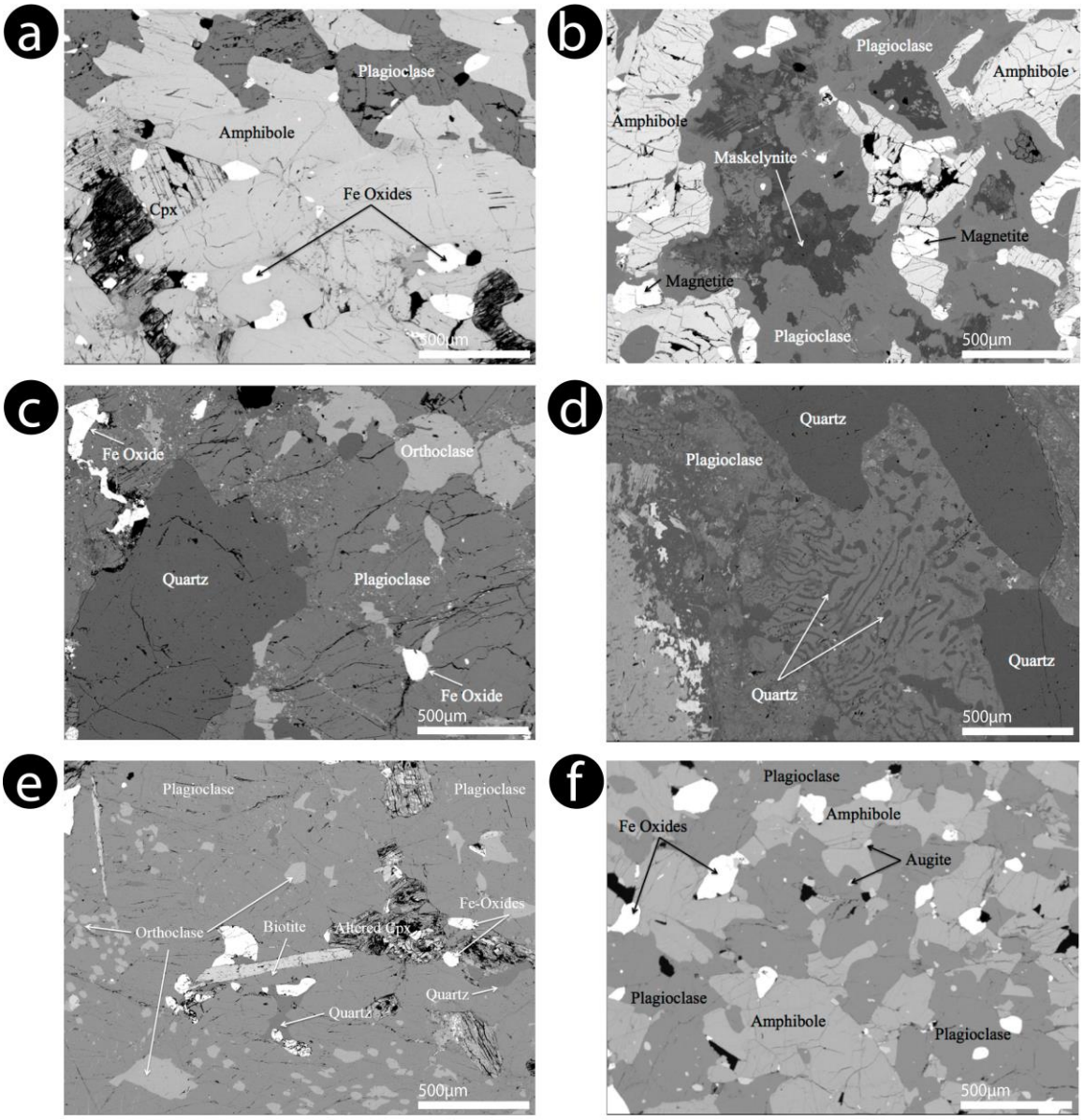

Figure 2.3: Backscattered SEM image of target rock thin sections. a) Drill core sample 1-385.6, an amphibolite that has experienced a degree of shearing. b) Surface sample MK-041 an altered amphibolite from the central islands which has experienced shock metamorphism as seen by the diaplectic glass (maskelynite) shock metamorphism of plagioclase. c) Drill core sample 5-600, a coarse-grained gneiss d) Drill core sample 1-1099 a coarse-grained gneiss with a myrmekite texture of quartz intergrowths within plagioclase feldspar. e) Drill core sample 1-398.9 a fine-medium grained granodiorite with little to no amphibole present f) Drill core sample 1-310 a medium-coarse grained diorite.

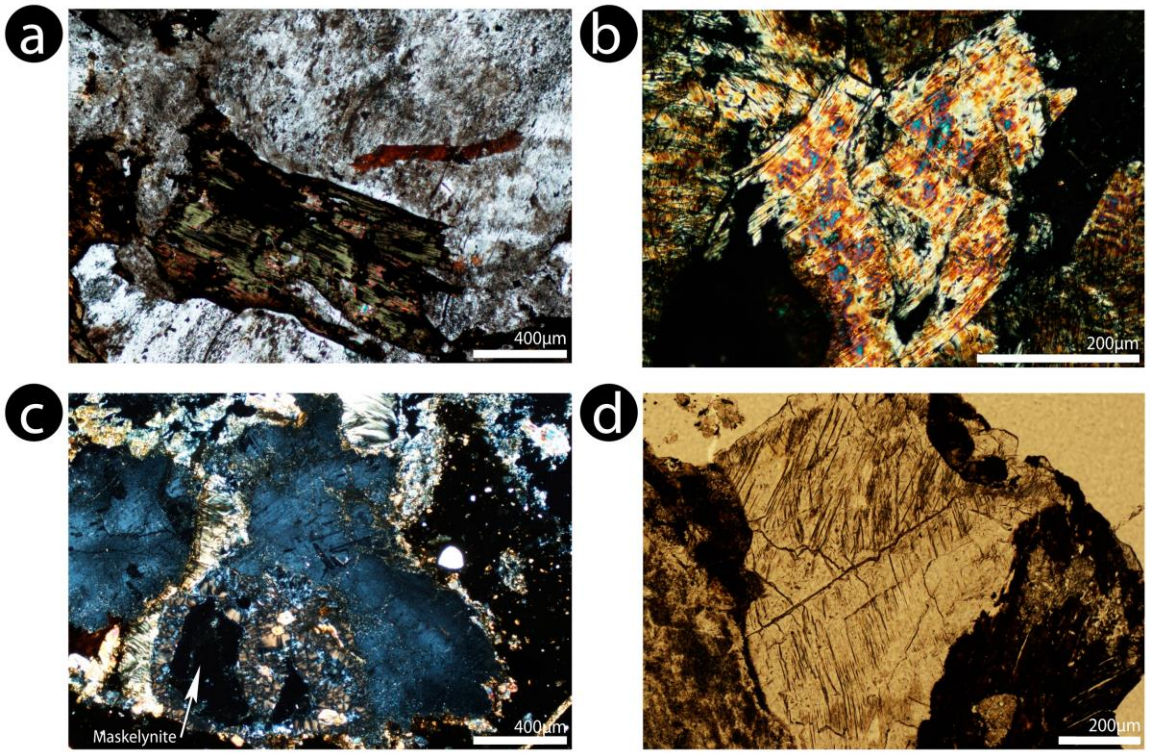

Figure 2.4: Petrographic thin section images a) Sample AR-016 showing a biotite grain almost completely altered to chlorite in XPL. b) Sample AR-017 showing an altered biotite grain with abundant secondary calcite and evident kink banding in XPL. c) Plagioclase in Sample MK-041which has undergone alteration to maskelynite (diaplectic glasss) in XPL d) Planar deformation features in a grain of quartz from sample RW-011.

2.3.2 Impact Melt Rock

A total of sixteen impact melt rock samples of both fine-grained and coarse-grained melt were used in this study to represent the impact melt rock average. Of these samples 6 were collected on Ile Kamikutanikaw, 7 from Ile Lepage, and 3 from Ile Atkinson (Figure 2.1). Using bulk chemical data the impact melt rocks plotted almost entirely within a trachyandesite composition on a total alkali to silica volcanic diagram (Le Maitre et al., 1989). The melt rock matrices vary depending on the melt rock type. The fine-grained melt rock matrix, which is generally 3-10µm in grain size (cf., Phinney et al., 1978) is composed of plagioclase and alkali feldspar laths. Minor amounts of pyroxene, iron oxide

and quartz are also present. Clast content is higher in the fine grained impact melt rock samples and included lithic and mineral clasts; they are predominantly quartz and plagioclase clasts however smaller 200 μm iron oxide clasts have also been observed. Pyroxene and iron oxide halos have been observed to form around quartz and iron oxide clasts in the fine grained matrices.

The coarse-grained impact melt matrix is more holocrystalline and has a subophitic texture, it is mineralogically similar to the fine-grained melt, with feldspar being the most dominate mineral; however, fewer clasts are observed. Pyroxene, feldspar and iron oxide reaction rims are still observed around quartz clasts.

2.3.3 Setting of Vein Samples

2.3.3.1 Core Samples

Drill Core 1-63: Core 1-63 contacts the fractured basement at 19 m below lake level (Figure 2.5). It is located near the centre of the structure and penetrates basement rock of the central uplift (Figure 2.1). At a depth 19 m coarse-grained gneiss (CGG) is contacted, this gneiss is coarse-grained pink granite in composition and shows various degrees of banding. A shear zone occurs from 20 m to 21 m where a fine to medium grained pink and grey clinopyroxene- and biotite-bearing granodiorite is contacted and continues to 26 m where a shear zone occurs again and marks the transition back to CCG until 29 m where the core grades back into the granodiorite. At 35 m the first evidence of melt veins is observed in a shear zone within the granodiorite. This alternation between granodiorite and CGG with numerous melt veins continues until 117 m where amphibolite with moderate shearing is encountered. The mafic component increases as clinopyroxene, amphibolite and plagioclase begin to dominate for a metre in depth until CGG with localized melt veins is contacted. At 129 m the core transitions back to amphibolite and dominates the remainder of the core; however, it is occasionally truncated by transitions to the more felsic lithologies of either CCG or granodiorite.

A melt vein sample was taken from this amphibolite region at ~163 m in depth, the sample is denoted 1-533.4; that is a sample from drill core 1-63 retrieved at 533.4 feet in

depth. This amphibolite sample hosts a dark black vein interpreted in the core logging to be pseudotachylite. The host is augite rich with some plagioclase and biotite grains (Figure 2.6a). The vein is highly zoned with a more clast-rich outside edge (Figure 2.6a). Element maps(Appendix D) of the vein-host contact highlight this zoning, with the centre of the vein being aphanitic, even glassy in appearance, and the outside edges more crystalline and clast rich. The element maps (Appendix D) show a deficit of Na, Al, Ca and Si in the central glassy portion with higher counts of Mg and slightly higher counts of Ti, meaning the central portion of the vein is not simply a smaller grain size but has a compositional difference when compared to the surrounding clast rich edges.

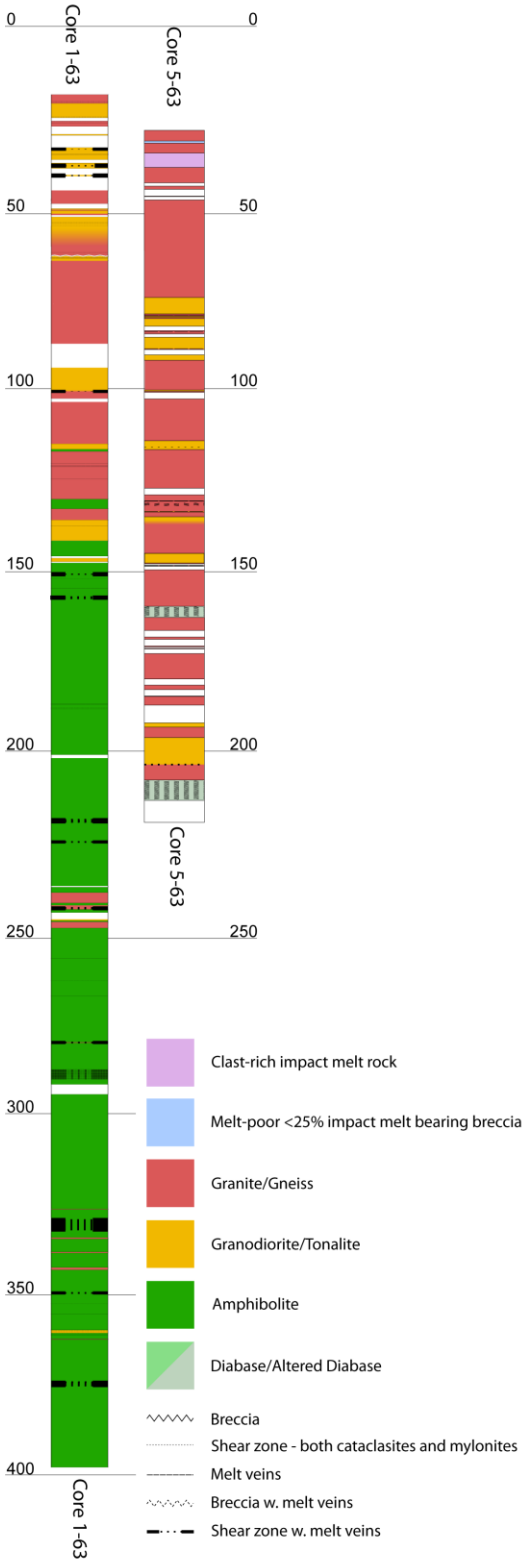

Figure 2.5: Stratigraphic section of drill cores modified from Rae et al. (2016).

The core was sampled again at ~197 m (sample 1-645) where a melt vein measuring 1 cm across interrupts the amphibolite. The host rock is divided by the vein into what appeared to be a relatively unaltered more mafic half and a heavily altered less mafic half. During optical microscope analysis the difference between sides was evident as the more mafic half had a higher frequency of pyroxene whereas the less mafic side was plagioclase dominated (Figure 2.6d). This difference was not apparent in the bulk chemical analysis however. The vein is very clast rich with mainly plagioclase clasts near the edges and pyroxene clasts dominate toward the centre of the vein. On the mafic side of the melt vein-host rock contact a separate thinner vein with a glass matrix and high quartz clast content is observed (Figure 2.6d). This vein matrix in the elemental maps (Appendix D) appears to be glassy as very small counts of Mn, S, Ni and Cl are evident around the clasts, but the maps do not show high counts of any other elements than the Si displayed in the quartz clasts. This glass vein is hosted by alkali feldspar grains, some of which appear elongated from the melt flow. Due to the presence of elongated alkali feldspar clasts on the side of the glass vein it can be interpreted as a separate melting event as it cross cuts the larger alkali feldspar rich melt vein. This smaller vein was not detectable in hand sample and therefore has been include in the bulk chemistry analysis along with the larger vein. The remainder of the melt vein does not have any other apparent elemental zoning. The element maps on the opposite side of the vein are harder to interpret as the host rock is much more heavily brecciated, this gives the appearance that a large portion of wall rock is being incorporated into the vein particularly pieces of feldspars on the wall. Many thinner veins are observed in the remainder of the core, as shear zones and pseudotachylite are prominent throughout this amphibolite portion to its final depth of 376 m.

Drill Core 5-63: Core 5-63 was sampled just off the southwest edge of the Ile Kamiskutanikaw coastline (Figure 2.1). It begins at 29 m below the lake surface and initially penetrates abundantly veined and fractured CGG with vein widths of 1 mm to 1 cm (Figure 2.5). At a depth of 32 m impact melt-bearing breccia occurs with an estimated 10% melt content; it then grades into a fine-grained gneiss after ~1 m. From 35−39 m the

core is clast-rich impact melt with an estimated 30% clast content; the clasts are typically less than 1 cm and are predominantly fine-grained gneiss. The clast-rich melt then contacts a CGG with infrequent veining and fracturing. This CGG continues for 37 m occasionally interrupted by missing core segments. At 52 m the first occurrence of hydrothermal alteration is observed in the form of epidote. At a depth of 58 m the CGG grades to a more intermediate composition with frequent veining of 1 mm thickness. At 62 m the core grades back to a CGG with frequent veining of 2 mm thick veins and infrequent epidote is observed. At a depth of 75 m granodiorite/tonalite with frequent 1 mm veining is encountered and continues for 5 m before grading back to CGG. This alternation between granodiorite/tonalite and CGG continues for 70 m with frequent red veining as well as occasional black glassy veining until pegmatite granite is encountered at 145 m. A sample was retrieved from ~134 m (sample 5-440) This is a sample of a clast rich red melt vein which divides the CGG and tonalite host rock lithologies. The tonalite host rock side is highly chloritized, with green chlorite rich veins crosscutting the host rock. The CGG host has some mafic banding; the bands have also undergone chlorite alteration as chlorite veining within the mafic banding is observed. The red melt vein is more heavily melted than the mafic banding (Figure 2.6c). Zoning of Mg within the vein is evident in this sample (Appendix D); however, is not due to grain size or clast content as this vein is more uniform in grain size and instead likely has something to do with the incorporation of the chlorite veins.

This drill core quickly transitions back to frequently veined granodiorite/tonalite with up to 2 mm wide red veins until 148 m where pegmatite granite is briefly encountered again. The CGG is then followed by brecciated section at 149 m in depth for 15 cm before the core becomes too broken up until 150 m where CGG is encountered again. This CGG is highly altered and continues for 6 m and the core has alternating patches of pegmatite granite and more mafic minerals. In this altered zone yellow-green epidote and creamy white crystals of carbonate are observed. At 160 m the CGG begins to exhibit more frequent mafic banding and contacts an altered and brecciated diabase lithology with frequent veining. A melt vein sample was collected at ~204 m (sample 5-670) The clast rich red melt vein is ~1 cm across and cuts through both CGG and tonalite host rock (Figure 2.6b). The CGG is plagioclase and quartz dominated and its contact with the melt

vein is highly brecciated. A similar zoning effect as 1-533.4 is evident on the CGG contact in this sample; however, the more clast rich portion of the vein is central and the finer grained clast poor region is closer to the wall. The element map data (Appendix D) shows enrichment in Fe and to a lesser degree Mg closer to the wall of the vein whereas the central area of the vein had higher counts of Na, Si and K. Based on the red colouring, flow textures and enrichment of feldspar clasts in this sample it appears that the CGG host rock is being incorporated into the vein to a much higher degree than the tonalite host rock. The CGG continues with alternating patches of more mafic banding, grading into tonalite at 192 m and then back to CCG briefly before 208 m where brecciated and altered diabase with frequent veining is observed again to the core's final depth of 220 m.

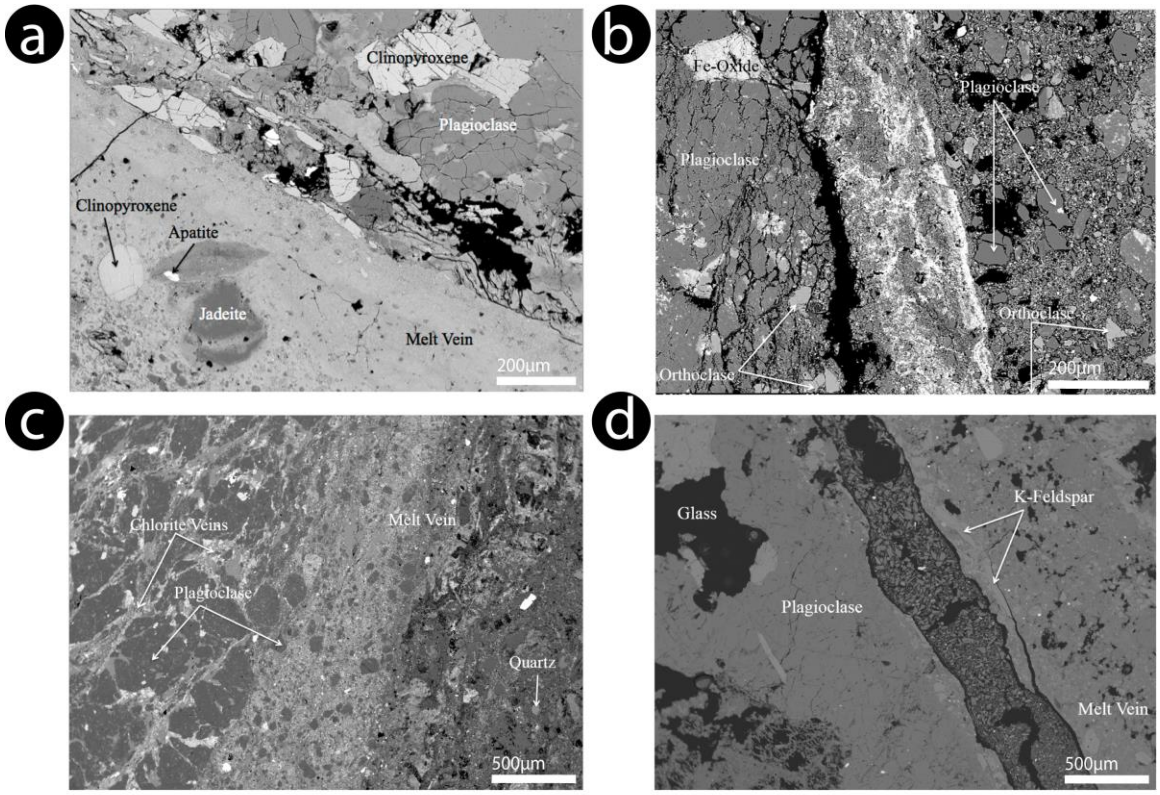

Figure 2.6: Backscattered SEM images of melt veins in drill core samples a) Sample 1-533.4 showing the mafic host rock on top and the contact with the melt vein on the bottom b) Sample 5-670, the brecciated CGG host rock on the right and the melt vein on the left displaying an iron rich zone at the contact and a very clast rich zone further from the wallc) Sample 5-440, the highly chloritized mafic host rock on the left and the contact with the clast rich melt vein on the right d) Sample 1-645 showing the contact between the mafic host rock and the melt vein.

2.3.3.2 Central Island Samples

AR-019: The host rock of AR-019 is gabbroic in composition and primarily composed of plagioclase and clinopyroxene with some accessory pyrite (Figure 2.7a). Small grains of augite and pyrite appear to congregate within the plagioclase grains that have undergone some degree of metamorphism close to the melt vein. The melt vein is made up of very fine-grained plagioclase laths with large clasts that appear to be jadeite with intergrowths of anorthite, also apparent in the vein are smaller clasts of augite (Figure 2.7b).

*AR-016:*AR-016 wascollected from one of the central islands (Figure 2.8a), the host rock is gabbroic in composition; predominantly made up of alkali feldspar and clinopyroxene with accessory iron oxides (Figure 2.7c). The melt vein is vitric and clast rich with flow banding; the clasts are primarily plagioclase and appear in various physical states (Figure 2.7d).

2.3.3.3 Ile Lepage Samples

AR-069: The host rock of AR-069 is a granitic pegmatite with large grains of quartz, orthoclase and plagioclase (Figure 2.7e). The melt vein varies from a fine-grained matrix to a glassier vitric texture. The melt has quartz clasts ranging in size from 10−600 μm across, some of which appear resorbed and fractured. One of these clasts within the devitrified matrix has an apparent iron oxide reaction rim forming on its right side and a darker rimmed halo around its entirety (Figure 2.7f). Quartz clasts within the glassier matrix have also been observed to possess the so-called ballen texture (Ferriere et al., 2009), especially near contacts with the melt.

*RW-013:*RW-013 was collected on Ile Lepage(Figure 2.8b) the host rock is granitic in composition and very quartz rich. A partially melted groundmass is evident in the host rock and exhibits flow banding (Figure 2.7g). Within this groundmass clasts of plagioclase, zircon, and iron oxides are apparent. Under XPL the melted groundmass appears to be a devitrified feldspathic matrix and displays recrystallization textures. The melt vein, however, is crystalline and made up of very fine-grained quartz, plagioclase, and pyroxene. Figure 2.7h shows a large quartz grain within the melt vein with a reaction

rim of small pyroxene grains surrounding it. Towards the top and especially on the right side of the clast are larger quartz and pyroxene grains. Petrographic analysis of the sample shows the melt vein cross cutting the host rock at the contact. Due to the textural and compositional differences of the vein and host rock we can ascertain that the host rock has undergone a degree of shock metamorphism but the melt observed in the host rock did not originate from the melt vein it is in contact with.

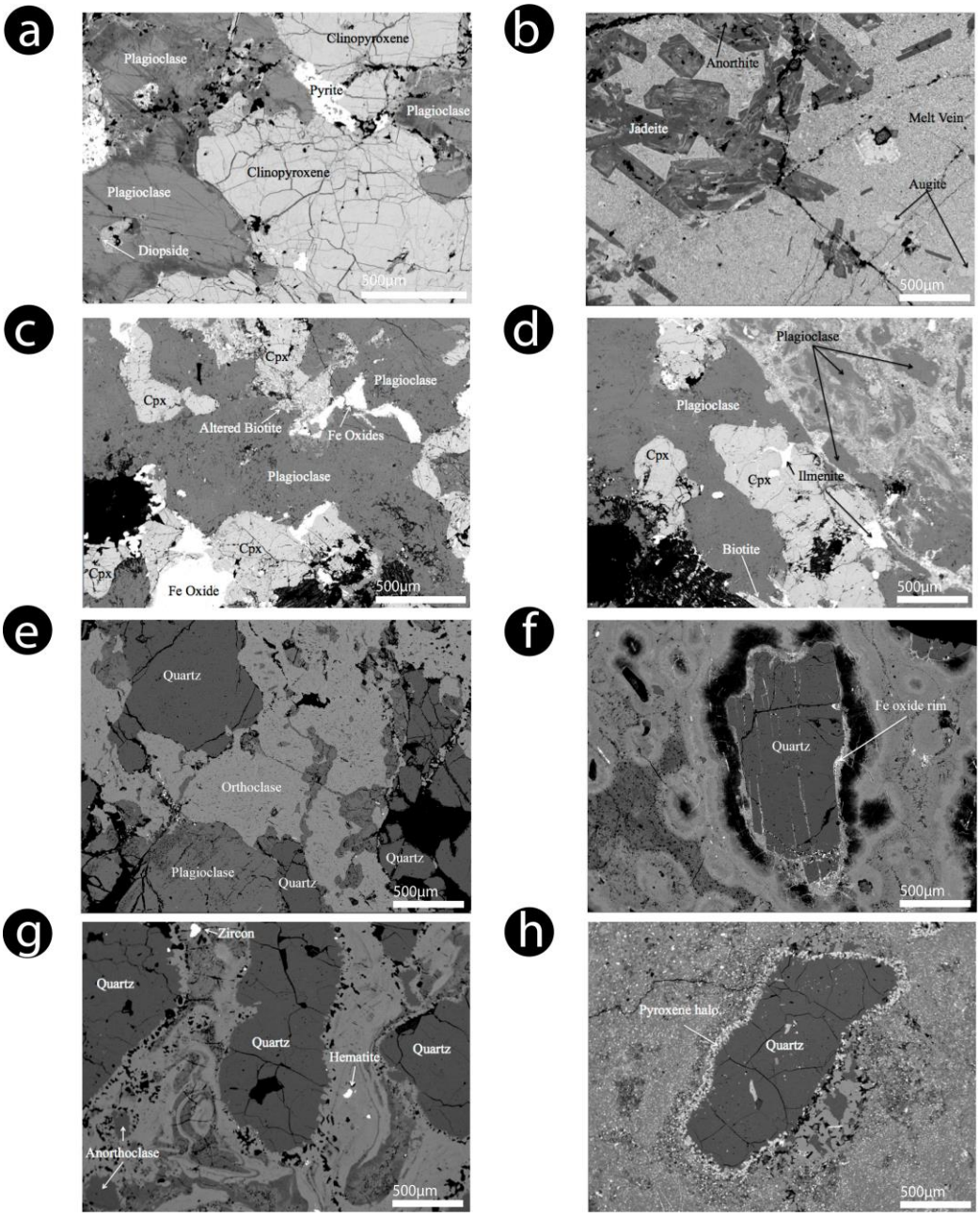

Figure 2.7: Backscattered SEM images of the surface sample host rocks and melt veins a) Mafic host rock of sample AR-019 and b) plagioclase dominated melt vein with various pyroxene clasts. c) Mafic host rock of sample AR-016 and d) contact between the host rock and the melt vein. e) Felsic host rock of sample AR-069 and f) a large quartz clast within the melt vein. g) Felsic host rock of sample RW-013 with a partially melted groundmass and h) the fine-grained feldspathic melt vein with a large quartz clast and pyroxene rim.

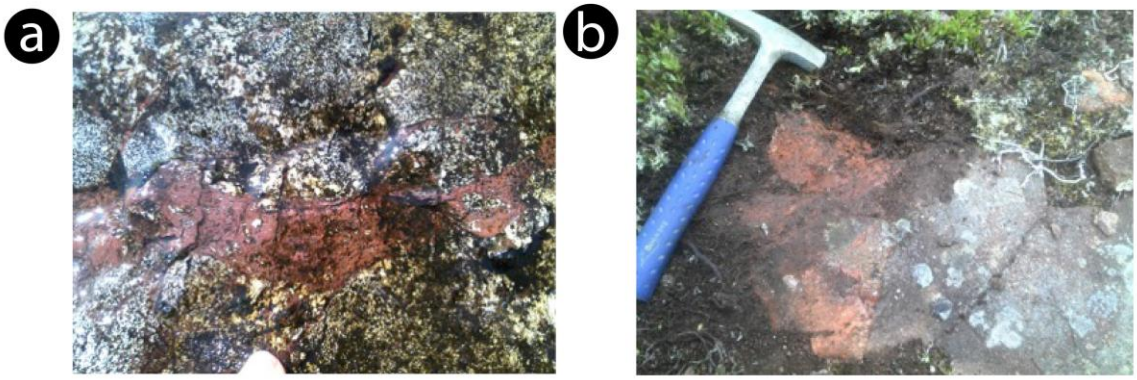

Figure 2.8: Field photos of surface samples. a) Sample AR-016 melt vein from central islands, finger for scale b) Sample RW-013 melt vein (red on left side) and basement rock (right) contact from Ile Lepage 13” rock hammer for scale.

2.3.4 Mixing Models

The samples used in this study were divided into a total of 5 end members based on their rock classifications; felsic rocks, intermediate rocks, mafic rocks with a sub category of diabase, and impact melt rock. For the surface samples all end members were used over the course of the mixing models; however, the drill core only used felsic, mafic and impact melt as realistic end members as diabase and was not observed proximal to the samples in either of the two cores. The melt vein samples can be divided based on location: 2 are from Ile Lepage, 2 are from the central islands and 3 are from the drill core. The Ile Lepage melt veins have a felsic host rock; the central island melt veins host rock consists of more mafic material as both are gabbroic in composition; and the drill core samples have both felsic and mafic hosts. It is expected, based on the total alkali to silica melt vein classification, that the Ile Lepage samples will more likely incorporate an impact melt component as these veins plotted close to the impact melt rock samples; whereas the central island samples and the drill core samplesdid not.

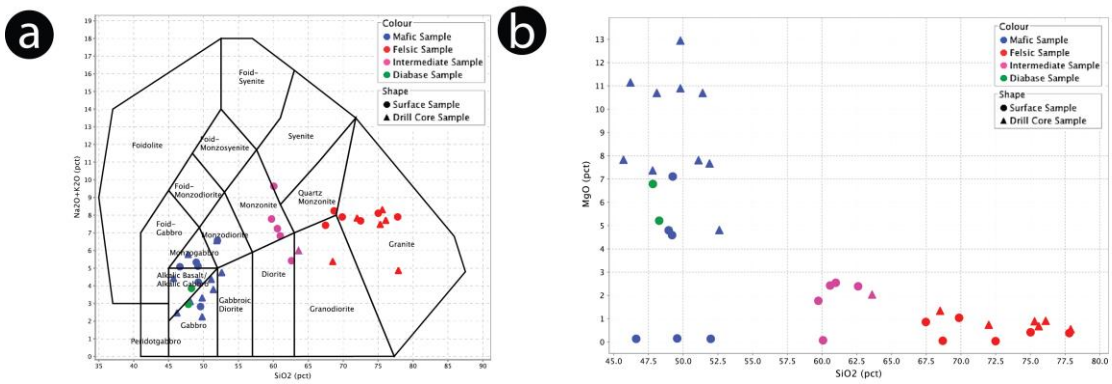

Figure 2.9: Rock classifications of target rocks a) A TAS plutonic diagram (Middlemost, 1994) b) SiO2-MgO Harker diagram.

2.3.4.1 Surface Samples

End member compositions were averaged using the surface sample suite, which were classified based on their total alkali to silica content (Figure 2.9a). Samples were selected primarily based on how unaltered they appeared, as many basement samples were highly altered or contained veining. A representative suite from different localities was also desired but difficult to achieve given the sparse basement outcrops on some islands. Of the felsic samples collected a total of 6 samples were used for the felsic end member, the majority consisted of granites with one sample of granodiorite. The mafic end member value was averaged from 6 samples which plotted as alkali gabbro, gabbro, monzogabbro and monzodiorite. Two diabase samples were averaged to represent the diabase component of the structure. A similar division of target rock end members was evident when plotted on a SiO_2-MgO harker diagram (Figure 2.9b).

Central Island Samples:

The central islands melt vein samples were both shown to be best modelled using a mixture of target rocks and their respective host rocks. Neither sample required a contribution from the impact melt average. In some cases particular samples with more

specific bulk chemistry were used instead of, or in addition to, the averages for each lithology member. Notably, a mafic sample was separated out and used as an end member for the central island sample models as it was determined to be a better representation of the surrounding mafic outcrops than the average. This sample was collected on one of the central islands proximal to the vein samples and represents an accurate mafic end member. A felsic end member was deemed as being unrealistic for the central island vein samples due to no felsic outcrops being observed proximal to the veins and their exceptionally low silica content of ~47%.

AR-016 was best modelled using 88.9% of the mafic target rock collected from the central islands and 11.1% of its host rock. No contribution from the melt or mafic average was needed. The model produced an acceptable p-value of 0.43 and a chi-squared value of 20.45. Figure 2.10b shows the modelled vein closely following the REE spider plot of the measured vein. The elements of interest used to model the vein included rare earth elements and immobile elements; however, some oxides and elements that were causing high chi-squared values were removed from the set. These included La, Ce and Nd, Sc, Co, Zr, TiO_2, MgO and Fe_2O_3. It is hypothesized that alteration may be playing a role in why these elements contributed high chi-squared values; perhaps these elements can not be modelled as well because an alteration component within the vein is not represented in the end members.

AR-019 was best modelled using 66% of the mafic host rock collected from the central islands and 33% of the host rock in contact with the melt vein, there was minimal (less than 1%) contributions from either the impact melt rock average or the mafic average. The model exceeds the p-value threshold of 0.05 with an observed p-value of 0.09 and a chi-squared value of 27.46. The modelled vein did not fit quite as well as AR-016, which is evident in Figure 2.10d. The set used to model the measured vein included rare earth elements and immobile elements with elements contributing large chi-squared values being removed, these were Sc, Co, Zr, Rb, Nd, La, Ce, MnO and CaO.

Lepage Island Samples:

AR-069 was best modelled using 64.3% impact melt average, 34.7% diabase, and needed minimal to no contributions from the granitic host rock and melt sample. The model is a good fit as the observed p-value exceeds the threshold at 0.64 and the chi-squared value is 18.15. A secondary melt sample was included as an end member since it was within the vicinity of AR-069 and had a strikingly different silica value when compared to the impact melt average. The most obvious take away from these spider diagrams is the positive Eu anomaly in the granitic host rock (Figure 2.10e); this anomaly is also observed in the other felsic samples. These felsic rocks likely formed in a reducing magma, which allowed for Eu to be preferentially incorporated into plagioclase as its divalent form Eu^{2+} can substitute for Ca^{2+} (Weill and Drake, 1973). The set used to model the vein included rare earth elements and immobile elements with elements contributing large chi-squared values being removed, these were Zn, Sc, Co, Zr, Y, Th, Nd, Nb, Pr, Rb, Sm, La, Gd, Cs, Ce.

RW-013 was best modelled using 88.5% melt average and 11.6% of the felsic host rock with no contribution from the diorite or diabase target rocks. Of the surface models this is the best fit with an observed p-value of 0.99 and chi-squared value of 4.61 and the modelled vein plots almost identically to the measured vein (Figure 2.10h). This model did not require removal of elements due to high chi-squared values.

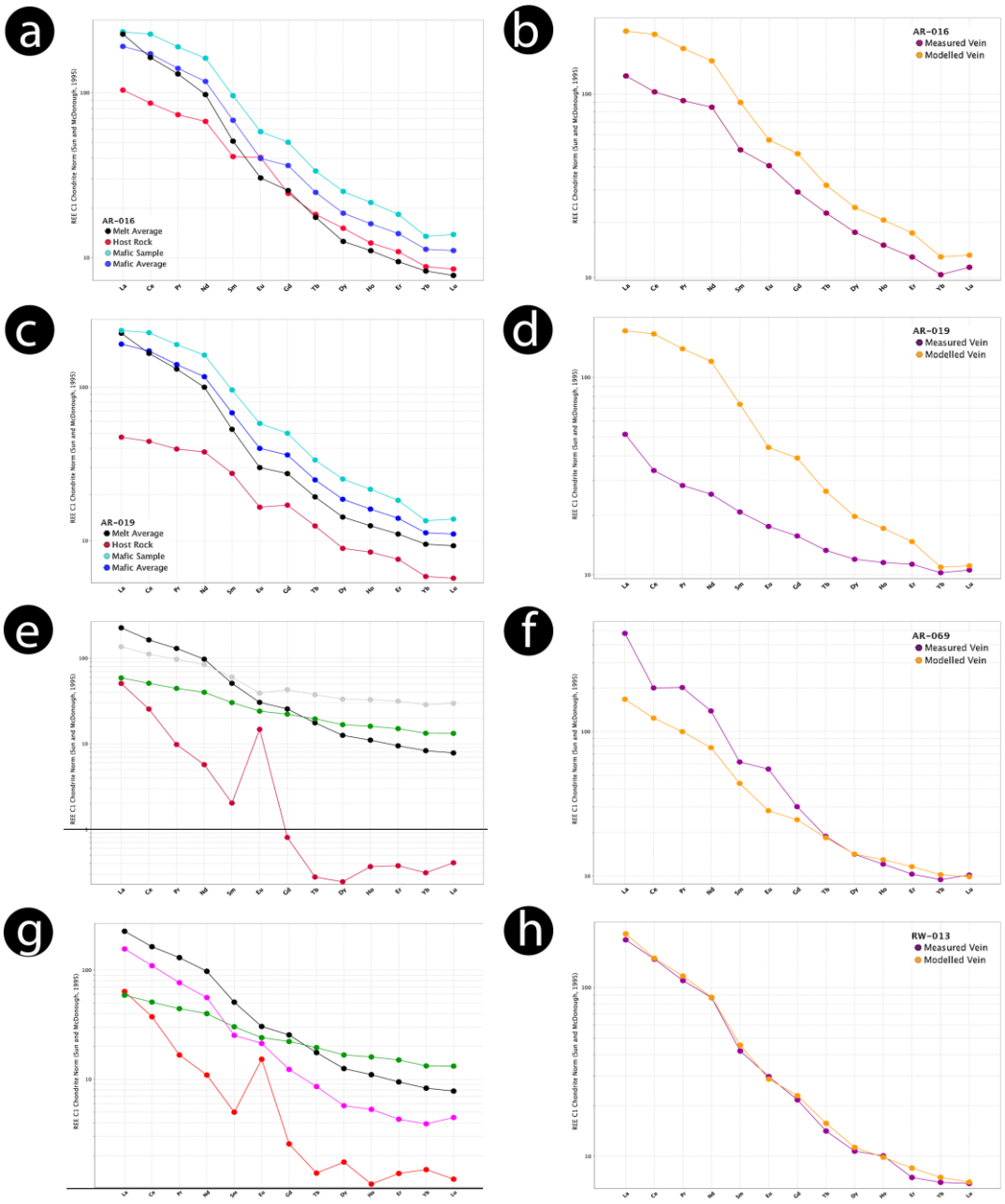

Figure 2.10: Rare earth element chondrite normalized spider diagrams (Sun and McDonough, 1989) of mixing model results for surface samples a) End members used for AR-016 b) Comparison of the modelled vein and the measured vein of AR-016. c) End members used for AR-019 d) Comparison of the modelled vein and the measured vein of AR-019. e) End members used for AR-069 f) Comparison of the modelled vein and the measured vein of AR-069. g) End members used for RW-013 h) Comparison of the modelled vein and the measured vein of RW-013.

2.3.4.2 Drill Core Samples

The end members used to model the core melt vein samples were restricted to the impact melt average and the dominant lithologies proximal to the veins. In both cores 1-63 and 5-63 these lithologies alternated between felsic and mafic composition (Figure 2.9); specifically amphibolite, tonalite and CGG (Figure 2.5). A total of 10 samples of target rock were used for the end members, 5 mafic and 5 felsic. These target rock samples were averaged for each respective core and acted as end members along with the impact melt average and the specific host rock of the sample. Two of the melt veins occurred in a shear zone between two different lithologies, in these cases both of the two host rock lithologies were used as end members along with the impact melt average.

Sample 5-670 had a melt vein with a strikingly similar chemistry to its felsic host. This is likely caused by sampling error as separating the melt vein from host rock can be a difficult process, it is possible that a notable portion of host was included in the melt vein sample or vice versa. When the granitic host was used as an end member results were limited to a 100% contribution from it, which was deemed unrealistic and likely caused by sample contamination. In the case of this sample, the felsic host rock end member was replaced by felsic target rock sample 5-440 which was of the same lithology and is within the same core; however, is not quite as similar chemically to avoid the 100% felsic contribution obtained when using the felsic host rock as an end member.

Three of the four drill core samples were successfully modelled: 1-645, 5-670, and 5-440, all of which were best modelled using target rocks with little to no contribution necessary from the impact melt average. Sample 1-533.4 had too low a silica value to be modelled; with a silica value of 44.9% it is the lowest silica value observed in this study and, therefore, due to the mixing model constraint on the silica content (Eq. 2) this sample could not be modelled using end members of higher silica values.

1-645 was best modelled using 89.3% of the mafic average from drill core 1-63, 6.7% of the host rock and less than 5% contribution from the impact melt rock. This model is a good fit which is evident in the spider diagram (Figure 2.11b), as it exceeds the threshold

value of 0.05 with an observed p-value of 0.99 and a chi-squared value of 3.01 The set used to model the vein included REE and immobile elements but removed Th and Nb.

The sample 5-440 was best modelled using 76.3% mafic host rock and 23.7% felsic host rock with no contribution needed from the impact melt average. This model is a good fit as the observed p-value is 0.54 and chi-squared value of 22.72 (Figure 2.11d). This model did not require removal of elements due to high chi-squared values.

Sample 5-670 was best modelled using 83.6% felsic host rock and 16.4% mafic host rock with no contribution from the impact melt average. The model provides an observed p-value of 0.95 and chi-squared value of 10.20. The set used to model this vein included rare earth elements and immobile elements. The high contribution from the felsic rock can be expected as the measured vein has the same positive Eu anomaly as the felsic host rock (Figure 2.11e and Figure 2.11f).

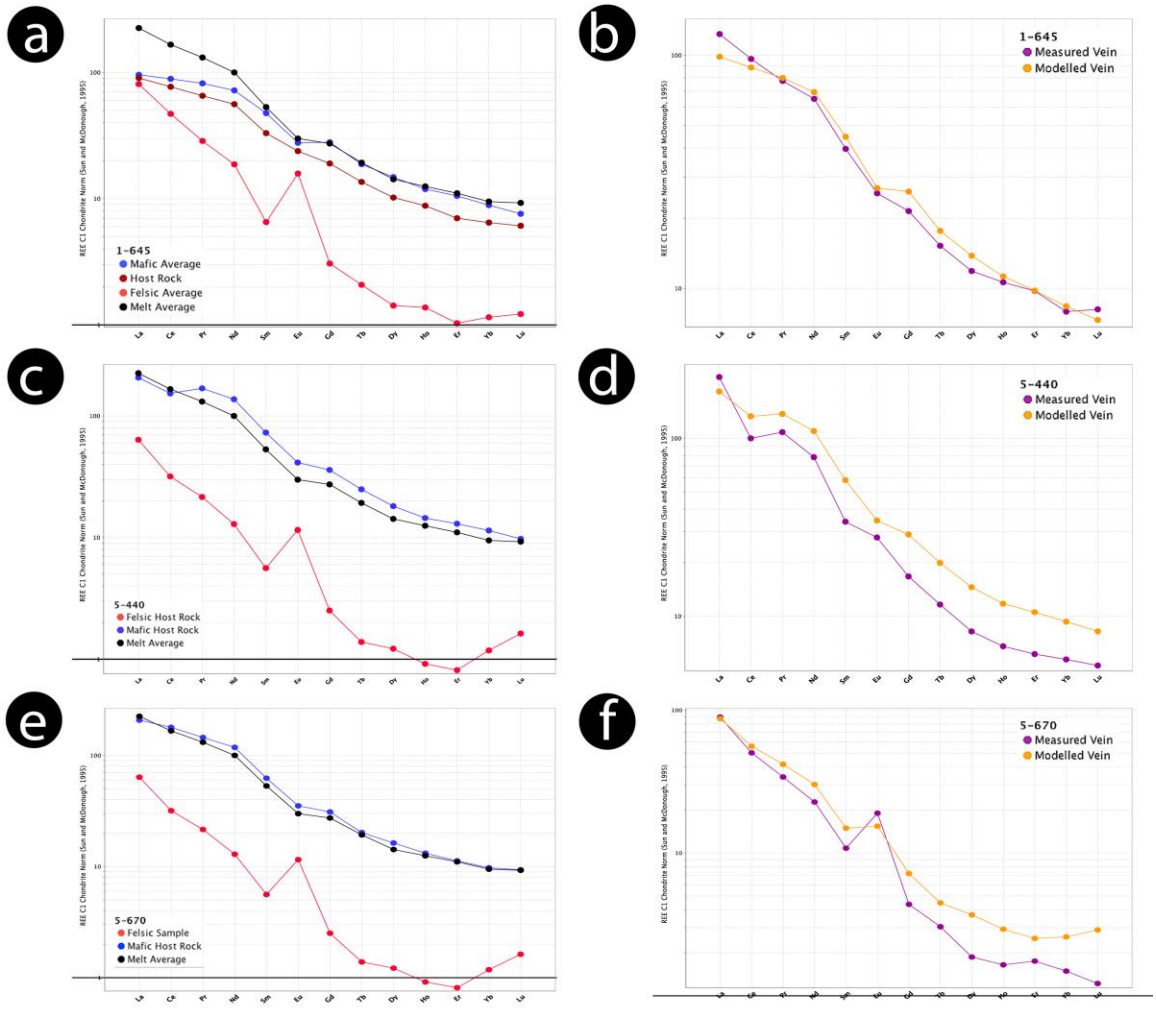

Figure 2.11: Rare earth element chondrite normalized spider diagrams (Sun and McDonough, 1989) of mixing model results for drill core samples a) End members used for modelling 1-645 b) Comparison of the modelled vein and the measured vein of 1-645 c) End members used for modelling 5-440 d) Comparison of the modelled vein and the measured vein of 5-440. e) End members used for modelling 5-670 f) Comparison of the modelled vein and the measured vein of 5-670.

2.4 Discussion and Conclusions

Melt veins have been observed by previous researchers at the West Clearwater Lake Impact Structure; primarily within the target rocks of the drill core and central islands but also cutting through the fragmental breccia (Dence, 1965; Simonds et al., 1978). These previous workers suggested that the veins observed in the drill core and on the central

islands were formed *in situ* by frictional melting, similar to the pseudotachylite detected in crater floors and central uplifts of other impact structures, including Manicougan (Dressler, 1970), Vredefort (Dietz, 1961), Sudbury (Dietz, 1964) and Ries (Dressler and Graup, 1969). However, these conclusions were based solely on textural similarities with pseudotachylite formed in endogenic faults zones. Until now, no geochemistry has been done on these veins and no study has incorporated melt veins within basement outcrops that are not observed at depth or from the central islands but instead collected from the ring of islands. We have conducted a geochemical and petrographic analysis of melt veins within target rock from the West Clearwater Lake Impact Structure in order to determine their formation processes, which in turn can aid in understanding how central uplifts are formed.

2.4.1 *In situ* Melt Veins

Mixing models for the drill core and central islands samples demonstrate that they are derived solely from local target rock lithologies and require no impact melt component in their modelled compositions (Figure 2.10 and Figure 2.11). These samples are, therefore, interpreted to have formed *in situ* and to represent pseudotachylite *sensustricto*.

Of the 4 drill core melt veins, only 3 were modelled successfully dueto mixing model restrictions on low silica content. There are two potential explanations for the silica value being lower than all potential end member silica values. First, there may be a missing component in the end member suite; this is an unlikely possibility as all lithologies observed have been sampled and used in this study, unless some degree of unknown alteration has occurred. The second potential explanation is the tendency for more mafic minerals to melt preferentially (Spray, 2010), therefore leaving the remnant melt vein with a deficit in silica when compared to its host rock.

Petrographic analysis of these veins suggests that some degree of transport occurred within the vein structures. Element maps (Appendix D) of drill core samples 1-533.4 and 5-670 show evidence of zoning between flow-banded textures within the melt veins. Sample 1-533.4 has three discrete sections of banded flow: a clast-rich flow closest to the wall, a glassy flow texture a little further from the wall and a very clast rich flow in the

middle of the vein. All sections of the vein appear different compositionally in the element maps (Appendix D), which may be due to preferential melting of some mineral clasts over others (Spray, 2010). This compositional zoning is again evident in core sample 5-670 which exhibits a finer grained Fe rich flow margin closest to the wall and a clast-rich flow texture further from the wall (Appendix D). Both these samples show elemental differences between the vein and host rock, which in conjunction with the heterogeneous composition of the melt vein may be indicative of some degree of transport to allow for banding and clast sorting. There may be some *ex-situ*melt within the pseudotachylite from other depths but not to such a degree that the models required a contribution from a lithology not proximal to the melt vein. Riller et al. (2010) argues that this is the case for the Sudbury breccia, which is on a much larger scale than observed here. It is possible, therefore, that *ex-situ*material is incorporated here, but on a smaller scale (i.e., transport from tens of metres rather than km).

An element map of sample 5-440 (Figure 2.12) shows clear evidence for melting of host rock and incorporation into the melt vein; whereas maps of samples 1-533.4 and 5-670 did not show any clear incorporation of host rock into the vein (Appendix D). A zone of high Mg content occurs in 5-440 for up to 400μm from the mafic wall rock before drastically dropping off when contacting a flow of Fe rich melt. The simplest interpretation is that this is due to incorporation of Mg from the chlorite veins in the mafic host rock. However, as this elevated Mg contentis only evident proximal to the wall this incorporation may be due to the vein flow melting the wall rock rather than a dominant *in situ* melting of the mafic host rock. This may have a large effect on the mixing model results, as a preferential incorporation of the Mg rich chlorite vein from the mafic host would likely have an influence on the high contribution from mafic lithology in comparison to the felsic, as was the case for this sample.

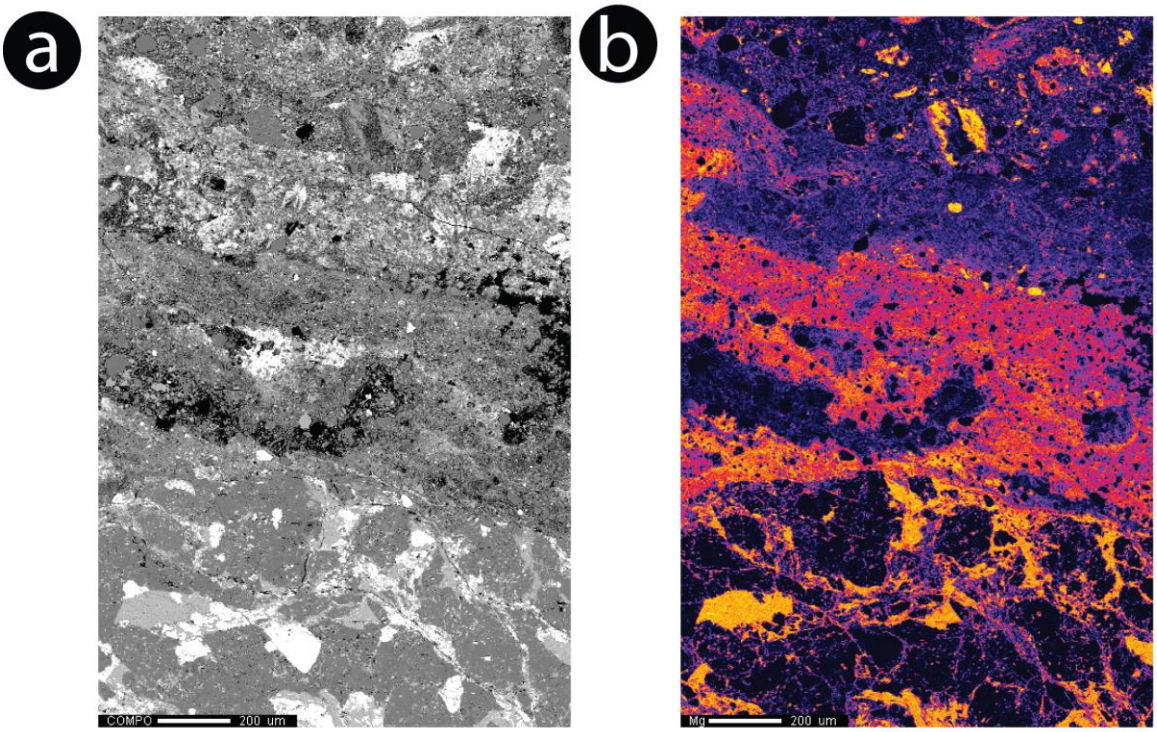

Figure 2.12: Element mapof sample 5-440: A) SEM backscatter electron image of sample spot B) Mg map where high concentrations appear magenta to yellow and low concentrations appear purple to black.

Petrography results of the drill core and central island melt veins show an array of contact types, none of which are diagnostic of a formation origin. Indeed, melt veins formed *in situ* exhibited both clean shear contacts and heavily embayed and brecciated contacts with their host rock (Figure 2.6). Only one sample, AR-016, exhibited clear evidence of minerals from the wall rock being rotated and incorporated into the vein, which in itself could be indicative of injected melt picking off wall rock, or of *in situ* melting of the wall, this can also be a mixture of both processes occurring simultaneously (Figure 2.7d). However, the thinnest veins, particularly from the drill core, only exhibited very straight margins with the host rock. It is suggest that this could be due to the widening of veins and subsequently higher frequency of larger clast there is an increased likelihood of impacting the wall rock and therefore more incorporation of grains along the wall resulting in a jagged contact. Thus, despite textures appearing to be more indicative of

one melt vein formation process over the other, the only way to be sure of melt vein origin is to use bulk chemical data to model melt vein composition.

An outstanding question surrounding the origin of pseudotachylite within impact craters is how to generate large volumes of melt with little apparent displacement? We observed evidence for displacement across some melt veins at shear zones in the drill core (Figure 2.5) but no evidence for large scale displacement to the degree of Spray and Thomson's (1995) pseudotachylite-rich zone theory of large scale displacement. The displacement seen in The West Clearwater Lake Impact Structure core is more similar to the displacement observed at the Vredefort dome where most cases of pseudotachylite breccia showed no sign of significant displacement; this minimal displacement was interpreted to potentially reflect a reactivation of melt lubricated shock induced fabric network during crater collapse (Lana et al. 2003).

Although melt veins are observed between different lithologies this cannot necessarily be attributed to displacement as it has been shown that pseudotachylite can form along pre-existing lithological boundaries without necessary displacement (Lana et al. 2003). It is also important to note that veining does not always separate contacts between different lithologies within the drill core. It is possible that *in-situ* melt veins formed by shock compression along pre existing heterogeneities within the rock and did not necessarily need a frictional melt component (Gibson and Reimold, 2003).

2.4.2 Injected Melt Veins

The Ile Lepage samples were shown to require a significant contribution from the impact melt rock average in their modelled compositions (Figure 2.10). These melt veins are, therefore, interpreted to have formed through injection of melt from the overlying impact melt sheet. Petrographic analysis of the melt veins supports this hypothesis, as we have observed textures within the melt veins that are not associated with pseudotachylite. Specifically, quartz clasts within both the Ile Lepage veins exhibited pyroxene or iron oxide reaction rims (Figure 2.7f and Figure 2.7h). These reaction coronae are common in impact melt sheets (Grieve, 1975; Simonds et al., 1978a; Bischoff and Stöffler, 1984; Kring and Boynton, 1992; Whitehead et al., 2002) but to our knowledge have not been

documented in pseudotachylite.Sample RW-013 also showed a very similar melt texture to that of the fine-grained impact melt (Figure 2.7h).

Based on the petrographic analysis of the host rock of RW-013, which shows a partially melted groundmass, it can be inferred that this relatively large contribution of host rock, in comparison to the other Ile Lepage melt, may be due to the host rock resembling a more similar chemistry to the melt as its ground mass is melted feldspars. Another possible explanation is that the host was in fact incorporated into the melt during injection; this melted groundmass may have been more preferentially eroded and incorporated in comparison to the large quartz grains within the host.

Since basement outcrops were observed at times within tens of metres from exposed impact melt outcrops on Ile Lepage, it is not surprising to see that these injected impact melt veins have a large contribution from the impact melt sheet. It is worth noting that other melt vein samples were retrieved from the central ring islands; however, they were too thin to be examined geochemically. Based on their similarity with the melt veins from the central islands, these thin glassy veinlets are also interpreted to have formed by *in situ* melting. They bear strong resemblance to the pseudotachylite in the drill core and are similar to those described by Dence, (1965). However, one sample retrieved from Ile Atkinson, although too small to be studied geochemically, was found to have very similar textures to that observed in sample AR-069. No reaction rims were observed in this melt vein but the resorbtion of quartz clasts and circular fracturing pattern was evident. Similarly to those from Ile Lepage this Ile Atkinson melt vein was observed proximal to impact melt rock outcrops. It is, therefore hypothesized, that this Ile Atkinson sample was likely formed by injected impact melt. Due to the proximity of impact melt outcrops to the injected melt veins we can not say that there is evidence for large scale transport of this injected material.

2.4.3 Implications for Central Uplift Formation

Anastomosing veins are common in the drill core of the West Clearwater Lake Impact Structure and at times are seen to exhibit cross-cutting relationships, which have also been observed at Vredefort (Mohr-Westheide et al., 2009) and were interpreted to have

formed by shock compression and/or decompression melting (Mohr-Westheide and Reimold, 2011). The large amount of lichen cover on outcrops precludes a determination as to whether similar anastomosing veins occur on the surface. Large scale shear was not observed in the Vredefort dome, therefore, a pervasive pseudotachylitic breccia vein-fracture network was proposed as a mechanism to allow for large scale coherent movement and central uplift formation (Lana et al., 2003). This network would accommodate central uplift formation by allowing small scale shear and rotation along its vein-fractures.

Although the West Clearwater Lake Impact Structure is a much smaller crater than Vredefort, which is estimated to be between 250 and 300 km in diameter, it can be hypothesized that this pervasive network of pseudotachylite veins can act as a mechanism for a large-scale coherent response in the rocks of the crater floor. This would allow for uplift even if only minimal shear was observed in the core. Although it appears that small-scale shear may be occurring we are unable to confirm if this is in fact displacement or if there is simply a preferential melting along pre-existing zones of weakness between different lithologies. We are limited to the core as no *in situ* veins at the surface displayed any displacement.

Overall it would appear that our findings coincide well with the Lana et al., (2003) theory of large-scale coherent response within the crater floor due to a pervasive pseudotachylite network of veins and fractures. This *in situ* melt may have been formed from frictional melting but this is not a necessary origin as it could have also been produced though shock compression melting after shockwave propagation during the compression phase (Martini, 1991; Spray, 1998). No clear evidence for large-scale displacement and megablock rotation was seen within the drill core, although small-scale displacement was observed. Therefore, a more even distribution of displacement may have occurred resulting in smaller slip displacements and rotations, potentially along the network of pseudotachylite melt veins (Lana et al., 2003). If a pre-existing network of fractures existed the shock induced pseudotachylite melt would act to lubricate the fractures and allow for an overall weakening of the crater floor's bulk strength, therefore accommodating the necessary slip and rotation for central uplift formation. Without

mapping of the crater floor structure it is not possible to say with certainty that there is no large displacement or occurrence of megablocks, but given the limited information from the existing drill core, as there is also limited exposure of basement in the central uplift at the surface, it appears a pseudotachylite lubricated fracture network can be the driving force behind central uplift formation at the West Clearwater Lake Impact Structure.

As noted above, the Ile Lepage melt veins require a significant impact melt rock component in the modelling of their compositions and can be interpreted to be impact melt dykes. Interpreting the injected melt dykes as having a potential influence on central uplift formation is not as easy, as there are fewer instances of them observed due to the low frequency of basement outcrops compared to melt outcrops on the ring of islands. The formation of these dykes may have occurred during the production of the breccia and melt units, specifically the layering of a clast-rich basal unit overlain by a clast poor melt, as this process is associated with a highly energetic melt (Grieve, 2006). This process is explained by Grieve (2006) who states that the leading edge of a melt sheet is driven downwards at high velocities into the transient cavity and when this occurs the melt picks up pieces of debris from the cavity walls and floor which results in it gradually increasing its viscosity. The now more viscous debris-rich impact melt is over ridden by the less viscous impact melt sheet behind it. In some places within the West Clearwater Lake Impact Structure the breccia unit is removed, likely having been swept away by this active outflowing impact melt (Grieve, 2006). In these cases, the impact melt sheet rests directly on basement, therefore, if impact induced or pre-existing fractures exist there is a strong likelihood that the overlying melt sheet would form melt dykes within the basement materials. This could also explain the formation of the dyke observed by Simonds et al., (1978) in the fragmental breccia.

2.4.4 Conclusions

We have been able to show that melt veins observed at the West Clearwater Lake Impact Structure are formed by both *in situ* melting and injected melt. By using a geochemical mixing model to determine the contributions of target rock and impact melt rock to the veins we were able to discern a clear spatial pattern to the formation processes of the melt veins. The samples collected from the central islands and at depth from the core do not

require any impact melt component; whereas the island ring samples predominately require an impact melt component. Petrographic analysis of the melt veins supports the mixing model findings, as injected melt veins displayed features and textures that have not been observed in pseudotachylite and are similar to that of the impact melt rock. *In situ* melt veins display zoning, flow banding and clast sorting which can be interpreted to represent a relatively small degree of transport within the vein. The high frequency of pseudotachylite observed in the core may potentially represent a pervasive network of veining and fracturing, which can allow for a large-scale coherent uplift of the crater floor. Support for both processes of injected melt and *in situ* melting is evident; however, pseudotachylite appears to have a larger potential influence on central uplift formation than injected melt dykes. Occurrences of the two vein types seem to be spatially dependent such that injected melt veins form within basement lithologies that are proximal to the impact melt sheet whereas *in situ* melting occurs relatively deeper in the structure, in the interior of the central uplift and at depth within the drill core.

Melt has been hypothesized to have a significant role in the process of central uplift formation (Senft and Stewart, 2009; Spray and Thompson, 1995; Lana et al. 2003). By understanding the formation processes of the melt veins observed at the West Clearwater Lake Impact Structure we have determined which mechanisms supported by melt production may have aided in the central uplift process. Establishing the relative proportions of target rock and impact melt to the suite of melt veins has allowed us to determine their formation processes. The mixing model results show evidence for both *in situ* and injected melt models, therefore supporting the argument for both pseudotachylite veins as well as allochthonous melt veins. While not disproving the importance of acoustic fluidization, this study does show that melt is important in supporting mechanisms that can weaken the crater floor and accommodate central uplift formation.

2.5 References

Bischoff A, and StöfflerD. 1984. Chemical and structural changes induced by thermal annealing of shocked feldspar inclusions in impact melt rocks from Lappajarvi crater, Finland. J Geophys. Res. 89 (Suppl):B645-B656.

Bostock H. H. 1969. The Clearwater Complex, New Quebec. Geological Survey of

Canada 178:63p.

Bunch T. E. 1968. Some characteristics of selected minerals from craters. In Shock metamorphism of natural materials, edited by French B.M. and Short N.M. Baltimore: Mono Book Corp. pp. 413-432.

Dence M. R. 1964. A comparative structural and petrographic study of probable Canadian meteorite craters. Meteoritics 2:249-269.

Dence M. R. 1965.The extraterrestrial origin of Canadian craters. Annals New York Academy of Science 123:941-969.

Dietz R. S. 1961. Vredefort Ring structure: Meteorite impact scar? The Journal of Geology 69:499-516.

Dietz R. S. 1964. Sudbury Structure as an astrobleme. The Journal of Geology 72:412-434.

Dressler B. and Graup G. 1969. Pseudotachylite aus dem Nördlinger Ries. Geologica Bavarica 60:170-171.

Dressler B. O. 1970. Die Beanspruchung der prakambrischenGesteine in der Kryptoexplosionsstruktur von Manicouagan in der Provinz Quebec, Canada. Ph. D. dissertation, University of Munich, Germany.

Ferriere L., Koeberl C., and Reimold W.U. 2009. Characterisation of ballen quartz and cristobalite in impact breccias: New observations and constraints on ballen formation. Eur. J. Mineral 21:203-217.

Gibson R. L, and Reimold W.U. 2003. Thermal and Dynamic Consequences of Impact: Lessons from large impact structures. Impact cratering: Bridging the gap between modelling and observations 1: 22-23.

Grieve R. A. F. 1975. Petrology and chemistry of the impact melt at Mistastin Lake crater, Labrador. Geological Society of America Bulletin 86(12):1617-1629.

Grieve R. A. F. and Therriault A. 2004. Observations at terrestrial impact structures: Their utility in constraining crater formation. Meteoritics & Planetary Science 39:199-216.

Grieve R. A. F. 2006. Impact Structures in Canada.GEOtext 5, Geological Association of Canada: 210 p.

Hische R., 1995. Geologie des Clearwater Impakstruktur / Quebec. Ph. D. thesis, WestfälichenWilhemsUniversität, Münster, Germany.

Krank S. H. and Sinclair G. W.1963. Clearwater Lake, New Quebec. Geological Survey of Canada 100:25p.

Kring D. A. and Andboynton W V. 1992. Petrogenesis of an Augite bearing melt rock in the Chicxulub structure and its relationship to K/T impact spherules in Haiti. Nature 258:141-144.

Lana C., Gibson R. L., and Reimold W. U. 2003. Impact tectonics in the core of the Vredefort dome, South Africa: Implications for central uplift formation in very large impact structures. Meteoritics & Planetary Science38:1093-1107.

Le Maitre, R. W., 1989. A Classification of Igneous Rocks and Glossary of Terms. Recommendations of the IUGS Commission on the Systematics of Igneous Rocks. Oxford: Blackwell 256 p.

Martini J. E. J. 1991. The nature, distribution and genesis of the coesite and stishovite associated with the pseudotachylite of the Vredefort Dome, South Africa. Earth and Planetary Science Letters103(1-4):285-300.

McIntyre D.B. 1968. Impact metamorphism at Clearwater Lake, Quebec. In Shock metamorphism of natural materials, edited by French B.M. and Short N.M. Baltimore: Mono Book Corp. pp. 363-366.

Melosh H. J. 1989. Impact Cratering: A Geologic Process. Oxford University Press, 245 p.

Middlemost E.A.K., 1994. Naming materials in the magma/igneous rock system; Earth-Science Reviews 37: 215-224.

Mohr-Westheide T., Reimold W. U., Riller U., and Gibson R. L. 2009. Pseudotachylitic breccia and microfracture networks in Archean gneiss of the central uplift of the Vredefort Impact Structure, South Africa. South African Journal of Geology112(1):1-22.

Mohr- Westheide T., and Reimold W. U. 2011. Formation of pseudotachylitic breccias in the central uplifts of very large impact structures: Scaling the melt formation. Meteoritics & Planetary Science46(4):543-555.

O'Callaghan J.W., Osinski G.R., Lightfoot P.C., Linnen R.L., and Weirich J.R. 2016. Reconstructing the geochemical signature of sudbury breccia, Ontario, Canada: Implications for its formation and trace metal content: Economic Geology (Forthcoming).

Osinski G. R., Brunner A., Collins G., Cohen B. A., Coulter A., Elphic R., Grieve R. A.

F., Heldmann J. L., Hodges K., Horne A., Kerrigan M., Lim D. S. S., Misener R., Morgan J. V., Rae A. S. P., Saint-Jacques D., Skok J. R., Squyres S., Tornabene L. L., Wilks R., and Young, K. 2015. Revisiting the West Clearwater Lake Impact Structure, Canada (abstract #1621) 46th Lunar and Planetary Science Conference.

Phinney W. C., Simonds C. H., Cochran A., and McGee P. 1978. West Clearwater, Quebec, Impact Structure, part II: Petrology Proc. 9th Lunar and Planetary Science Conference: pp. 2659-2693.

Rae A. S. P, Collins G. S., Grieve R. A. F., Osinski G. R., Morgan J. V. 2016. Complex crater formation: Insights from combining observations of shock pressure distribution with numerical models at the West Clearwater Lake Impact Structure. Meteoritics & Planetary Science (forthcoming).

Reimold W. U. 1995. Pseudotachylite in impact structures—generation by friction melting and shock brecciation?: A review and discussion. Earth-Science Reviews 39(3):247-265.

Riller U., Lieger D., Gibson R. L., Grieve R. A., and Stöffler D. 2010. Origin of large-volume pseudotachylite in terrestrial impact structures. Geology38(7):619-622.

Robertson P. B., Dence M. R. and Vos M. A. 1968. Deformation in rock-forming minerals from Canadian craters. In Shock metamorphism of natural materials, edited by French B.M. and Short N.M. Baltimore: Mono Book Corp: pp. 433-452.

Schmieder M., Schwarz W. H., Trieloff M., Tohver E., Buchner E., Hopp J., and Osinski G. R. 2015. New 40 Ar/39 Ar dating of the Clearwater Lake impact structures (Québec, Canada)–Not the binary asteroid impact it seems?. Geochimicaet Cosmochimica Acta 148:304-324.

Senft L. E., and Stewart S. T. 2009. Dynamic fault weakening and the formation of large impact craters. Earth and Planetary Science Letters 287:471-482.

Simonds C. H., Phinney W. C., McGee P. and Cochran A. 1978. West Clearwater, Quebec, Impact Structure, part I: Field geology, structure and bulk chemistry. Proc. 9th Lunar and Planetary Science Conference: 2633-2658.

Simonds C. H., Floran R. J., Mcgee P. E., Phinney W. C. and Warner J. L. 1978. Petrogenesis of melt rocks, Manicouagan impact structure, Quebec. J Geophys. Res. 83:2773-2788.

Spray J. G., and Thompson L. M. 1995.Friction melt distribution in a multi-ring impact basin. Nature 373:130-132.

Spray, J. G. 1998. Localized shock-and friction-induced melting in response to

hypervelocity impact. Geological Society, London, Special Publications140(1):195-204.

Spray J. G. 2010. Frictional melting processes in planetary materials: From hypervelocity impact to earthquakes. Annual Review of Earth and Planetary Sciences38:221-254.

Weill D. F. and Drake M. J. 1973. Europium anomaly in plagioclase feldspar: experimental results and semiquantitative model. Science80(4090):1059-1060.

Weirich J. R., Osinski G. R., Pentek A., Bailey J.,O'Callaghan J and Grieve R. A. F. 2016.Trace element geochemistry and texture of Sudbury breccia in the North Range of the Sudbury impact structure, Canada.Meteoritics& Planetary Science (forthcoming).

Whitehead J., Grieve R. A. F., and Spray, J. G. 2002. Mineralogy and petrology of melt rocks from the Popigai impact structure, Siberia. Meteoritics & Planetary Science 37(5):623-647.

Chapter 3

3 Conclusions and Future Work

3.1 Summary

Central uplift formation remains one of the most enigmatic processes of crater formation. Although it is generally accepted that a weakening mechanism is a necessary precursor to uplift, whether this mechanism is dynamic fault weakening, melt lubricated blocks or acoustic fluidization is undetermined. Multiple researchers have hypothesized that *in situ* melt may play a large role in enabling the weakening of the crater floor in order for subsequent uplift to occur. These theories for crater collapse require the role of *in situ* melting; whether it be in the form of pseudotachylite rich zones allowing for large displacement (Spray and Thompson, 1995), pseudotachylitic breccia along a network of vein fractures accommodating shear and rotation (Lana et al., 2003), or frictional melt within fault zones acting to reduce the bulk strength of overlying rock (Senft and Stewart, 2009).

We have successfully modelled melt vein compositions using melt and target rock end members to determine the origin processes of the melt veins collected at the West Clearwater Lake Impact Structure. The results can provide insight into what role melt may have had on central uplift formation at the West Clearwater Lake Impact Structure and what may have been the most likely mechanism for weakening, our major results and conclusions are:

- Melt vein formation processes appear to be heavily influenced by their location within the structure. The mixing model results show that melt veins sampled from the interior of the central uplift and at depth in the crater floor are formed *in situ;* whereas veins from the ring of islands ,which are more proximal to the impact melt sheet,are formed through the injection of impact melt. Although thin veinlets interpreted to be pseudotachylite are observed on the island rings we are unable to

include them in the bulk chemical and mixing model study due to insufficient material and exposure.

- Melt veins collected from the central islands and at depth in the drill core did not require an impact melt component in their modelled geochemical signature and instead were successfully modelled using only target rock lithologies as end members. They are, therefore, interpreted to have been formed*in situ*. These veins display element zoning, clast sorting and flow banding which are interpreted to display some degree of in vein melt transport but given the mixing model results this transport is not interpreted to represent large scale transport of injected melt from the impact melt sheet.

- Melt veins collected from the ring of islands required an impact melt component in order to successfully model their geochemical signature and are therefore interpreted to have been formed by injected melt. Petrographic analysis supports the result that these veins are injected melt dykes as they show textures and features that have not been observed in pseudotachylite and instead are very similar to the impact melt sheet.

- Formation of the injected melt dykes may have occurred during the layering of a clast rich basal unit below a clast poor melt, as this appears to have been the result of a particularly high energy melt at the West Clearwater Lake Impact Structure (Grieve, 2006). In cases where the clast rich unit is removed, the impact melt sits directly above basement, if this basement had pre-existing fractures it is likely that the impact melt will have form injected melt dykes, similar to the ones observed in this study.

- Petrographic analysis of contact types between the melt veins and host rock proved to be unable to aid in defining their formation process, as both clean sharp contacts and heavily brecciated contacts were observed in both vein types.

- The high frequency of pseudotachylite observed in the core and no sign of significant displacement may potentially represent a pervasive network of veining and fracturing. This network suggested by Lana et al (2003) may have allowed for a large-scale coherent response of the crater floor at the West Clearwater Lake Impact Structure resulting in central uplift formation.

- The pseudotachylite within the crater floor may not have formed through frictional melting, as only small scale displacement is observed, instead a likely origin is that of shock melting during the shock compression stage (Martini, 1991; Spray, 1998) along pre-existing heterogeneities within the rock (Gibson and Reimold, 2003) such as lithological boundaries (Lana et al., 2003). If a pre-existing fracture network existed the pseudotachylite melt would act to lubricate the fractures, allowing for an overall weakening of the crater floor's bulk strength.

- Support for both processes of injected melt and *in situ* melting is evident at West Clearwater; however, pseudotachylite appears to have a larger potential influence on central uplift formation than the injected melt dykes.

3.2 Future Work

Some outstanding questions remain, as the sample suite of this study was restricted. We were limited by the number of surfacemelt veins sampled; of the veins retrieved only a small fraction were thickenough to be analysed for bulk chemical data and subsequently used for modelling purposes. Ideally a more expansive study including surface veins from a wider variety of islands would allow for more substantial answers to be reached in regards to the disparity of *in situ* versus injected melt on the central ring of islands. Although melt veins were much more prolific in the drill core, similarly to the surface samples, the drill core melt veins were rarely thick enough to retrieve bulk chemical data which was necessary in order to be modelled successfully.

A better understanding of the common alteration processes which have taken place at the West Clearwater Lake Impact Structure would be advantageous in helping to discriminate between elements of interest in the mixing model. At this time it is unknown why specific elements were providing high chi-squared values and had to be deleted from the elements of interest in order for the model to run successfully. By filling in this gap of knowledge about alteration at the impact structure future work will be able to better justify why some elements needed to be removed from the model.

Due to limited surface exposure of the central uplift we are left to rely heavily on the drill core in order to hypothesize about large-scale displacement and potential megablock movement. The concept of listric fault zones as being likely places to accommodate early stages of floor uplift for large scale displacement (Senft and Stewart, 2009) goes unexamined here due to location of drill cores; it is possible that should an examination of the core from closer to the crater wall take place evidence for dynamic fault weakening by pseudotachylite may be observed. In addition to this, structural mapping of the crater floor would be helpful in allowing us to better apply what we know about pseudotachylite in the drill core to the mechanisms of large-scale movement and subsequent central uplift formation.

3.3 References

Gibson R. L, and Reimold W.U. 2003. Thermal and Dynamic Consequences of Impact: Lessons from large impact structures. Impact cratering: Bridging the gap between modelling and observations 1:22-23.

Grieve R. A. F. 2006. Impact Structures in Canada.GEOtext 5, Geological Association of Canada: 210 p.

Lana C., Gibson R. L., and Reimold W. U. 2003. Impact tectonics in the core of the Vredefort dome, South Africa: Implications for central uplift formation in very large impact structures. Meteoritics & Planetary Science38:1093-1107.

Senft L. E., and Stewart S. T. 2009. Dynamic fault weakening and the formation of large impact craters. Earth and Planetary Science Letters 287:471-482.

Spray J. G., and Thompson L. M. 1995.Friction melt distribution in a multi-ring impact basin. Nature 373:130-132.

Appendices

Appendix A: Locations of surface samples.

Table A.1 - Sample list with locations and rock type.

Location	Rock Type	Sample Number	Latitiude	Longtitude
Ile Kamiskutanikaw	Melt	MK-033-0	56°14'0.42"N	74°21'3.03"W
Ile Kamiskutanikaw	Melt	MK-033-1	56°14'0.42"N	74°21'3.03"W
Ile Kamiskutanikaw	Melt	MK-033-9	56°14'0.42"N	74°21'3.03"W
Ile Kamiskutanikaw	Melt	MK-033-14	56°14'0.42"N	74°21'3.03"W
Ile Kamiskutanikaw	Melt	MK-033-19	56°14'0.42"N	74°21'3.03"W
Ile Kamiskutanikaw	Melt	AR-036	56°14'0.42"N	74°21'3.03"W
Ile Kamiskutanikaw	Felsic	AR-034	56°13'38.17"N	74°20'58.82"W
Ile Kamiskutanikaw	Mafic	AR-030	56°13'42.24"N	74°21'13.22"W
Ile Lepage	Melt	MK-075	56°15'56.89"N	74°27'21.02"W
Ile Lepage	Melt	MK-076	56°16'1.29"N	74°26'58.49"W
Ile Lepage	Melt	MK-077	56°15'59.40"N	74°26'49.56"W
Ile Lepage	Melt	MK-078	56°16'6.47"N	74°26'44.83"W
Ile Lepage	Melt	MK-079	56°16'8.12"N	74°26'44.88"W
Ile Lepage	Melt	MK-071	56°16'22.13"N	74°25'40.48"W
Ile Lepage	Felsic	AR-045	56°16'41.37"N	74°27'38.61"W
Ile Lepage	Felsic	AR-069-H	56°17'20.66"N	74°29'0.86"W
Ile Lepage	Diabase	BAC-003	56°16'41.03"N	74°27'52.93"W
Ile Lepage	Diabase	AR-074D	56°16'41.84"N	74°29'32.21"W
Ile Lepage	Intermediate	AR-077	56°15'4.40"N	74°25'55.40"W
Ile Lepage	Melt	RW-012	56°17'12.20"N	74°28'58.50"W
Ile Lepage	Melt Vein	AR-069-M	56°17'20.66"N	74°29'0.86"W
Ile Lepage	Felsic	RW-013-H	56°17'6.57"N	74°29'59.09"W
Ile Lepage	Melt Vein	RW-013-M	56°17'6.57"N	74°29'59.09"W
Ile Atkinson	Melt	RW-019	56° 9'12.66"N	74°32'17.48"W
Ile Atkinson	Melt	RW-024	56° 9'8.00"N	74°32'13.00"W
Ile Atkinson	Melt	RW-025	56° 9'10.15"N	74°28'9.70"W
Ile Atkinson	Intermediate	AR-081	56° 8'27.96"N	74°35'19.22"W
Ile Atkinson	Intermediate	AR-087	56° 8'5.06"N	74°30'27.44"W
Central Islands	Mafic	MK-041	56°13'21.49"N	74°31'18.09"W
Central Islands	Felsic	AR-013	56°13'12.18"N	74°29'55.31"W
Central Islands	Mafic	AR-015.5	56°12'42.43"N	74°30'37.17"W
Central Islands	Mafic	AR-019-H	56°12'19.59"N	74°29'25.07"W
Central Islands	Melt Vein	AR-019-M	56°12'19.59"N	74°29'25.07"W
Central Islands	Felsic	AR-016-H	56°12'42.43"N	74°30'37.17"W
Central Islands	Melt Vein	AR-016-M	56°12'42.43"N	74°30'37.17"W
Eastern Islands	Felsic	MK-003	56°11'25.57"N	74°20'33.22"W
Eastern Islands	Intermediate	MK-006	56° 9'44.07"N	74°18'47.98"W
Eastern Islands	Mafic	MK-011	56°10'34.43"N	74°18'22.44"W
Western Islands	Intermediate	KEY-018	56°14'6.21"N	74°43'4.37"W

Appendix B: Chemical compositions of rock samples obtained from the surface and drill core at the West Clearwater Lake Impact Structure.

Table B.1 – Oxide compositions of surface samples (1 of 2).

SAMPLE	SiO2	Al2O3	Fe2O3	CaO	MgO	Na2O	K2O	Cr2O3	TiO2	MnO	P2O5	SrO	BaO	L.O.I	Total
MK-033-0	62.32	15.68	5.07	3.98	2.56	3.59	3.17	0.09	0.61	0.06	0.22	0.05	0.11	1.91	99.415
MK-033-1	61.78	15.40	5.27	4.78	2.95	3.54	3.07	< 0.01	0.64	0.06	0.23	0.05	0.11	2.01	99.879
MK-033-9	62.45	16.25	4.71	4.06	2.37	3.73	3.26	< 0.01	0.63	0.05	0.23	0.06	0.10	2.09	99.99
MK-033-14	62.07	16.17	4.84	4.17	2.51	3.79	3.23	< 0.01	0.68	0.05	0.26	0.06	0.10	2.03	99.96
MK-033-19	61.92	15.95	5.51	4.29	2.65	3.70	3.12	0.02	0.67	0.06	0.25	0.06	0.10	1.75	100.047
AR-036	61.57	15.72	5.84	4.34	2.55	3.60	3.22	0.01	0.69	0.07	0.25	0.05	0.11	1.94	99.948
AR-034	67.47	14.46	4.35	2.54	0.86	3.57	3.86	< 0.01	0.80	0.04	0.30	0.04	0.13	1.5	99.928
AR-030	49.25	16.43	9.64	9.37	7.11	2.73	1.47	0.01	0.95	0.14	0.39	0.12	0.08	2.16	99.837
MK-075	58.12	15.21	5.85	8.85	3.93	3.56	2.38	0.01	0.61	0.11	0.20	0.05	0.08	0.96	99.906
MK-076	61.57	15.85	5.70	4.63	2.51	3.71	3.57	< 0.01	0.78	0.09	0.29	0.06	0.11	0.86	99.718
MK-077	61.67	15.98	5.75	4.42	2.39	3.64	3.60	< 0.01	0.78	0.06	0.29	0.06	0.11	1.29	100.048
MK-078	61.49	15.82	6.15	4.40	2.54	3.65	3.65	< 0.01	0.78	0.06	0.28	0.06	0.11	1.04	100.042
MK-079	61.36	15.97	5.83	4.30	2.37	3.65	3.65	< 0.01	0.77	0.05	0.28	0.06	0.11	1.5	99.916
MK-071	59.52	15.50	5.76	6.14	3.67	3.53	3.05	< 0.01	0.67	0.09	0.24	0.05	0.09	1.36	99.67
AR-045	69.86	14.61	2.62	1.26	1.04	2.26	5.64	< 0.01	0.41	0.05	0.11	0.04	0.19	2.04	100.136
AR-069-H	75.01	12.63	0.75	0.72	0.41	2.42	5.69	< 0.01	0.05	0.05	0.01	0.01	0.04	2.04	99.834
KEY-018	62.59	16.89	6.27	5.04	2.39	4.53	0.89	< 0.01	0.53	0.12	0.20	0.06	0.02	0.49	100.01
BAC-003	47.82	15.24	13.03	9.97	6.79	2.23	0.72	0.02	1.34	0.15	0.14	0.04	0.03	2.64	100.15
AR-074D	48.27	16.40	13.08	8.79	5.21	2.69	1.16	0.05	1.50	0.12	0.19	0.04	0.04	2.4	99.933
AR-077	60.99	15.67	5.59	4.71	2.54	3.57	3.26	< 0.01	0.72	0.06	0.27	0.05	0.10	2.33	99.868
RW-012	62.12	15.58	6.06	3.84	1.84	3.58	3.88	< 0.01	0.84	0.09	0.30	0.05	0.09	1.54	99.804
AR-069-M	56.31	16.95	5.15	1.33	2.09	2.12	6.38	< 0.01	0.78	0.18	0.25	0.04	0.15	8.28	100.009
RW-013-H	77.80	12.10	1.49	0.83	0.38	2.79	5.11	<0.01	0.16	0.01	0.03	0.04	0.14	0.74	101.62
RW-013-M	62.80	14.30	6.48	3.27	2.19	3.24	3.97	0.01	0.92	0.06	0.27	0.06	0.13	1.82	99.52
RW-019	58.78	15.98	6.57	4.43	2.99	3.86	3.03	< 0.01	0.89	0.10	0.37	0.06	0.10	2.62	99.765
RW-024	60.63	15.61	5.49	4.42	2.71	3.44	3.82	< 0.01	0.81	0.08	0.33	0.06	0.11	2.48	99.978
RW-025	60.10	16.54	6.59	4.24	1.84	3.57	3.68	< 0.01	0.90	0.08	0.40	0.07	0.13	1.85	99.992
AR-081	60.58	15.30	6.27	4.16	2.42	3.41	3.83	< 0.01	0.86	0.06	0.34	0.06	0.12	2.37	99.772
AR-087	59.73	16.70	6.76	4.10	1.77	3.95	3.83	0.01	0.99	0.06	0.37	0.03	0.08	1.42	99.802
MK-041	48.96	16.92	11.51	8.02	4.79	4.35	0.98	< 0.01	1.61	0.13	0.50	0.10	0.03	2.04	99.93
AR-013	68.69	14.66	2.07	0.94	0.05	4.67	3.58	< 0.01	0.29	0.05	0.09	0.04	0.14	4.14	99.988
AR-015.5	46.61	18.98	11.85	8.33	0.13	3.63	1.44	< 0.01	1.27	0.13	0.57	0.15	0.09	2.34	100.055

Table B.2 Oxide compositions of surface samples (2 of 2).

SAMPLE	SiO2	Al2O3	Fe2O3	CaO	MgO	Na2O	K2O	Cr2O3	TiO2	MnO	P2O5	SrO	BaO	L.O.I	Total
AR-019-H	49.57	9.94	10.07	10.51	0.15	2.26	0.56	0.06	0.46	0.15	0.08	0.04	0.03	2.76	99.801
AR-019-M	47.63	14.69	10.73	9.61	0.18	2.95	0.56	0.03	0.80	0.18	0.07	0.06	0.05	4.43	99.931
AR-016-H	49.20	16.40	11.75	7.68	4.59	3.71	1.40	<0.01	1.42	0.09	0.21	0.10	0.10	2.8	99.45
AR-016-M	46.90	15.85	15.75	6.19	4.13	3.08	1.72	<0.01	1.46	0.09	0.32	0.09	0.11	4.13	99.82
MK-003	72.49	14.33	1.89	1.75	0.04	3.17	4.51	< 0.01	0.23	0.04	0.04	0.05	0.18	0.73	99.712
MK-006	60.07	18.19	4.99	3.44	0.07	3.75	5.88	0.03	0.65	0.07	0.30	0.09	0.29	0.34	99.993
MK-011	51.98	18.13	9.50	7.28	0.13	4.61	1.95	< 0.01	1.24	0.13	0.58	0.09	0.09	0.4	99.478

Table B.3 Chemical compositions of surface samples (1 of 4).

SAMPLE	Ba	Ce	Cr	Cs	Dy	Er	Eu	Ga	Gd	Hf	Ho	La	Lu	Nb	Nd	Pr	Rb	Sm	Sn	Sr	Ta	Tb	Th	Tm
MK-033-0	1060	88.6	40	0.17	2.71	1.21	1.5	20.4	4.27	5.6	0.49	49.2	0.16	6.5	39.2	10.65	71.4	6.57	1.00	531.00	0.30	0.51	4.82	0.17
MK-033-1	947	86.7	50	0.19	2.67	1.35	1.43	20.3	4.43	4.9	0.52	47.2	0.18	6.7	38.5	10.55	75.3	6.76	1.00	521.00	0.30	0.57	5.32	0.17
MK-033-9	1070	91.6	40	0.16	2.73	1.34	1.62	20.6	4.49	5.1	0.52	51.2	0.17	5.8	41.2	11.05	70.3	6.69	1.00	546.00	0.20	0.55	4.46	0.16
MK-033-14	1085	99	40	0.17	2.93	1.48	1.68	21.4	5.05	5.9	0.55	54.7	0.19	6.6	45.5	12.15	71.7	7.5	1.00	568.00	0.30	0.62	4.38	0.18
MK-033-19	1110	95.4	40	0.17	3.07	1.44	1.64	21.6	4.77	6.2	0.56	52.6	0.17	6.5	42.8	11.65	70.6	7.54	1.00	582.00	0.30	0.64	4.35	0.18
AR-036	1095	96	50	0.21	2.87	1.46	1.58	21.4	4.52	5.8	0.56	52.7	0.18	7.1	42	11.3	79.2	6.74	1.00	544.00	0.30	0.57	5.11	0.16
AR-034	1310	167	20	0.18	3.31	1.42	1.78	21	5.96	11.4	0.58	76.3	0.17	12.2	69.4	18.9	85.5	10.65	2.00	458.00	0.40	0.69	1.34	0.19
AR-030	860	86.7	110	0.28	3.62	1.85	2.04	20.9	5.96	3.4	0.71	36	0.21	4.3	48.3	11.5	37	9.11	1.00	1190.00	0.10	0.73	0.46	0.25
MK-075	826	69.5	110	0.16	2.47	1.3	1.32	19.3	3.72	4.7	0.48	40.1	0.17	5.2	31.2	8.32	53.7	5.42	1.00	559.00	0.20	0.48	3.92	0.16
MK-076	1180	117	40	0.31	3.75	1.81	1.95	21.4	6.04	6.7	0.72	64.5	0.21	8.5	52.8	14.45	102	9.02	1.00	620.00	0.30	0.79	5.78	0.22
MK-077	1110	107.5	40	0.3	3.15	1.57	1.88	20.7	5.38	6.7	0.62	57.3	0.19	8.5	47.6	12.95	100.5	7.97	1.00	587.00	0.30	0.66	5.63	0.20
MK-078	1120	102.5	40	0.29	3.02	1.51	1.8	21.3	5.19	6.2	0.6	55	0.2	8.1	46.4	12.55	95.6	7.87	1.00	579.00	0.30	0.62	5.35	0.20
MK-079	1090	105	40	0.36	3.04	1.38	1.62	20.6	5.06	6.4	0.59	51.7	0.19	7.9	44.7	12.05	96.2	7.35	1.00	599.00	0.30	0.62	5.40	0.21
MK-071	952	86.1	60	0.08	2.75	1.3	1.36	19.3	4.24	5.1	0.49	43.5	0.17	6	36.5	9.79	65.5	6.24	1.00	567.00	0.30	0.54	4.93	0.18
AR-045	1940	33.4	10	0.27	0.81	0.4	1.17	15.5	1.29	8.3	0.15	19.2	0.07	3.8	11.7	3.25	118	1.97	1.00	456.00	0.10	0.16	1.92	0.07
AR-069-H	451	15.6	<10	0.05	0.06	0.06	0.83	13.1	0.16	1.4	0.02	12	0.01	<0.2	2.6	0.91	95.1	0.3	<1	98.40	<0.1	0.01	0.87	0.01
KEY-018	241	67.2	40	0.05	1.41	0.69	1.2	21.9	2.45	4.7	0.29	37	0.11	4.5	25.6	7.11	9.8	3.74	1.00	606.00	0.20	0.31	0.54	0.11
BAC-003	265	26.8	130	0.21	3.82	2.17	1.21	19.2	3.9	2.6	0.79	12	0.3	6.3	16.5	3.64	21.1	3.99	1.00	356.00	0.40	0.65	0.68	0.33
AR-074D	354	35.6	70	0.28	4.4	2.64	1.5	20.4	4.93	3.3	0.96	15.9	0.35	8.3	20	4.59	34.4	4.97	1.00	383.00	0.50	0.76	0.97	0.38
AR-077	1060	101.5	50	0.23	2.92	1.47	1.5	20.1	4.93	6	0.56	50.4	0.18	6.8	43.1	11.6	83.4	7.28	1.00	571.00	0.30	0.61	5.13	0.21
RW-012	1015	112.5	40	0.25	3.55	1.84	1.69	20.4	5.54	6.6	0.71	51.7	0.24	9.4	46.2	12.35	112.5	7.9	1.00	571.00	0.40	0.72	6.49	0.25
AR-069-M	1605	123	30	0.11	3.48	1.65	3.1	21	6.01	6.9	0.66	113.5	0.25	8	63.5	18.75	131	9.12	1.00	456.00	0.30	0.68	6.32	0.26
RW-013-H	1235	22.9	10	0.19	0.43	0.22	0.86	14.3	0.51	5.4	0.06	15.1	0.03	1.7	5	1.55	145.5	0.74	1.00	378.00	<0.1	0.05	0.83	0.02
RW-013-M	1140	90.3	40	0.37	2.64	1.2	1.67	23.2	4.3	7	0.55	45.4	0.17	10	39.8	10.2	120.5	6.23	2.00	586.00	0.40	0.51	6.40	0.20
RW-019	997	131	50	0.29	3.77	1.83	1.79	22	6.2	6.8	0.72	62.4	0.22	8.9	56	14.85	84.1	9.29	1.00	654.00	0.30	0.76	3.20	0.24
RW-024	1170	132	30	0.31	3.52	1.64	1.89	20.2	6.14	7.8	0.66	61.7	0.21	8.5	55.3	14.55	112.5	9.46	1.00	632.00	0.30	0.75	5.92	0.23
RW-025	1260	132	50	0.31	3.53	1.59	2	21.5	6.15	6.1	0.7	75.2	0.21	8.6	61.1	16.7	95.3	9.48	1.00	706.00	0.30	0.72	7.16	0.23
AR-081	1150	133.5	40	0.4	3.7	1.68	1.77	20.4	5.89	7.7	0.67	63.4	0.23	9.1	54.7	14.6	110	9.04	2.00	580.00	0.30	0.77	6.27	0.24
AR-087	888	142	20	0.56	3.55	1.84	1.83	22.4	5.86	10.6	0.69	65.9	0.26	9.8	58.2	15.85	110	9.08	2.00	366.00	0.40	0.71	2.91	0.24
MK-041	226	158.5	60	0.06	7.21	3.59	2.65	25.4	10.7	7.2	1.41	64	0.47	15.8	77.3	19.4	12.6	14.5	2.00	1010.00	0.70	1.38	2.10	0.53
AR-013	1555	35.1	10	0.07	0.43	0.21	0.7	16.3	0.88	1	0.07	22	0.03	2.2	11.5	3.45	45.2	1.51	1.00	449.00	0.10	0.09	0.33	0.03
AR-015.5	876	139	30	0.28	6.2	2.93	3.27	26.2	9.97	3.5	1.18	55.5	0.34	9.4	74	17.6	40	14.2	2.00	1550.00	0.30	1.21	1.31	0.39

Table B.4 Chemical compositions of surface samples (2 of 4).

SAMPLE	Ba	Ce	Cr	Cs	Dy	Er	Eu	Ga	Gd	Hf	Ho	La	Lu	Nb	Nd	Pr	Rb	Sm	Sn	Sr	Ta	Tb	Th	Tm
AR-019-H	231.00	27.20	440.00	0.31	2.19	1.21	0.93	11.50	3.39	1.50	0.46	11.20	0.14	1.30	17.30	3.67	17.30	4.06	1.00	402.00	0.10	0.45	1.08	0.17
AR-019-M	371.00	20.70	250.00	0.20	2.95	1.81	0.99	18.00	3.13	1.50	0.63	12.20	0.26	3.10	11.70	2.63	19.50	3.08	1.00	636.00	0.10	0.48	0.44	0.27
AR-016-H	886.00	53.00	20.00	0.25	3.71	1.74	2.28	24.40	4.88	8.30	0.67	24.60	0.21	7.10	30.60	6.83	38.00	6.07	1.00	874.00	0.10	0.66	0.41	0.25
AR-016-M	1010.00	62.90	20.00	0.24	4.34	2.07	2.29	28.50	5.82	7.60	0.82	29.70	0.28	7.30	38.70	8.53	44.10	7.34	2.00	761.00	0.20	0.81	0.53	0.28
MK-003	1820.00	42.60	10.00	0.03	0.38	0.18	0.94	16.20	0.88	5.50	0.08	27.50	0.02	1.40	12.90	3.95	81.10	1.50	<1	442.00	<0.1	0.10	2.82	0.02
MK-006	2750.00	99.50	20.00	1.49	2.69	1.39	2.06	21.70	4.41	6.60	0.51	50.60	0.22	10.00	41.10	11.15	187.00	6.69	1.00	945.00	0.50	0.53	5.27	0.22
MK-011	811.00	169.50	60.00	0.48	4.53	2.11	2.32	24.60	8.32	8.50	0.83	80.30	0.26	8.50	73.50	19.20	61.00	12.50	2.00	959.00	0.30	0.96	4.04	0.27

Table B.5 Chemical compositions of surface samples (3 of 4).

SAMPLE	Tl	Ag	Cd	Co	Cu	Li	Mo	Ni	Pb	Sc	Zn	U	V	W	Y	Yb	Zr	As
MK-033-0	<10	<0.5	<0.5	14.00	26.00	<10	<1	22.00	12.00	10.00	41.00	0.55	84.00	<1	13.30	1.10	221.00	<5
MK-033-1	<10	<0.5	<0.5	15.00	20.00	<10	<1	25.00	12.00	11.00	45.00	0.67	91.00	<1	14.10	1.11	195.00	<5
MK-033-9	<10	<0.5	<0.5	11.00	33.00	<10	1.00	16.00	13.00	10.00	44.00	0.47	80.00	<1	13.30	1.09	207.00	<5
MK-033-14	<10	<0.5	<0.5	14.00	31.00	<10	1.00	22.00	12.00	11.00	50.00	0.49	90.00	<1	14.30	1.23	234.00	6.00
MK-033-19	<10	<0.5	<0.5	13.00	23.00	<10	<1	22.00	13.00	11.00	60.00	0.52	89.00	<1	14.60	1.31	254.00	<5
AR-036	<10	<0.5	<0.5	14.00	18.00	10.00	<1	20.00	12.00	10.00	67.00	0.58	93.00	<1	14.40	1.26	234.00	<5
AR-034	<10	<0.5	<0.5	5.00	11.00	10.00	<1	6.00	14.00	5.00	28.00	0.17	60.00	<1	14.90	1.05	476.00	6.00
AR-030	10.00	<0.5	<0.5	38.00	37.00	20.00	1.00	73.00	5.00	27.00	77.00	<0.05	218.00	<1	17.70	1.51	134.00	6.00
MK-075	<10	<0.5	<0.5	17.00	42.00	<10	<1	39.00	9.00	13.00	82.00	0.53	100.00	1.00	12.50	1.15	187.00	<5
MK-076	<10	<0.5	<0.5	13.00	17.00	20.00	1.00	21.00	12.00	11.00	48.00	0.65	97.00	<1	18.60	1.56	296.00	<5
MK-077	<10	<0.5	<0.5	13.00	11.00	30.00	1.00	19.00	13.00	10.00	54.00	0.61	101.00	<1	15.80	1.37	279.00	<5
MK-078	<10	<0.5	<0.5	13.00	13.00	20.00	<1	19.00	13.00	11.00	59.00	0.59	86.00	<1	15.30	1.36	269.00	<5
MK-079	<10	<0.5	<0.5	12.00	13.00	20.00	<1	19.00	14.00	10.00	57.00	0.58	99.00	<1	15.00	1.24	263.00	<5
MK-071	<10	<0.5	<0.5	15.00	9.00	30.00	3.00	27.00	13.00	12.00	56.00	0.46	103.00	<1	12.90	1.17	198.00	8.00
AR-045	<10	<0.5	<0.5	5.00	12.00	20.00	<1	6.00	18.00	4.00	36.00	0.34	40.00	<1	4.00	0.43	334.00	<5
AR-069-H	<10	<0.5	<0.5	2.00	5.00	10.00	<1	3.00	18.00	<1	6.00	0.15	9.00	<1	<0.5	0.05	34.00	<5
KEY-018	<10	<0.5	<0.5	14.00	12.00	<10	<1	16.00	15.00	8.00	88.00	0.12	83.00	<1	7.00	0.63	179.00	<5
BAC-003	<10	<0.5	<0.5	48.00	36.00	30.00	<1	72.00	4.00	32.00	50.00	0.10	311.00	<1	20.50	1.98	93.00	<5
AR-074D	<10	<0.5	<0.5	46.00	47.00	20.00	<1	60.00	<2	24.00	67.00	0.15	259.00	<1	23.00	2.29	117.00	<5
AR-077	<10	<0.5	<0.5	13.00	7.00	10.00	<1	22.00	12.00	11.00	64.00	0.56	100.00	<1	14.30	1.18	240.00	6.00
RW-012	<10	<0.5	<0.5	13.00	12.00	10.00	<1	15.00	17.00	11.00	52.00	0.67	163.00	<1	18.10	1.62	270.00	6.00
AR-069-M	<10	<0.5	1.00	11.00	20.00	20.00	<1	13.00	40.00	10.00	35.00	1.44	96.00	<1	20.10	1.52	279.00	<5
RW-013-H	<10	<0.5	<0.5	2.00	6.00	10.00	<1	3.00	17.00	1.00	9.00	0.35	16.00	<1	1.90	0.24	218.00	<5
RW-013-M	<10	<0.5	<0.5	14.00	12.00	30.00	<1	16.00	18.00	9.00	47.00	0.63	124.00	<1	13.20	1.13	281.00	<5
RW-019	10.00	<0.5	<0.5	15.00	31.00	20.00	1.00	24.00	13.00	12.00	97.00	0.40	116.00	<1	17.90	1.48	288.00	6.00
RW-024	10.00	<0.5	<0.5	13.00	7.00	10.00	<1	17.00	14.00	11.00	47.00	0.55	99.00	<1	16.90	1.41	322.00	5.00
RW-025	<10	<0.5	<0.5	13.00	20.00	20.00	<1	23.00	17.00	14.00	28.00	0.44	179.00	<1	17.40	1.23	248.00	5.00
AR-081	<10	<0.5	<0.5	12.00	18.00	10.00	1.00	19.00	13.00	10.00	59.00	0.61	104.00	<1	18.20	1.47	316.00	<5
AR-087	<10	<0.5	<0.5	11.00	10.00	10.00	1.00	11.00	15.00	9.00	52.00	0.45	109.00	<1	18.30	1.71	462.00	<5
MK-041	<10	<0.5	<0.5	36.00	65.00	10.00	<1	50.00	7.00	25.00	95.00	0.35	274.00	1.00	36.20	3.15	305.00	<5
AR-013	<10	<0.5	<0.5	2.00	8.00	<10	<1	4.00	13.00	1.00	30.00	<0.05	24.00	<1	2.00	0.16	38.00	<5
AR-015.5	10.00	<0.5	<0.5	27.00	67.00	10.00	1.00	19.00	5.00	20.00	86.00	0.22	274.00	<1	28.60	2.17	127.00	<5

Table B.6 Chemical compositions of surface samples (4 of 4).

SAMPLE	Tl	Ag	Cd	Co	Cu	Li	Mo	Ni	Pb	Sc	Zn	U	V	W	Y	Yb	Zr	As
AR-019-H	<10	<0.5	0.60	65.00	180.00	10.00	1.00	265.00	<2	45.00	65.00	0.15	167.00	<1	11.00	0.94	48.00	<5
AR-019-M	<10	<0.5	<0.5	44.00	108.00	10.00	1.00	117.00	<2	31.00	61.00	<0.05	234.00	<1	15.90	1.65	49.00	5.00
AR-016-H	<10	<0.5	0.50	32.00	43.00	10.00	<1	28.00	6.00	23.00	76.00	0.12	236.00	<1	16.50	1.42	329.00	<5
AR-016-M	<10	<0.5	<0.5	36.00	60.00	10.00	<1	25.00	7.00	17.00	109.00	0.18	261.00	<1	19.60	1.67	317.00	<5
MK-003	<10	<0.5	<0.5	2.00	2.00	10.00	<1	3.00	12.00	1.00	21.00	<0.05	25.00	<1	1.80	0.14	234.00	5.00
MK-006	<10	<0.5	<0.5	11.00	8.00	10.00	<1	15.00	27.00	7.00	67.00	1.04	76.00	<1	13.60	1.37	278.00	<5
MK-011	<10	<0.5	<0.5	22.00	35.00	10.00	1.00	29.00	10.00	18.00	92.00	0.71	186.00	<1	21.20	1.67	366.00	<5

Table B.7 Oxide compositions of drill core samples.

SAMPLE	SiO2	Al2O3	Fe2O3	CaO	MgO	Na2O	K2O	Cr2O3	TiO2	MnO	P2O5	SrO	BaO	LOI	Total
5-63-158.5	75.3	13.55	1.58	1.15	0.89	3.8	3.68	<0.01	0.15	0.02	0.05	0.05	0.14	0.64	101
5-63-430	75.6	13.25	1	1.12	0.68	3.7	4.61	<0.01	0.09	0.01	0.01	0.03	0.09	1.01	101.2
5-63-180	68.5	15.85	2.74	4.23	1.34	4.4	0.98	<0.01	0.39	0.05	0.13	0.05	0.03	1.37	100.06
5-63-687.5	52.6	12.65	14.2	6.25	4.81	3.79	0.96	0.01	2.1	0.16	0.35	0.03	0.04	2.33	100.28
5-63-263.8	51.9	17.75	9.93	1.77	7.67	5.74	0.82	<0.01	1.03	0.1	0.53	0.02	0.03	4.1	101.39
1-63-969	49.8	8.06	9.44	14.7	12.95	1.44	0.81	0.13	0.7	0.16	0.28	0.04	0.03	1.93	100.47
1-63-502.2	45.7	14.35	11.9	7.53	7.83	3.05	1.37	0.03	0.89	0.18	0.54	0.1	0.05	4.65	98.17
1-63-1099-A	46.2	8.8	8.27	12.65	11.15	1.77	0.7	0.1	0.43	0.15	0.05	0.04	0.02	1.59	91.92
1-63-1099-G	77.9	11.55	0.94	2.01	0.55	3.58	1.29	<0.01	0.03	0.02	<0.01	0.04	0.04	0.97	98.92
1-63-398.9	63.6	16.3	4.5	4.02	2.04	4.91	1.08	0.01	0.83	0.11	0.11	0.06	0.05	1.74	99.36
5-63-670-G	72	14.25	1.89	2.01	0.74	4.35	3.49	<0.01	0.16	0.03	0.06	0.06	0.15	1.11	100.3
5-63-670-A	51.1	15.5	9.97	6.72	7.81	3.71	0.66	0.08	0.77	0.13	0.42	0.05	0.03	3.31	100.26
5-63-670-M	72	14.8	2.25	2.29	0.72	4.44	3.67	<0.01	0.18	0.03	0.06	0.06	0.16	1.17	101.83
5-63-440-G	76.1	13.05	1.16	0.57	0.91	4	3.71	<0.01	0.09	0.01	0.02	0.02	0.1	1.13	100.87
5-63-440-A	47.8	17.15	11.4	4.39	7.37	5.41	0.37	<0.01	2.01	0.13	1.21	0.05	0.03	4.2	101.52
5-63-440-M	54.5	15.6	10.1	1.21	7.01	2.28	1.72	0.01	0.48	0.09	0.24	0.03	0.04	8.06	101.37
1-63-645-AF	48.1	11	10.55	9.65	10.7	2.38	0.73	0.05	0.61	0.15	0.18	0.07	0.04	5.83	100.04
1-63-645-A	49.8	11.5	10.05	10.55	10.9	2.19	1.13	0.05	0.72	0.13	0.1	0.08	0.05	2.98	100.23
1-63-645-M	47.8	10.7	9.74	10.4	10.6	2.16	0.63	0.05	0.56	0.14	0.16	0.07	0.03	6.59	99.63
1-63-533.4-A	51.4	11.5	10.05	10.05	10.7	2.57	1.22	0.05	0.65	0.17	0.2	0.08	0.05	1.17	99.86
1-63-533.4-M	44.9	12.3	10.8	8.89	10.8	1.74	0.85	0.05	0.73	0.27	0.19	0.07	0.05	8.43	100.07

Table B.8 Chemical compositions of drill core samples (1 of 2).

SAMPLE	Ba	Ce	Cr	Cs	Dy	Er	Eu	Ga	Gd	Hf	Ho	La	Lu	Nb	Nd	Pr	Rb	Sm	Sn	Sr	Ta	Tb	Th	Tm
5-63-158.5	1270	36.5	<10	0.07	0.36	0.13	0.74	15.5	0.74	4.7	0.07	26.8	0.03	0.8	11	3.39	57.5	1.33	<1	467	0.1	0.07	1.18	0.03
5-63-430	820	85.9	<10	0.1	0.57	0.27	1	16.5	1.53	2.5	0.12	56.4	0.05	0.8	26	8.31	109.5	3.53	<1	228	0.1	0.17	14.75	0.03
5-63-180	243	37.4	10	0.04	0.98	0.49	0.71	17.6	1.44	2.9	0.18	24.8	0.07	4.5	14.9	4.65	18.4	2.36	1	477	0.4	0.18	1.1	0.07
5-63-687.5	360	63.3	30	0.1	7.35	4.18	2.16	21.2	8.14	6.1	1.53	29.3	0.55	12.5	36	8.37	19.2	8.49	2	250	0.8	1.22	1.86	0.52
5-63-263.8	316	36.3	10	0.24	1.56	0.92	0.71	23.7	2.26	3.5	0.32	19.4	0.15	6.4	18.3	4.91	27.5	3.18	2	152	0.3	0.29	1.72	0.14
1-63-969	313	49.8	930	0.34	3.37	1.48	1.73	12.9	5.41	2.5	0.58	20.6	0.18	2.8	32.1	7.49	24.3	6.98	1	371	0.2	0.65	1.79	0.2
1-63-502.2	474	73.1	190	0.37	4.93	2.32	1.67	18.8	7.51	2.2	0.87	29.2	0.24	6.3	44.4	10.05	34.6	9.5	1	844	0.3	0.9	3.09	0.28
1-63-1099-A	202	40.6	700	0.16	2.63	1.25	1.28	10.5	3.77	1.6	0.5	18.3	0.14	1.5	22.3	5.28	21.1	4.66	1	384	0.1	0.48	1.1	0.19
1-63-1099-G	350	26.8	10	0.06	0.11	0.04	0.68	13.1	0.26	<0.2	0.03	19.9	0.01	0.2	6	2.13	33.8	0.5	<1	377	<0.1	0.03	0.61	0.01
1-63-398.9	436	30.8	50	<0.01	0.59	0.29	1.1	18.9	0.96	2.9	0.12	18.4	0.05	8.1	11.1	3.19	8.5	1.43	1	515	0.3	0.12	0.42	0.05
5-63-670-G	1475	32	10	0.04	0.49	0.24	1.01	15	0.9	2	0.08	22.2	0.04	1.1	10.5	3.16	51.5	1.28	<1	491	0.1	0.11	0.26	0.03
5-63-670-A	304	109.5	580	0.05	4.01	1.8	1.98	19.6	6.17	3.9	0.72	49.2	0.23	9.9	54	13.45	6.6	9.23	2	460	0.5	0.73	3.64	0.27
5-63-670-M	1475	30.8	440	0.03	0.46	0.28	1.07	15.1	0.87	2.2	0.09	21.2	0.03	1.9	10.4	3.16	51.4	1.6	<1	502	0.1	0.11	0.15	0.03
5-63-440-G	922	19.5	<10	0.04	0.3	0.13	0.65	12.3	0.5	2.9	0.05	15.1	0.04	0.4	5.9	2	62	0.83	<1	206	<0.1	0.05	0.39	0.03
5-63-440-A	241	93.9	10	0.11	4.46	2.08	2.33	22.5	7.16	5.7	0.79	49	0.24	11.4	62.7	15.65	10.7	10.8	2	378	0.5	0.9	1.36	0.27
5-63-440-M	410	61.3	50	0.38	2.02	0.98	1.56	21.7	3.33	5.1	0.37	52.4	0.13	3.5	35.8	10.05	35.6	5.03	3	204	0.2	0.42	2.49	0.14
1-63-645-AF	333	47.2	340	0.25	2.51	1.12	1.34	13.2	3.78	2.1	0.48	21.4	0.15	2.6	25.6	6.06	21.2	4.89	1	518	0.1	0.49	1.2	0.17
1-63-645-A	472	43.7	340	0.46	2.6	1.36	1.31	14	4.02	1.8	0.47	19.2	0.17	3.5	24.7	5.72	39.8	5.02	1	654	0.2	0.52	0.77	0.17
1-63-645-M	225	59.1	320	0.25	2.92	1.56	1.44	12.9	4.27	2.3	0.58	29.2	0.2	2.8	29.7	7.2	18.8	5.87	2	548	0.2	0.55	4.07	0.21
1-63-533.4-A	457	66.4	350	0.31	4.03	2.2	1.35	14.2	5.67	2.8	0.8	26.1	0.3	5.6	37.4	8.97	50.7	7.49	1	620	0.3	0.75	0.83	0.32
1-63-533.4-M	479	95.3	300	0.22	3.63	1.74	1.69	12.9	5.41	3.1	0.65	44.7	0.23	7.1	43.7	11.35	17	7.56	4	565	0.3	0.66	2.39	0.24

Table B.8 Chemical compositions of drill core samples (2 of 2).

SAMPLE	Ag	As	Cd	Co	Cu	Li	Mo	Ni	Pb	Sc	Tl	Zn	U	V	W	Y	Yb	Zr
5-63-158.5	<0.5	<5	<0.5	1	5	10	2	6	23	1	<10	23	0.39	28	3	2.1	0.27	193
5-63-430	<0.5	<5	<0.5	<1	2	10	1	5	28	2	<10	10	0.67	12	<1	3	0.24	83
5-63-180	<0.5	<5	<0.5	4	9	10	1	7	9	3	<10	44	0.42	28	<1	5.1	0.53	126
5-63-687.5	<0.5	<5	<0.5	38	29	20	1	34	5	26	10	137	0.37	303	<1	40.2	3.8	232
5-63-263.8	<0.5	<5	<0.5	21	12	50	1	26	4	14	<10	109	0.95	189	1	8.4	1.05	140
1-63-969	<0.5	<5	<0.5	50	46	20	<1	225	4	54	10	73	0.51	220	<1	16.5	1.33	81
1-63-502.2	<0.5	<5	0.6	38	4	20	1	103	7	23	10	65	0.77	237	<1	22.2	1.93	68
1-63-1099-A	<0.5	<5	0.6	49	81	10	1	209	8	48	10	82	0.24	169	<1	11.9	1.03	50
1-63-1099-G	<0.5	<5	<0.5	<1	13	<10	1	22	12	<1	<10	18	0.07	<5	<1	0.6	0.03	2
1-63-398.9	<0.5	<5	<0.5	15	60	10	1	36	19	4	<10	37	0.25	58	<1	3.1	0.34	110
5-63-670-G	<0.5	<5	<0.5	2	5	10	1	4	8	1	<10	18	0.12	21	<1	2.1	0.21	70
5-63-670-A	<0.5	<5	<0.5	39	23	30	1	97	13	24	<10	137	1.06	187	<1	18.3	1.57	134
5-63-670-M	<0.5	<5	<0.5	2	9	10	1	5	9	2	<10	18	0.1	18	<1	2.3	0.24	74
5-63-440-G	<0.5	<5	<0.5	1	4	10	<1	5	8	1	<10	12	0.34	15	<1	1.6	0.19	92
5-63-440-A	<0.5	<5	<0.5	23	14	40	1	38	7	14	10	130	0.66	217	1	19.4	1.84	226
5-63-440-M	<0.5	<5	<0.5	17	286	110	2	36	18	6	<10	84	2.6	69	3	8.5	0.92	190
1-63-645-AF	<0.5	<5	0.6	52	99	20	1	209	10	34	10	72	0.36	190	<1	11.4	1.04	60
1-63-645-A	<0.5	<5	<0.5	53	216	10	1	193	8	36	<10	77	0.24	195	<1	12.3	1.1	61
1-63-645-M	<0.5	<5	0.5	48	325	10	2	202	15	37	<10	99	0.41	168	<1	13.8	1.28	77
1-63-533.4-A	<0.5	<5	0.6	51	133	10	1	174	10	30	<10	299	0.33	172	<1	19.8	2.1	101
1-63-533.4-M	<0.5	<5	<0.5	43	1100	60	1	203	15	29	<10	342	0.43	164	<1	16.5	1.6	101

Appendix C: Electron microprobe mineral compositions.

Table C.1 – Feldspar mineral compositions (1 of 2).

Sample	SiO2	MgO	Na2O	Al2O3	FeO	MnO	K2O	CaO	TiO2	Total
1-502.2_Plag-01	57.414	0.007	6.210	26.656	0.159	0.001	0.279	8.544	0.011	99.322
1-502.2_Plag-02	54.925	0.000	5.316	28.249	0.106	0.006	0.164	10.356	0.000	99.112
1-502.2_Plag-03	62.722	0.017	8.749	22.887	0.042	0.000	0.359	4.027	0.004	98.807
1-502.2_Plag-04	58.533	0.011	7.062	25.485	0.086	0.028	0.295	7.098	0.000	98.609
1-502.2_Plag-05	57.981	0.002	6.729	26.090	0.084	0.015	0.270	7.751	0.000	98.895
1-645_Plag-01	55.948	0.009	5.703	27.646	0.087	0.000	0.310	9.698	0.012	99.387
1-645_Plag-02	56.912	0.001	6.243	26.958	0.102	0.010	0.253	8.869	0.016	99.385
1-645_Plag-03	56.969	0.003	6.130	27.004	0.089	0.000	0.242	8.806	0.013	99.263
1-645_Plag-04	56.473	0.000	5.968	27.206	0.105	0.007	0.356	9.138	0.021	99.291
1-645_Plag-05	56.413	0.014	6.039	26.812	0.105	0.000	0.279	8.901	0.005	98.588
1-1084.3_Plag-01	59.386	0.002	7.334	25.157	0.070	0.000	0.339	6.970	0.012	99.218
1-1084.3_Plag-02	59.457	0.007	7.279	25.119	0.089	0.000	0.284	6.915	0.012	99.121
1-1084.3_Plag-03	58.832	0.011	7.102	25.804	0.091	0.020	0.231	7.447	0.010	99.551
1-1084.3_Plag-04	63.180	0.014	0.842	18.307	0.107	0.005	15.117	0.158	0.014	97.729
1-969_Plag-02	54.888	0.004	5.489	28.037	0.087	0.041	0.158	10.139	0.005	98.900
1-969_Plag-03	55.928	0.004	5.927	27.583	0.059	0.000	0.192	9.455	0.013	99.163
5-440_Plag-01	61.868	0.046	9.195	20.584	2.067	0.046	0.376	4.352	0.003	98.553
5-440_Plag-02	67.937	0.000	11.640	19.613	0.048	0.012	0.082	0.166	0.018	99.519
5-440_Plag-03	66.835	0.007	11.153	20.206	0.109	0.017	0.185	0.831	0.003	99.363
5-440_Plag-04	67.685	0.012	11.467	19.339	0.075	0.001	0.059	0.094	0.000	98.732
5-440_Plag-05	64.428	0.006	2.495	18.657	0.077	0.030	13.029	0.188	0.020	98.930
5-440_Plag-06	63.538	0.006	0.298	18.433	0.042	0.001	16.308	0.097	0.020	98.743
5-440_Plag-07	64.342	0.004	0.900	18.702	0.019	0.000	15.611	0.056	0.018	99.661
5-440_Plag-08	63.824	0.001	0.200	18.474	0.008	0.000	16.457	0.192	0.017	99.194
5-440_Plag-09	68.005	0.008	11.545	19.639	0.000	0.000	0.438	0.185	0.000	99.823
1-533.4_Plag-01	59.253	0.027	7.413	24.632	0.070	0.002	0.262	6.356	0.005	98.025
1-533.4_Plag-03	55.351	0.005	5.578	28.129	0.108	0.010	0.164	10.168	0.000	99.518
1-533.4_Plag-04	55.919	0.000	5.944	27.681	0.069	0.004	0.202	9.751	0.011	99.581
1-533.4_Plag-05	57.422	0.000	6.484	26.559	0.095	0.000	0.343	8.362	0.015	99.295
1-533.4_Plag-06	57.721	0.003	6.583	26.342	0.075	0.000	0.391	8.228	0.012	99.393
5-670_Plag-01	63.587	0.014	0.515	18.653	0.041	0.023	15.910	0.075	0.022	98.840
5-670_Plag-02	63.349	0.006	0.393	18.498	0.037	0.029	16.186	0.060	0.031	98.609
5-670_Plag-03	63.529	0.009	0.538	18.618	0.027	0.000	15.853	0.064	0.015	98.656
5-670_Plag-04	63.478	0.000	0.748	18.733	0.023	0.000	15.680	0.079	0.021	98.762
5-670_Plag-05	63.560	0.003	0.319	18.484	0.016	0.000	16.272	0.048	0.010	98.727
5-670_Plag-06	66.162	0.012	10.677	21.134	0.017	0.016	0.347	1.683	0.000	100.066
5-670_Plag-07	64.205	0.000	1.604	18.781	0.028	0.025	14.443	0.040	0.017	99.143
5-670_Plag-08	65.051	0.076	9.993	21.832	0.154	0.015	0.789	1.581	0.000	99.513
5-670_Plag-09	63.084	0.000	0.306	18.430	0.012	0.000	16.310	0.034	0.015	98.191
5-670_Plag-10	60.527	0.007	8.136	24.670	0.149	0.001	0.150	6.236	0.018	99.907
5-263.8_Plag-01	68.461	0.000	11.865	19.491	0.013	0.005	0.030	0.026	0.000	99.919
5-263.8_Plag-02	63.434	0.000	0.277	18.733	0.015	0.029	16.055	0.047	0.000	98.595

Table C.2 – Feldspar mineral compositions (2 of 2).

Sample	SiO2	MgO	Na2O	Al2O3	FeO	MnO	K2O	CaO	TiO2	Total
5-263.8_Plag-03	68.156	0.009	11.820	19.580	0.028	0.000	0.040	0.037	0.001	99.671
5-263.8_Plag-04	63.746	0.000	0.277	18.704	0.015	0.000	16.270	0.037	0.040	99.126
5-263.8_Plag-05	68.272	0.008	11.892	19.509	0.004	0.013	0.024	0.014	0.000	99.738
5-263.8_Plag-06	68.596	0.000	11.950	19.555	0.015	0.004	0.024	0.035	0.003	100.187
5-263.8_Plag-07	68.460	0.000	11.929	19.551	0.024	0.013	0.022	0.027	0.000	100.051
5-263.8_Plag-08	67.947	0.085	11.907	19.762	0.309	0.023	0.061	0.143	0.000	100.251
5-263.8_Plag-09	66.742	0.748	11.313	20.002	1.043	0.042	0.110	0.285	0.004	100.289
5-263.8_Plag-10	66.355	0.512	11.060	20.240	0.630	0.023	0.384	0.558	0.034	99.812
1-398.9_Plag-01	64.029	0.004	0.477	18.721	0.043	0.005	16.037	0.041	0.024	99.395
1-398.9_Plag-02	60.880	0.000	7.976	24.715	0.102	0.039	0.365	6.080	0.006	100.201
1-398.9_Plag-03	63.734	0.005	0.565	18.726	0.030	0.027	15.929	0.054	0.017	99.100
1-398.9_Plag-04	62.855	0.004	0.387	18.753	0.016	0.006	15.961	0.055	0.024	98.093
1-398.9_Plag-05	60.587	0.006	7.706	24.848	0.052	0.000	0.321	6.436	0.013	99.969
1-398.9_Plag-06	60.212	0.000	7.616	25.103	0.127	0.000	0.470	6.676	0.014	100.264
1-398.9_Plag-07	64.849	0.007	4.610	19.250	0.087	0.000	9.740	0.091	0.033	98.690
1-398.9_Plag-08	60.230	0.004	7.724	24.837	0.176	0.011	0.379	6.426	0.014	99.814
1-720.9_Plag-01	63.682	0.002	0.991	18.771	0.009	0.000	15.119	0.049	0.025	98.665
1-720.9_Plag-02	59.229	0.007	7.168	25.646	0.088	0.010	0.328	7.323	0.014	99.821
1-720.9_Plag-03	59.541	0.004	7.229	25.596	0.135	0.000	0.464	7.186	0.023	100.205
1-720.9_Plag-04	59.326	0.005	7.178	25.607	0.091	0.000	0.332	7.383	0.017	99.967
1-720.9_Plag-05	58.133	0.007	6.746	26.338	0.077	0.000	0.330	8.216	0.015	99.867
1-720.9_Plag-06	62.851	0.000	0.535	18.682	0.078	0.000	15.656	0.106	0.034	97.957
1-720.9_Plag-06	63.122	0.003	0.562	18.740	0.064	0.004	15.662	0.096	0.030	98.283
1-1113_Plag-01	59.273	0.013	7.272	25.844	0.090	0.022	0.242	7.399	0.003	100.158
1-1113_Plag-02	59.495	0.000	7.277	25.780	0.076	0.028	0.290	7.319	0.008	100.283
1-1113_Plag-03	64.738	0.004	1.707	18.775	0.011	0.000	14.346	0.128	0.021	99.743
1-1113_Plag-04	59.137	0.000	7.296	25.725	0.053	0.002	0.251	7.340	0.000	99.835
1-1113_Plag-05	64.638	0.000	1.959	18.808	0.023	0.000	14.154	0.138	0.018	99.738
1-1113_Plag-06	68.367	0.002	11.595	19.920	0.005	0.000	0.074	0.272	0.003	100.238
5-540_Plag-01	63.482	0.000	0.442	18.696	0.017	0.000	16.020	0.107	0.043	98.815
5-540_Plag-01	63.560	0.000	0.541	18.795	0.038	0.013	15.881	0.087	0.023	98.938
5-540_Plag-02	63.605	0.000	0.711	18.527	0.039	0.000	15.728	0.059	0.028	98.697
5-540_Plag-02	63.847	0.002	1.092	18.710	0.036	0.000	15.135	0.050	0.015	98.901
5-540_Plag-03	65.020	0.000	10.269	21.887	0.048	0.011	0.037	2.695	0.004	99.971
5-540_Plag-04	63.808	0.000	0.369	18.474	0.025	0.015	16.337	0.020	0.021	99.069
5-540_Plag-05	61.515	0.000	8.172	23.886	0.137	0.012	0.507	5.333	0.004	99.589
5-540_Plag-06	63.875	0.003	0.876	18.747	0.025	0.006	15.487	0.079	0.025	99.123

Table C.3 – Pyroxene mineral compositions (1 of 2).

Sample	SiO2	Al2O3	Na2O	MgO	MnO	Cr2O3	FeO	NiO	TiO2	CaO	Total
1-502.2_Px-01	52.062	2.633	0.506	14.088	0.158	0.057	7.229	0.016	0.155	22.532	99.436
1-502.2_Px-02	51.527	2.169	0.505	14.075	0.221	0.055	9.203	0.021	0.192	21.100	99.068
1-502.2_Px-03	52.146	1.949	0.416	14.638	0.170	0.036	6.303	0.012	0.119	23.313	99.102
1-502.2_Px-04	51.716	2.282	0.526	13.867	0.228	0.052	7.625	0.023	0.277	22.411	99.007
1-645_Px-01	51.254	2.797	0.535	13.608	0.134	0.092	7.930	0.018	0.330	22.103	98.801
1-645_Px-02	51.111	2.835	0.558	13.442	0.182	0.047	7.659	0.014	0.332	22.368	98.548
1-645_Px-03	51.154	2.437	0.511	14.003	0.150	0.083	8.051	0.022	0.295	21.641	98.347
1-645_Px-04	51.467	2.279	0.529	13.924	0.160	0.018	7.383	0.008	0.264	22.496	98.528
1-645_Px-05	51.653	2.380	0.493	14.236	0.161	0.091	7.305	0.024	0.271	22.365	98.979
1-1084.3_Px-01	51.381	1.738	0.550	13.879	0.313	0.123	8.482	0.006	0.153	21.832	98.457
1-1084.3_Px-02	52.067	1.693	0.540	14.110	0.302	0.143	7.857	0.005	0.135	22.009	98.861
1-1084.3_Px-03	51.757	1.862	0.579	13.812	0.340	0.217	8.846	0.032	0.179	21.197	98.821
1-969_Px-01	51.482	2.530	0.531	13.990	0.159	0.182	7.277	0.016	0.262	22.298	98.727
1-969_Px-02	51.433	2.658	0.554	14.212	0.152	0.062	7.023	0.032	0.316	21.944	98.386
1-969_Px-03	51.692	2.254	0.504	14.072	0.137	0.187	7.040	0.020	0.228	22.424	98.558
1-969_Px-04	51.519	2.134	0.537	14.085	0.186	0.182	7.408	0.018	0.280	22.096	98.445
1-533.4_Px-01	51.614	2.635	0.598	13.720	0.195	0.102	7.925	0.015	0.299	22.477	99.580
1-533.4_Px-02	51.906	2.402	0.592	13.871	0.212	0.072	7.859	0.025	0.272	22.399	99.610
1-533.4_Px-03	52.651	1.363	0.014	22.863	0.494	0.035	20.952	0.027	0.086	0.528	99.013
1-533.4_Px-04	51.571	2.349	0.554	13.755	0.213	0.117	7.999	0.021	0.258	22.179	99.016
1-533.4_Px-05	52.448	1.198	0.000	22.794	0.500	0.018	21.616	0.043	0.066	0.512	99.195
1-533.4_Px-06	52.669	2.145	0.503	14.227	0.204	0.059	7.498	0.025	0.213	22.569	100.112
1-533.4_Px-07	52.165	2.637	0.610	13.901	0.188	0.078	7.762	0.032	0.259	22.242	99.874
1-533.4_Px-08	51.694	2.792	0.570	13.789	0.211	0.117	8.002	0.007	0.296	22.395	99.873
1-533.4_Px-09	51.760	2.628	0.520	13.855	0.216	0.063	7.681	0.011	0.275	22.444	99.453
1-533.4_Px-10	52.701	1.917	0.538	14.977	0.147	0.078	6.452	0.027	0.219	22.809	99.865
398.9_Px-01	52.758	0.898	0.000	22.882	0.670	0.009	21.654	0.014	0.094	0.499	99.478
398.9_Px-02	52.740	1.158	0.003	22.808	0.641	0.008	22.074	0.000	0.099	0.550	100.081
398.9_Px-03	53.028	1.038	0.004	22.992	0.699	0.018	21.545	0.032	0.111	0.580	100.047
398.9_Px-04	51.280	1.006	0.000	21.691	0.681	0.015	21.578	0.000	0.097	0.625	96.973
398.9_Px-05	50.825	0.775	0.005	22.181	0.720	0.027	21.671	0.000	0.086	0.533	96.823
398.9_Px-06	52.448	0.997	0.016	22.587	0.691	0.000	21.740	0.006	0.099	0.613	99.197
398.9_Px-07	52.536	1.135	0.001	22.646	0.698	0.005	21.765	0.000	0.107	0.559	99.452
1-720.9_Px-01	52.828	1.761	0.533	14.479	0.208	0.067	7.224	0.000	0.235	22.410	99.745
1-720.9_Px-02	51.747	2.030	0.552	13.637	0.226	0.066	8.171	0.027	0.286	22.444	99.186
1-720.9_Px-03	52.596	1.722	0.506	14.324	0.180	0.158	7.230	0.000	0.185	22.570	99.471
1-720.9_Px-04	52.203	1.289	0.021	22.142	0.633	0.021	22.172	0.043	0.085	0.629	99.238
1-720.9_Px-05	52.129	1.879	0.520	13.842	0.317	0.000	8.309	0.000	0.207	22.359	99.562
1-720.9_Px-06	51.604	2.036	0.463	13.722	0.259	0.000	8.406	0.000	0.203	22.203	98.896
1-720.9_Px-07	52.002	1.224	0.000	22.135	0.799	0.008	21.886	0.003	0.087	0.576	98.720
1-1113_Px-01	52.284	1.870	0.549	14.094	0.201	0.083	7.655	0.018	0.201	22.537	99.492

Table C.3 – Pyroxene mineral compositions (2 of 2).

Sample	SiO2	Al2O3	Na2O	MgO	MnO	Cr2O3	FeO	NiO	TiO2	CaO	Total
1-1113_Px-02	52.8	1.595	0.508	14.544	0.289	0.096	8.095	0.022	0.145	22.206	100.3
1-1113_Px-03	54.881	1.133	0.242	17.328	0.448	0.064	11.469	0	0.031	12.081	97.677
1-1113_Px-04	52.883	1.831	0.51	14.14	0.275	0.176	7.35	0.031	0.161	22.605	99.962
5-540_Px-01	44.065	9.751	1.724	14.029	0.211	0.08	12.156	0.007	1.738	11.417	95.178
5-540_Px-02	44.793	9.906	1.694	14.22	0.136	0.113	11.938	0.012	1.909	11.445	96.166

Appendix D: Element maps of melt veins.

Figure D.1 - Element maps of sample 5-670: A) SEM backscatter electron image of sample spot B) Fe map C) K map D) Mg map E) Na map F) Si map.

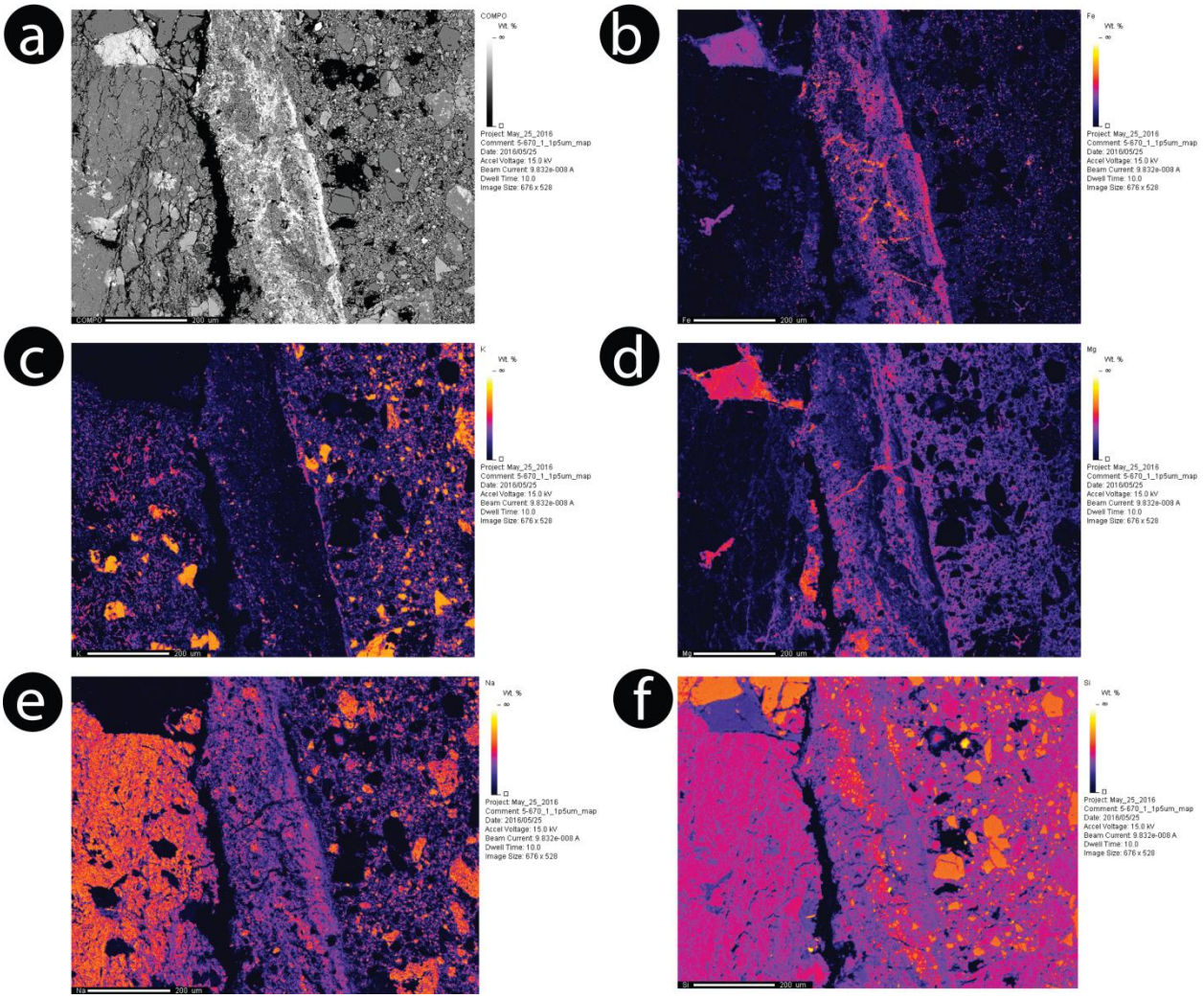

Figure D.2 - Element maps of sample 1-533.4: A) SEM backscatter electron image of sample spot B) Al map C) Ca map D) Mg map E) Na map F) Si map G) Ti map.

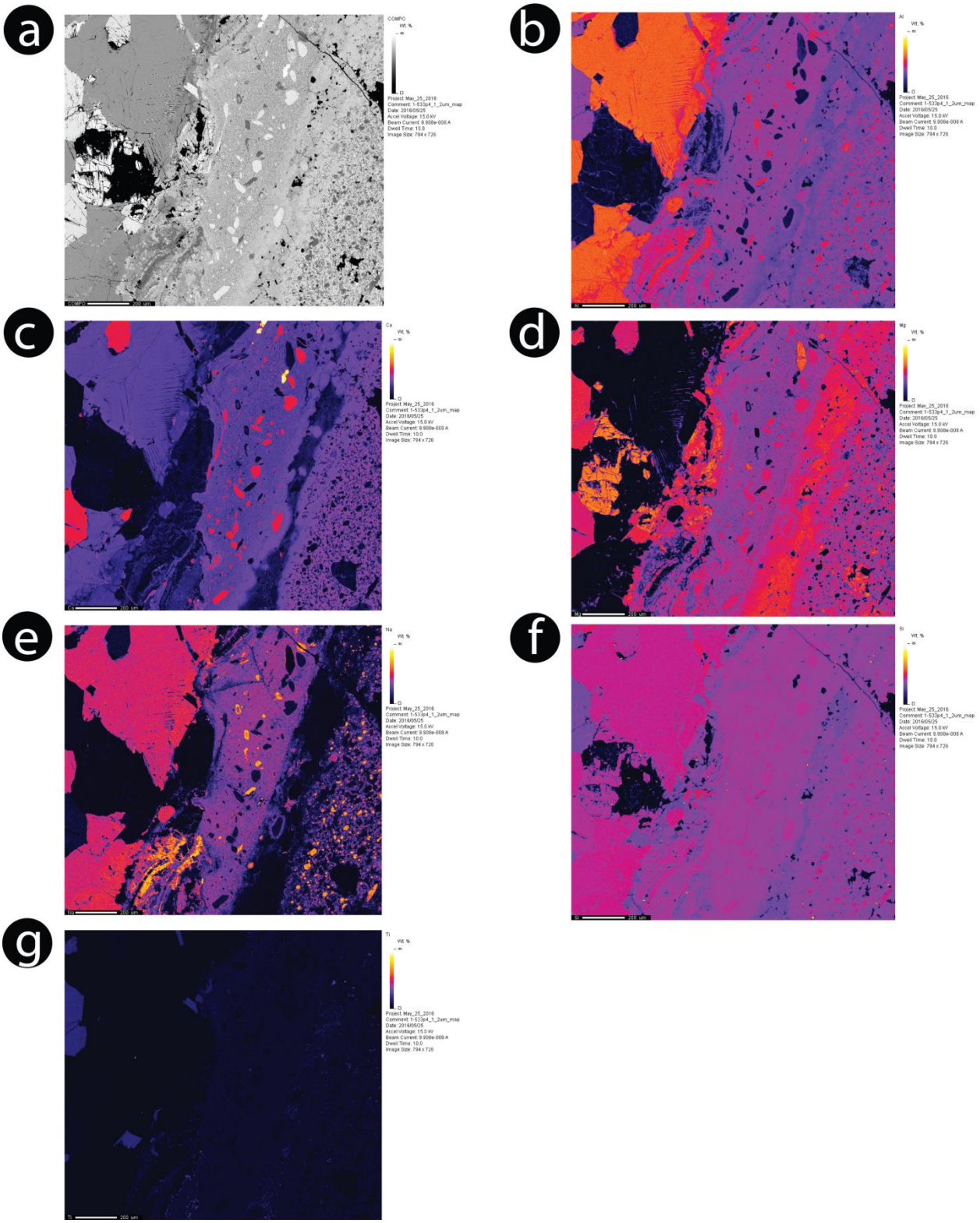

Figure D.3 - Element maps of sample 1-645: A) SEM backscatter electron image of sample spot B) Cl map C) Mn map D) Ni map E) S map.

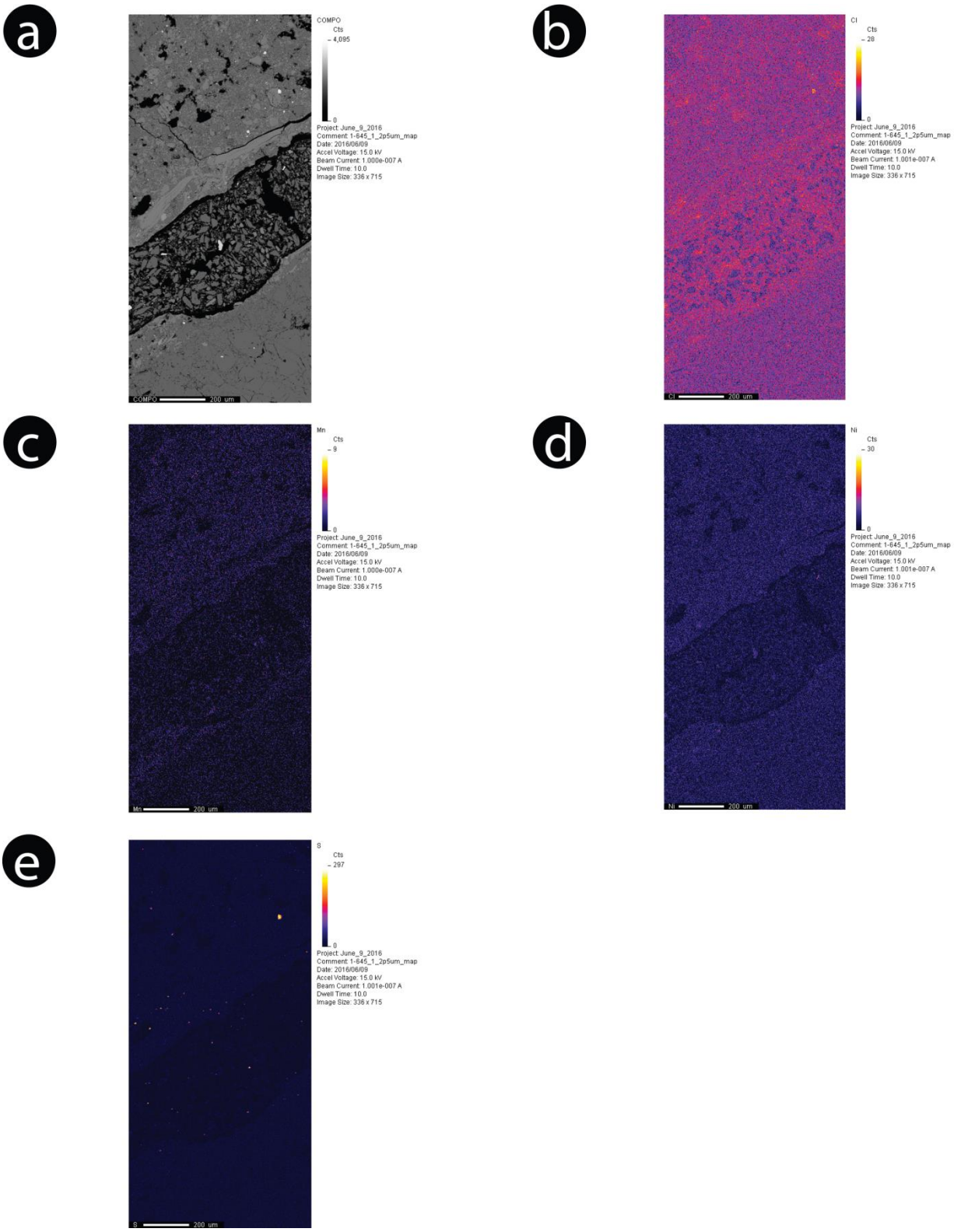

Curriculum Vitae

Name: Rebecca Wilks

Post-secondary Education and Degrees:
University of Winnipeg
Winnipeg, Manitoba Canada
2009-2014 B.Sc. in Geography with Honours

Honours and Awards

Canadian Graduate Scholarship – Masters Program Natural Sciences and Engineering Research Council of Canada
2015

Astromaterials Research and Training Opportunities Student Travel Grant
2015

Brian Evans Memorial Scholarship
University of Winnipeg
2013, 2012, 2011

Victor Dolmage Memorial Scholarship in Geography
University of Winnipeg
2013

Deans Honours List – Student of Distinction
University of Winnipeg
2013

Special Entrance Scholarship
University of Winnipeg
2009

Related Work Experience
Teaching Assistant
The University of Western Ontario
2014-2016

Research Assistant
Isotope Lab University of Winnipeg Geography Department
2011-2013

Earth Science Lab Marker and Demonstrator
University of Winnipeg Geography Department
2012-2013

Earth Science Tutor
University of Winnipeg Geography Department
2011

Publications:

Wilks, R.,and Osinski, G. (2016). Melt veins at the West Clearwater Impact Structure: In situ vs injected melt. 47th Lunar and Planetary Science Conference, Abstract #1570.

Wilks, R.,and Osinski, G. (2015). Impact Melt Veins in the Central Uplift of the West Clearwater Lake Impact Structure, Northern Quebec, Canada. 46th Lunar and Planetary Science Conference, Abstract #1397.

Wilks R, Applin D, Cloutis E, and Bandfield J. (2014). Spectral properties of shocked and unshocked granites: Implications for detection on Mars. 45th Lunar and Planetary Science Conference, Abstract #2579.

Carlson, J.C. Julie C. Anderson, Jennifer E. Low, Pascal Cardinal , Scott D. MacKenzie, Sarah A. Beattie , Jonathan K. Challis, Renae J. Bennett , Stephanie S. Meronek, Rebecca P.A. Wilks, William M. Buhay, Charles S. Wong, Mark L. Hanson. (2013). Presence and hazards of nutrients and emerging organic micropollutants from sewage lagoon discharges into Dead Horse Creek, Manitoba, Canada.*Science of the Total Environment;* Vol. 445 - 446: 64-78.